2015

Synthesis and characterization of Ni(II), Cu(II), Zn(II), Cd(II) and Pb(II) complexes with ligands of N,O and N,S donor atoms containing long chain pendant arms and study of their antimicrobial activities

Begum, Mst. Sabina

University of Rajshahi

PhD Thesis

Synthesis and characterization of Ni(II), Cu(II), Zn(II), Cd(II) and Pb(II) complexes with ligands of N,O and N,S donor atoms containing long chain pendant arms and study of their antimicrobial activities

A Thesis submitted to Rajshahi University for the degree of Doctor of Philosophy in Chemistry

SUBMITTED BY

MST. SABINA BEGUM

ROLL NO. 10203

REGISTRATION NO. 11629

SESSION: 2010-2011

MST. SABINA BEGUM

NOVEMBER, 2015

INORGANIC RESEARCH LABORATORY

DEPARTMENT OF CHEMISTRY

RAJSHAHI UNIVERSITY, RAJSHAHI-6205

BANGLADESH.

November, 2015

Synthesis and characterization of Ni(II), Cu(II), Zn(II), Cd(II) and Pb(II) complexes with ligands of N,O and N,S donor atoms containing long chain pendant arms and study of their antimicrobial activities

A Thesis submitted to Rajshahi University for the degree of Doctor of Philosophy in Chemistry

SUBMITTED BY

MST. SABINA BEGUM

ROLL NO. 10203

REGISTRATION NO. 11629

SESSION: 2010-2011

NOVEMBER, 2015

INORGANIC RESEARCH LABORATORY

DEPARTMENT OF CHEMISTRY

RAJSHAHI UNIVERSITY, RAJSHAHI-6205

BANGLADESH.

ACKNOWLEDGEMENT

All praises and gratefulness to the almighty Allah, the most merciful who manages each and everything soundly and enabled me to complete my work.

I am grateful to my honorable teacher and guide, ***Dr. Md. Belayet Hossain Howlader, Professor, Department of Chemistry, Rajshahi University, Rajshahi-6205, Bangladesh,*** *for his encouragement, guidance and generous help throughout the course of this research work. It's a great honor and privilege for me to work with him and to share his valuable knowledge and experience. Once more do I express my gratefulness to Professor Belayet Hossain Howlader who instilled in me the love for Inorganic Chemistry during my M.Sc. studies and eventually introduced me to the beauty of Synthetic Chemistry of Dithiocarbazate Compounds for my PhD.*

I would like to express my deepest sense of gratitude and indebtedness to ***Dr. Ennio Zangrando****,* ***Professor, Department of Chemical and Pharmaceuticals Sciences, via Giorgieri 1, 34127 Trieste, Italy,*** *for providing funds for X-ray crystallography.*

Thanks also to ***Dr. Ruyata Miyatake****, Associate professor, Center for Environmental Conservation and Research Safety, University of Toyama, 3190 Gofuku, Toyama 930-8555, Japan for his collaboration in my research. I also express my thanks and gratefulness to* ***Dr. Md. Chanmiya Sheikh****, Post Doctoral Fellow, Department of Applied Chemistry, Faculty of Engineering, University of Toyama, 3190 Gofuku, Toyama 930-8555, Japan for providing spectroscopic and analytical facilities.*

I am also grateful to the authority of Rajshahi University for providing necessary laboratory facilities. Thanks also to the Chairman, Department of

Chemistry, Rajshahi University and all of my respectable teacher's, Department of Chemistry, Rajshahi University for their cooperation.

Also I would like to thank the authority of Shahjalal University of Science and Technology, Sylhet-3114, Bangladesh, for granting me study leave.

I would like to thank the Ministry of Science and Technology, Bangladesh for providing NST fellowship for this research purpose.

And finally, I wish to thank my dearest mother, father, brothers and sisters for their endless love and encouragement.

Mst. Sabina Begum

Declaration

This is to certify that the thesis submitted by Mst. Sabina Begum entitled **'Synthesis and characterization of Ni(II), Cu(II), Zn(II), Cd(II) and Pb(II) complexes with ligands of N,O and N,S donor atoms containing long chain pendant arms and study of their antimicrobial activities'** was carried out under my supervision and guidance. The candidate has fulfilled all the terms and conditions for the award of **Doctor of Philosophy** in Chemistry. This work has not been submitted anywhere for any other degree.

Prof. Dr. Md. Belayet Hossain Howlader
Supervisor
Department of Chemistry
Rajshahi University, Rajshahi-6205
Bangladesh

Declaration

I do hereby state that the thesis entitled **'Synthesis and characterization of Ni(II), Cu(II), Zn(II), Cd(II) and Pb(II) complexes with ligands of N,O and N,S donor atoms containing long chain pendant arms and study of their antimicrobial activities'** is my own work. This work has not been presented elsewhere except for publication. All quotations, illustrations and citations have been duly acknowledged. I also declare that it has not been previously, and is not concurrently, submitted anywhere for any other degree.

Mst. Sabina Begum
PhD Fellow
Roll No. 10203
Registration No. 11629
Session: 2010-2011
Dept. of Chemistry
Rajshahi University, Rajshahi-6205
Bangladesh.

Dedicated

To My

Beloved Parents

Chapter 1

General Introduction

Chapter 2

Methods and Materials

Chapter 3

Synthesis, characterization, X-ray crystal structure, photoluminescence and electrochemistry of the N, S Schiff base ligand derived from 4-methylbenzaldehyde and S-hexyldithiocarbazate and of its bivalent metal complexes

Chapter 4

Synthesis, characterization, photoluminescence and electrochemical studies of Ni(II), Cu(II), Zn(II), Cd(II) and Pd(II) complexes of the bidentate S-hexyl-β-N-(2-thienyl)methylenedithiocarbazate ligand

Chapter 5

Synthesis, spectroscopic characterization, photoluminescence and antibacterial activities of some bivalent metal complexes of N,S donor ligand containing dithiocarbazate moiety. X-ray crystal structure of S-hexyl 3-(4-methoxybenzylidene)dithiocarbazate

Chapter 6
Conclusion

Appendix

ABSTRACT

Transition metal chelates of dithiocarbazic acid, its S-alkyl/aryl esters and their Schiff bases have been studied, mainly due to their potential anticancer, antibacterial, antifungal, antimoebic, nonlinear optical and insecticidal activities. The number of ligands synthesized continues to increase because of the intriguing observation that different ligands show different biological properties, although they may differ only slightly in their molecular structures. It is well known that coordination of metals to Schiff base ligands may enhance their biological activities. The electrochemical behavior and photoluminescence properties of many Schiff bases and of corresponding metal complexes are reported in the literature.

In view of this, the present work focuses on the synthesis of three new bidentate Schiff base ligands, formed by the condensation of S-hexyldithiocarbazate with 4-methylbenzaldehyde, thiophene-2-carboxaldeyde and 4-methoxybenzaldehyde, and on their Ni(II), Cu(II), Zn(II), Cd(II), Pd(II) and Pb(II) complexes. The synthesized ligands and the complexes have been characterized by various physico-chemical and spectroscopic methods such as ^{1}H and ^{13}C NMR, mass, IR and UV-Vis spectra, elemental analysis, magnetic moment, conductance and melting point measurements. A total of six X-ray single crystals structures have been determined in this work. In order to provide more insight into the behavior of these compounds in solution, the photoluminescence properties and the electrochemical analyses have also been performed.

Ligands and metal complexes structurally characterized by X-ray single crystal diffraction study are here reported. Both ligands **1** and **14** crystallize in triclinic system, space group $P\bar{1}$, and unit cell parameters and cell volume are as follows:

Crystal data of ligand **1**: a = 4.79244(9), b = 11.3790(2), c = 14.5382(3) Å, α = 100.1666(7), β = 91.2117(7), γ = 94.6754(7)°, V = 777.26(3) Å^3, Z = 2.

Crystal data of ligand **14**: a = 4.55596(8), b = 12.4224(3), c = 14.9619(3) Å, α = 75.7300(9), β = 84.7599(10), γ = 84.6141(9)°, V = 814.99 (3) Å^3, Z = 2.

In both the ligands **1** and **14**, the dithiocarbazate group adopts an *E* configuration with respect to the C=N bond of the benzylidene moiety. The *β*-nitrogen and the thioketo sulfur are *trans* located with respect to the C(9)-N(2) bond. Each molecule is in its thione tautomeric (also confirmed by IR and NMR) and the co-planarity of atoms (with the exception of the S-hexyl chain) indicates an electron delocalization within it.

Crystal data of Ni(II) complex **2**: triclinic system, space group $P\bar{1}$, a = 4.6738(3), b = 10.5132(5), c = 16.4789(8), Å, α = 86.522(3), β = 84.850(3), γ = 79.057(3)°, V = 791.00(7) Å^3, Z = 1.

Crystal data of Pd(II) complex **6**: monoclinic system, space group $C2$, a = 18.3559(11), b = 9.6747(5), c = 10.3368(6) Å, β = 116.810(2)°, V = 1638.37(16) Å^3, Z = 2.

The X-ray crystallographic structural analysis of **2** and **6** confirmed that the two Schiff bases, in their deprotonated imino thiolate form, act as chelating ligands to the metal center via the azomethine nitrogen N(1) and thiolate sulfur S(1) atoms. In complex **2**, the Ni-S(1) and Ni-N(1) bond distances are of 2.1777(11) and 1.933(4) Å, respectively, with a S(1)-Ni-N(1') chelating angle of 86.06(10)°, whereas in complex **6** the Pd-S(1) and Pd-N(1) coordination bond distances are of 2.264(4) and 2.154(12) Å, respectively, with an N(1)-Pd-S(1) chelating angle of 83.2(3)°. The complex **2** stacks at a distance of 4.6738(3) Å (along axis *a*), which exclude any significant interactions between the aromatic rings. The most interesting structural feature between these complexes is the different configuration of ligands, that is *trans* and *cis* in the square planar geometry of NiL_2, **2** and PdL_2, **6** complex, respectively.

In addition the configuration of dithiocarbazate group about the imine bond N1=C8 is E in the Pd(II) complex **6** and Z in Ni(II) complex **2**. In fact the torsion angle N2−N1−C8−C5 in **6** is 172.1(14)°, different from that observed in the nickel derivative **2** of 1.2(7)°. This allows an approach between the rings of the methylbenzylidene moieties, with a centroid-to-centroid distance of 4.114(8) Å, indicating a very weak π-π interaction.

The X-ray structural analysis of the bischelated nickel(II) **9** and copper(II) **10** complexes indicates that the crystals are isostructural crystallizing in monoclinic system, space group $P2_1/c$.

Crystal data of Ni(II) complex **9**: a = 13.9738(3), b = 10.31877(19), c = 20.4549(4) Å, β = 102.4271(7) °, V = 2880.34(10) Å^3, Z = 4.

Crystal data of Cu(II) complex **10**: a = 13.9228(3), b 10.33945(19), c = 20.6389(4) Å, β = 103.1778(7)°, V = 2892.82(10) Å^3, Z = 4.

Here the two ligands are crystallographically independent and chelate the metal in *trans* configuration. In the NiL_2 complex **9**, the Ni-S and Ni-N the bond distances are of 2.1785(4), 2.1812(4) and 1.9112(12), 1.9177(12) Å, respectively and S-Ni-N chelating bond angle averages to 85.88(4)°. The corresponding parameters in the CuL_2 derivative **10** are 2.2591(4), 2.2637(4) and 1.9988(12), 2.0047(12) Å, respectively, with a S-Cu-N chelating angle of 84.57(3)° (mean value). The observed differences in the bond lengths are to be ascribed to the different metal ionic radius. It is worth noting that in the complexes **9** and **10** both the M-S and M-N bond distances are within the range of the derivatives having a *trans* configuration. The crystal packing evidences the complexes **9** and **10** arranged in such a way that the alkyl chains point towards the center of the unit cell giving rise to a hydrophobic area.

According to spectroscopic and crystallographic studies, the Ni(II), Cu(II) and Pd(II) complexes exhibit a square planar geometry, the other being tetrahedral.

The fluorescence intensity of all the three Schiff base ligands is quenched upon complexation with metal ions with the exception of complexes **7** and **15** where the fluorescence intensity is enhanced (with respect to the ligand).

The electrochemical properties of Cu(II) complexes **3** and **10** have been studied by cyclic voltammetry. Both the compounds exhibit one electron quasi-reversible redox activity in the applied potential range. Electrochemical Impedance Spectral (EIS) measurements also ensure the electron transfer properties of complex **3**.

In order to evaluate the effect of antimicrobial activity of metal ions upon chelation, both the ligand **14** and its metal complexes **15-20** were screened for their antibacterial activity by disc diffusion method. The results revealed that neither ligand **14** nor any complexes **15-20** were found any activity against the organisms tested.

The work plane of the thesis is represented by the following flow sheet diagram:

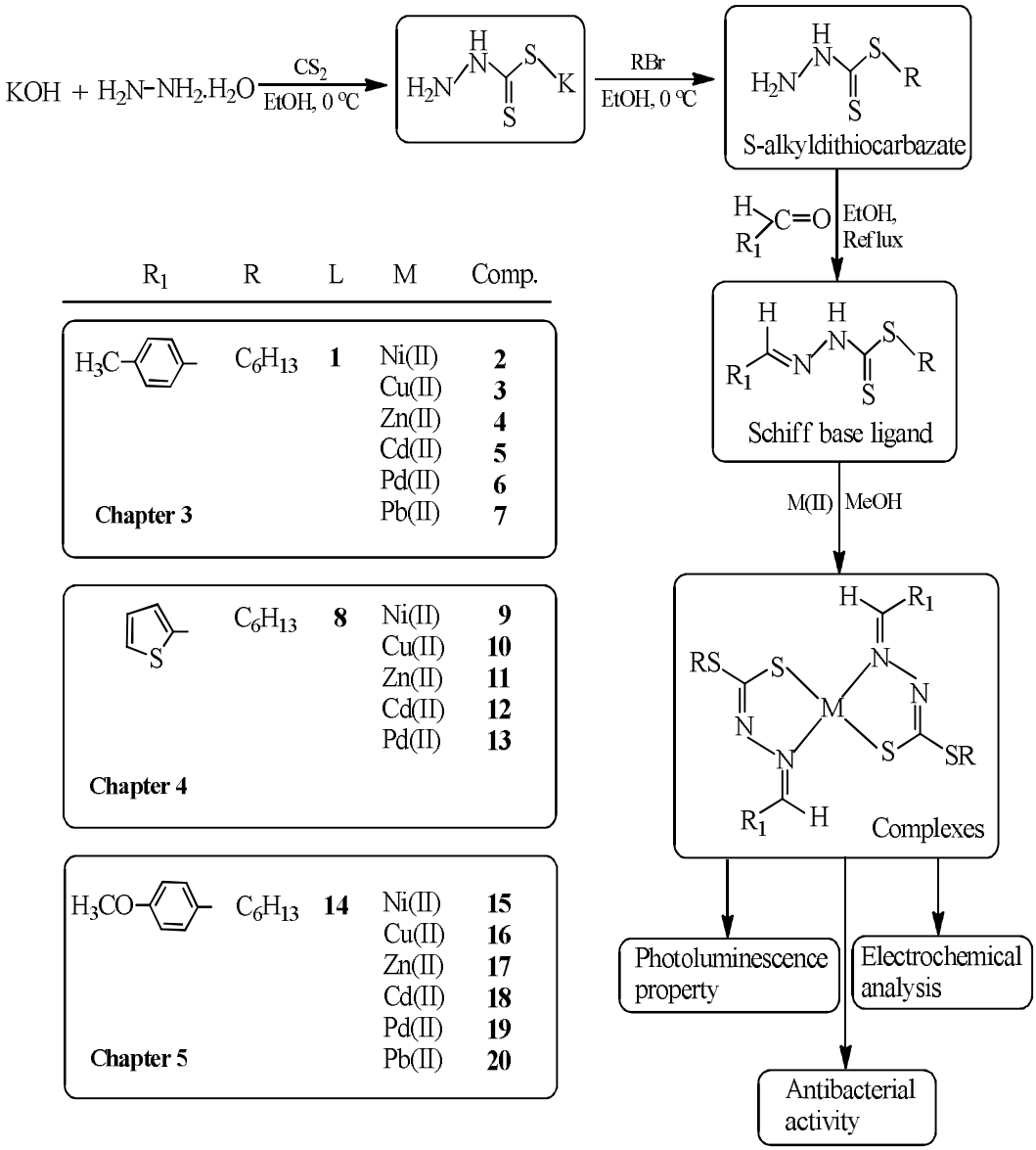

TABLE OF CONTENTS

LIST OF TABLES

LIST OF FIGURES

LIST OF SCHEMES

LIST OF SYMBOLS AND ABBREVIATIONS

Symbols

^{o}C	Degree Celcius
g	Gram
Å	Angstrom
%	Percentage
μ	Magnetic moment
λ	Wave length
χ_M	Molar Susceptibility
ν	Wave number
δ	Chemical shift
Λ_m	Molar conductance
ε	Molar extinction coefficient
χ_g	Gram Susceptibility
A	Absorbance
M	Molar ($molL^{-1}$)
μ_{eff}	Effective magnetic moment

Abbreviation

ml	milliliter
m.p.	Melting point
Hz	Hertz
MHz	Mega Hertz
cm^{-1}	Per centimeter
nm	nanometer
ppm	Pars per million
mmol	millimol
IR	Infra Red
UV	Ultra Violet
Vis	Visible
^{1}H NMR	Proton Nuclear Magnetic Resonance
^{13}C NMR	Carbon-13 Nuclear Magnetic Resonance
THF	Tetrahydrofurane
DMF	Dimethylformamide
DMSO	Dimethyl sulfoxide
$CDCl_3$	Deuterated chloroform
KDTC	Potassium dithiocarbazate
SBDTC	S-benzyldithiocarbazate
SMDTC	S-methyldithiocarbazate
SHDTC	S-hexyldithiocarbazate
MFC-7	Human breast carcinoma with positive estrogen receptor
MDA-MB-231	Human breast carcinoma with negative estrogen receptor

General Introduction

1.1 Historical background on the discovery of dithiocarbazic acid esters

Selection method is an important factor for the preparation of drugs because it is related to the production cost, compound purity and stability in air. Methods have been described for the preparation of 5-pyrazolemercaptan derivatives useful for the synthesis of sulfonylurea base herbicides represented by the following general formula (**1a**):

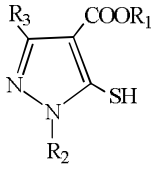

(**1a**)

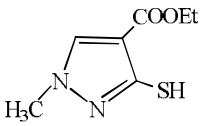

(**1b**)

Wherein, R_1 represents hydrogen, C_1-C_4 alkyl, aryl or propargyl, R_2 represents hydrogen, C_1-C_4 alkyl, or a phenyl group which contain one or more substituent selected from the group consisting of halogen, nitro or methyl at an optional position, and R_3 represents hydrogen, methyl, ethyl or phenyl. As for example a method was developed for the preparation of compound (**1a**) as a three step process starting from dimethoxymethylene malonate represented by the following reaction **Scheme 1.1**:

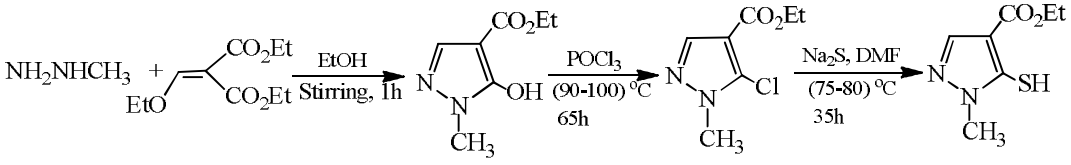

(**1d**) (**1c**) (**1b**)

Scheme 1.1

The method depicted in **Scheme 1.1**, has several disadvantages, namely, the desired compound is prepared through a complex reaction procedure comprising three reaction steps, the product from the first cyclization step may contain ragioisomeric compound (**1b**) as a by-product that reduces the purity of the product (**1a**) and needs for further purification and the whole reaction procedure requires a high reaction temperature, a long reaction time and provides low yield. Thus study was continued to develop a novel method which can be used more efficiently and economically to prepare the compound (**1a**). As a consequence, an alternative method was developed starting from a certain ethylene dithiocarbazic acid derivative which is sufficiently one step procedure as represented by the reaction **Scheme 1.2**.

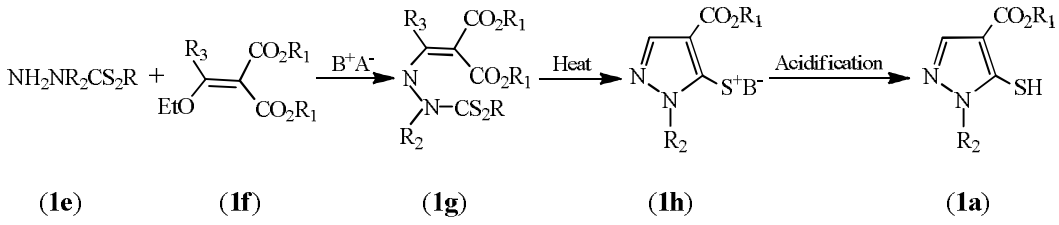

(**1e**) (**1f**) (**1g**) (**1h**) (**1a**)

Scheme 1.2

The advantages of scheme 1.2 over scheme 1.1 are

(i) The reaction can be carried out in the absence of solvent; however it is carried out in the presence of solvent and is completed within 8 to 20 hours. For this purpose, any solvent which has no adverse effect on the reaction, e.g. alcohols such as methanol, ethanol, t-butanol etc. Alkyl halides such as ethylene dichloride, methylene dichloride etc. or benzene, n-hexane, toluene and the like can be used with alcohols particularly ethanol being preferable. Although the reaction temperature can be in the range of 0 ^{o}C to 150 ^{o}C, it is preferably carried out at the refluxing temperature of the solvent.

(ii) The base which can be preferably used includes alkoxides (C_1-C_5), hydroxides and carbonates of alkali metals (sodium, potassium or lithium) or tertiary amine bases such as pyridine, triethylamine etc. with alkali metal alkoxide or hydroxide particularly sodium ethoxide or hydroxide being most preferable.

(iii) According to the reaction **Scheme 1.2** the desired compound can be obtained simply and efficiently in one step procedure in any case without any bi-product and can be obtained in high purity and high yield.

However when the compound of formula (**1e**) is prepared according to the known method, there is a problem related to the reaction selectivity in many cases. For example the compound (**1e**) can be prepared by reacting a monoalkyl hydrazine with potassium hydroxide and carbon disulfide in a polar solvent such as alcohols and then subjecting to esterification with methyl iodide (**Scheme 1.3**) [1]. According to such known methods, since the reaction selectivity in the esterification step is low, there is a problem is that the byproduct of formula (**1h**) may be produced and the yield of the desired compound (**1a**) is lowered to (60-80%). However, the reaction selectivity in the esterification step can be significantly improved by using a two-phase reaction comprising a non-polar solvent and a phase transfer catalyst (as shown in **Scheme 1.3**) and the desired compound can be obtained in high yield.

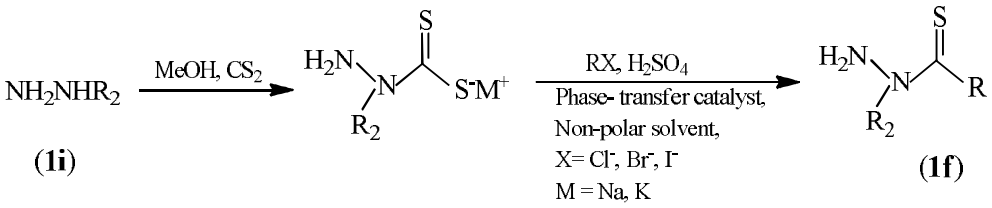

Scheme 1.3

The above scheme is significantly explained herein after. First, the base is completely dissolved in solvent and then carbon disulfide is added there in one portion and the alkyl hydrazine (**1i**) is slowly added drop wise and the mixture is thoroughly stirred until the reaction is no longer progressed. As a base for this procedure, a metal hydroxide is used and particularly sodium hydroxide or potassium hydroxide is preferable. Each of carbon disulfide and a base is used in an amount of 1.0 to 1.5 equivalent weight and the preferable 1.0 to 1.5 equivalent weight with respect to the compound (**1i**). Although the base which can be used in the reaction includes water or alcohols, it is advantageous that the use of water in an amount of four equivalent

weights or more can generally induce a uniform reaction. The reaction temperature is maintained conventionally in the range of 0 ^{o}C to 40 ^{o}C and preferably in the range of 0 ^{o}C to 15 ^{o}C to prevent the loss of reactants. Particularly, it is preferable to reduce the internal temperature of the reaction vessel to 0 ^{o}C to 5 ^{o}C prior to addition of carbon disulfide. The alkyl compound is slowly added in a manner that the internal temperature of the reaction vessel does not exceed to 15 ^{o}C. Subsequently, to the reaction mixture containing a carbazic acid derivatives thus produced are added to a non-polar organic solvent and a phase-transfer catalyst and then an electrophilic substance suitable for the desired compound is added thereto to practice the esterification reaction.

1.2 Introduction

The chemistry of carbon-nitrogen double bonds has played a vital role in the progress of chemical sciences. Schiff bases are very important class of ligands in coordination chemistry due to their wide applications in synthesis of a large variety of transition metal complexes with various structural architectures [2]. Transition metal complexes with oxygen, nitrogen and sulfur donor Schiff bases are of particular interest because of their ability to possess unusual configurations, be structural labile and their sensitivity to molecular environment [3]. The azomethine group >C=N of the Schiff base forming a stable metal complexes by coordinating through nitrogen atom. Schiff base ligands are able to coordinate many different metals, and to stabilize them in various oxidation states, enabling the use of the Schiff base metal complexes for a large variety of useful catalytic transformations [4]. The efficiency of the Schiff bases as therapeutic agents has often been enhanced upon coordination with a metal [5]. In many cases, the pharmacological activity has been found to be highly dependent on the identity of the metal with different ligands showing widely different biological activities although they may vary only slightly in their molecular structure [6,7,8]. Nitrogen and sulfur containing Schiff bases derived from S- alkyl dithoicarbazate and complexes have NNCSS backbone and can act multidentate ligand. The presence of hard nitrogen- and soft sulfur- donor atoms in the backbones of these ligands enable them to react readily with both transition and the main group metal ions yielding stable metal complexes some of which have been shown to exhibit interesting physico-chemical properties and significant biological properties [9].

During the past years, the synthesis of new coordination compounds containing nitrogen and sulfur donor atoms have been significantly developed. Among these materials, dithiocarbazates have been significantly considered by researchers mainly due to their potential anticancer [5,10,11], antibacterial [12-14], antifungal [13,15-17], antitumor [18,19] and insecticidal properties [20]. In the recent years there has also been interest in the non-linear optical properties of complexes having deprotonated Schiff bases of dithiocarbazates as ligands [21,22]. The interest in this field has been stimulated because the ligand incorporating donor atoms at both medium crystal field strength (nitrogen donor) and low crystal field strength (sulfur donor) might lead to

complexes of unusual stereochemistry, anomalous magnetic and spectroscopic as well as biological properties. In fact, nitrogen-sulfur ligands and their metal complexes have been reported to possess bio and cancerostatic activities. Actually, dithiocarbazates constitute one of the most important classes of mixed hard-soft nitrogen- sulfur donor ligands [23]. Although the synthesis and complexation of S-benzyldithiocarbazate and its derivatives have been under study for many years, considerable attention continues to be given to these and related ligands and their metal complexes, since their properties can be greatly modified by introducing different substituents. A change in the substitution pattern if these compounds can create new ligands with different properties. In dithiocarbazate compounds, owing to the thione-thiol tautomer, N and S donor atoms are connected to the metal atom with the formation of five- or six-membered rings. The presence of additional donor atoms in suitable position in the compounds can increase the coordination ability of the ligand giving rise to different coordination geometries [24].

Moreover, S-alkyldithiocarbazate complex can provide thiol during thermolysis that can act as internal stabilizing agent and also the presence of excess thiol in the reaction medium may prevent unwanted oxidation of nanoparticles. The transition metal complexes of dithiocarbazates have different geometric, electronic, optical [25], magnetic [26] and radiopharmaceuticals properties as well [24].

1.3 Chemistry of nitrogen- sulfur donor ligands containing dithiocarbazate

It is more than hundred years from the first synthesis of dithiocarbazic acid by Curtius [27]. Since then the study of nitrogen- sulfur donor ligands continues to be of great interest to the researchers. Dithiocarbazate ($NH_2NHCS_2^-$) and its substituted derivatives have been synthesized and investigated over the past few decades [13].

Dithiocarbazic acid and its S-alkyl and S-aryl esters form an interesting series of Schiff base ligands and metal chelates. Researchers in this area have been continuing the synthesis of new nitrogen-sulfur donor ligands through Schiff base condensation with aldehydes and ketones. The chemistry of such ligands warrants further studies owing to the following various reasons:

Firstly, Schiff bases containing S-alkyl/S-aryl derivatives of dithiocarbazate form an interesting series of compounds, whose properties can be greatly modified by introducing organic substituents in to the ligand molecule thereby causing variation in the ultimate donor properties and inducing different stereochemistry in the resultant metal complexes.

Secondly, most of the ligands and their metal complexes are potentially biologically active. S-alkyl/S-aryl dithiocarbazates undergo facile reactions with most of the aldehydes and ketones even at room temperature and produce air stable Schiff bases and their metal complexes. The number of ligands synthesized continues to increase because of the intriguing observation that different ligands show different biological properties, although they may differ slightly in their molecular structure [13,28]. Complexes of dithiocarbazic acid, its S-alkyl/ S-aryl esters and their Schiff bases have been studied, mainly due to their potential antibacterial [12-14], antifungal [13,15,29], anticancer [5,10,11], antiviral [16,17], antitumor [18,19] and inhibitory cell migration activities [12,16,20,30].

In the recent years, there has also been interest in the non-linear optical properties of complexes having deprotonated Schiff bases of dithoicarbazates as ligands, high second order hyperpolarizability are found for these complexes due to the extended π-conjugaton of the deprotonated ligands [20,31,32]. Recently, the synthetic chemistry of MS semiconductor nanocrystals have been highlighted by using metal complexes as single source of molecular precursors [33]. The Schiff bases of S-alkyl/ S-aryl dithiocarbazate are all important class of nitrogen-sulfur chelating agents with nitrogen-sulfur donor atoms in their structural backbones and are also capable of reacting with transition metal and some main group metal ions forming air stable complexes [34,35]. Although vast investigation have been carried out on the biomedical activities of the S-alkyl/aryl dithiocarbazate Schiff bases and their metal chelates, very little attraction have been paid on the antioxidant activities of such compounds.

1.4 Properties associated with nitrogen and sulfur as donor ligands

Ligands with sulfur as donor atoms have the following characteristics:

(i) Those with sulfur bind more strongly to class (b) metals than do oxygen donors. [Class (a) metals are small, not very easily polarized and have greater affinity for F^- than I^-. Class (b) metals are essentially opposite in character].

(ii) The polarizabilities of sulfur donors and the number of lone pair decreases in the order S^{2-}> RS^-> R_2S. Consequently, thiolo ligands are more polarizable but not as effective d_π - electron acceptors as thioethers which implies that the thiolo ligands can coordinates to the metal ions in a uninegatively charged manner.

(iii) Normally, the permanent dipole moment and the coordinating ability decrease in the order: H_2O> ROH> R_2O. However, the reverse order holds for sulfur, H_2S> RSH> R_2S.

(iii) The strength of bonding to a metal (considering both electrostatic models and covalent models) is in the following order: RO> RS and R_2O> R_2S. However sulfur has vacant *d*-orbitals that can be used for d_π - d_π bonding with later transition metals and with early transition metals in unusually low oxidation states.

(iii) Ligands containing nitrogen and sulfur donors are more soluble in low boiling non-polar solvents such as dichloromethane, chloroform etc. than ligand containing nitrogen and oxygen donors that enhances the possibility to grow single crystals.

The properties of complexes of sulfur donor ligands apply also to the complexes of nitrogen-sulfur chelating agents. However, there are additional characteristics in the case of the latter due to the presence of nitrogen in the complexes. In general the presence of nitrogen tends to lower the solubility of complexes in the non-polar solvents. This causes the complexes of nitrogen-sulfur donor ligands to be either sparingly soluble or completely insoluble in non-polar solvents. Nitrogen- sulfur donor ligands seem to cause a small reduction in the inter-electronic repulsion energy than do sulfur-sulfur ligands. It is assumed that this is due to the lower position of nitrogen in the nephelauxetic series compared to sulfur [36].

1.5 Literature Review

1.5.1 Dithiocarbazate anion as chelating agent

Potassium dithiocarbazate (KDTC), the starting material of dithiocarbazate Schiff base, itself a coordinating ligand [37]. Literature study suggests that the dithiocarbazate anion ($DTCA^-$) coordinates with various transition and non-transition metal ions by its imine nitrogen and thiolate sulfur atom in mono or bischelated fashion (**Fig. 1.2** and **Fig. 1.3**). Their study also revealed that the complexes of non-transition metal ions are more effective antibacterial agents than the transition metal complexes against *P. aeruginosa* and *B. cereus.* Their study suggests that Sb(II) and Al(III) complexes showed stronger activity than the standard drug Kanamycin against *P. aeruginosa*. They also concluded that neither KDTC nor its complexes showed cytotoxic activity against human T-lymphoblastic cell line (CEM-SS).

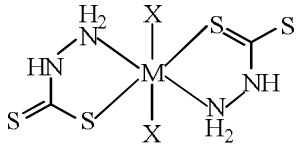

M = Ni(II), X = 0
M = Zn(II), X = 0
M = Th(IV), $X = NO_3^-$

Fig. 1.2

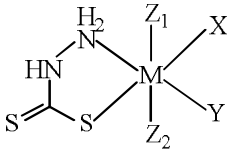

M = Cu(II), $X = NO_3^-$, $Y = H_2O$, $Z_1 = Z_2 = 0$
M = Al(III), $X = Y = Cl^-$, $Z = H_2O$
M = Sn(II), $X = Cl^-$, $Y = H_2O$, $Z = 0$
M = Sn(IV), $X = Cl^-$, $Y = H_2O$, $Z_1 = Z_2 = Cl^-$
M = Bi(III), $X = Y = NO_3^-$, $Z_1 = Z_2 = H_2O$
M = Sb(III), $X = Y = Cl^-$, H_2O, $Z_1 = Z_2 = H_2O$
M = U(IV), $X = Cl^-$, $Y = H_2O$, $Z_1 = Z_2 = 0$
M = Zr(IV), $X = NO_3^-$, $Y = H_2O$, $Z_1 = Z_2 = 0$

Fig. 1.3

1.5.2 S-alkyl or S-aryldithiocarbazates as chelating agent

S-benzyldithiocarbazate has four potential donor atoms of which two are sterically available, at a time, for coordination with a metal ion. Thus in principle both NS (**Fig. 1.4**) and SS (**Fig. 1.5**) chelated structure are possible [38]:

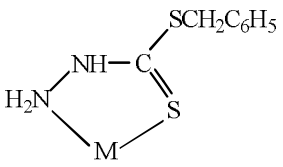

Fig. 1.4

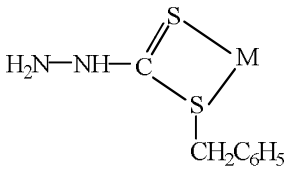

Fig. 1.5

For instance, both S-benzyldithiocarbazate and S-methyldithiocarbazate behave as potentially bidentate chelating agent with NS donor site for both transition and non-transition metal ions [14,20,38-40] and generates complexes of variable coordination geometry. However, the geometry of the coordinated metal complexes depends on the metal ions, metal to ligand ratio and in some cases the nature of the ions associated with the metal salts. As for example, the interaction of SBDTC [38] with ethanolic solutions of Ni(II) salts in an 1:3 metal-ligand molar ratio yields tris chelated complexes (**Fig. 1.6**). However, reaction of excess nickel(II) salts with the ligand produced bis-chelated complexes (**Fig. 1.7)** [20,38]; whereas the reaction of SBDTC with Ni(II) and Zn(II) salts under alkaline conditions yields neutral complexes of the deprotonated ligand.

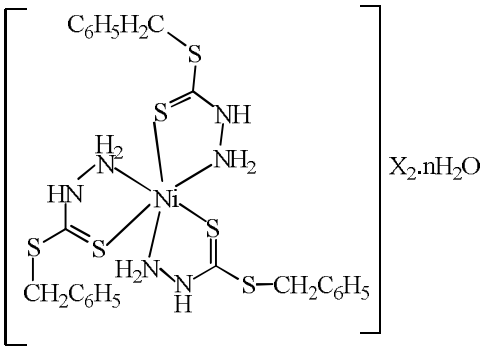

X = NO_3^-, Cl^-, Br^-, CNS^-

Fig. 1.6

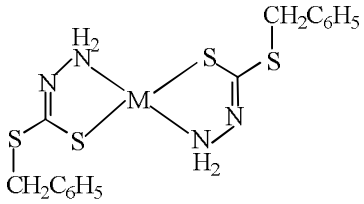

M = Ni(II), Zn(II)

Fig. 1.7

SBDTC was also reported to yield penta coordinated chlorobridged dimeric Cd(II) complex in the presence of chloride ion (**Fig. 1.8**) forming five membered chelate rings [39,40] with each SBDTC ligands, coordinated by thione sulfur and β-nitrogen atoms of each SBDTC unit and another four membered ring between two cadmium atoms bridged by two chlorine atoms, while both SBDTC and SMDTC was described to produce hexa coordinated [39] complexes (**Fig. 1.9**) with Cd(II) in the presence of nitrate as counter ion, also coordinated in their thioketo form.

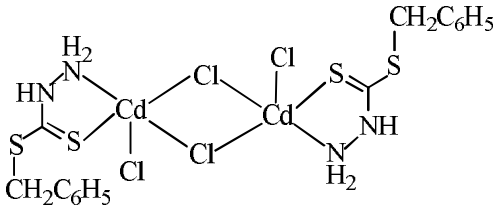

Fig. 1.8

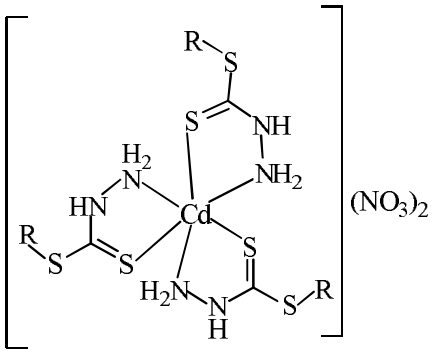

R = -CH_3, -$CH_2C_6H_5$

Fig. 1.9

In contrast, SBDTC was reported to afford tris-chelated complexes (**Fig. 1.10**) with Cr(III) and Sb(III) and bis-chelated complexes (**Fig. 1.11**) with Fe(II), Sb(III), Zr(VI) and U(VI) ions where SBDTC coordinated with the metal ions in thiolate form [14].

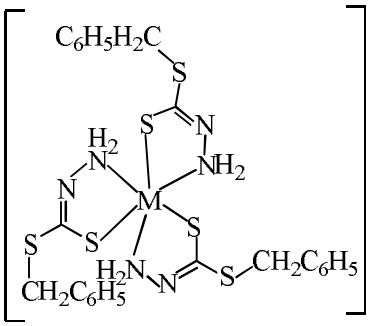

M = Cr(III), Sb(III)

Fig. 1.10

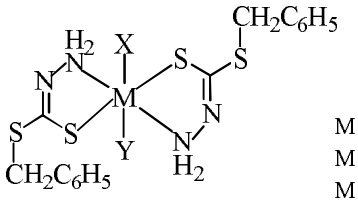

M = Fe(II), X = 0, Y = 0
M = Sb(III), X = Cl^-, Y = H_2O
M = Zr(IV), X = O^{2-}, Y = H_2O
M = U(IV), X = Y = O^{2-}

Fig. 1.11

1.5.3 Coordination behaviors of Schiff bases of SBDTC, SMDTC and SADTC with metal ions

As reported earlier [41] SBDTC reacts with acetaldehyde and benzaldehyde to form two bidentate NS Schiff bases which upon reaction with M(II) ions generated bis-chelated octahedral complexes (M=Ni) with thiocyanate and chloride ions as co-ligand (**Fig. 1.12**), but they formed bis-chelated four coordinated complexes with Cu(II) ion (**Fig. 1.13**). In all the complexes, they behave as neutral bidentate ligand in neutral or

slightly acidic medium. However, they coordinated as uninegative bidentate ligand with Ni(II) ion in alkaline medium to give bis-chelated complex (**Fig. 1.14**).

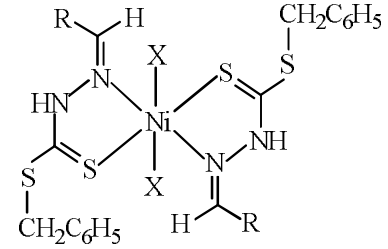

X = Cl^-, CNS^- ; R = -CH_3, -C_6H_5

Fig. 1.12

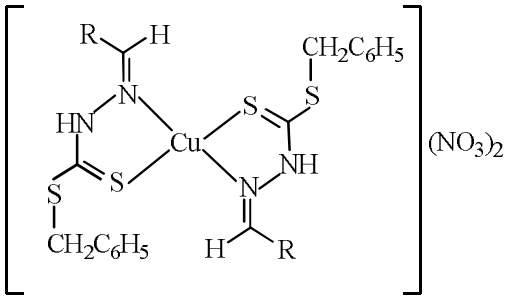

R = -CH_3, -C_6H_5

Fig. 1.13

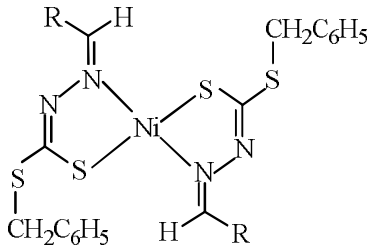

Fig. 1.14

Bidentate NS Schiff bases of SBDTC and SMDTC derived from acetone was shown to exhibit variable coordination behavior with different metal ions [9,18]. The Schiff bases of SBDTC was suggested to coordinate with Ni(II), Cu(II) and Co(II) ions as neutral bidentate chelating agent in slightly acidic or neutral medium to yield trischelated octahedral complexes (**Fig. 1.15**) in presence of chloride, bromide and nitrate ions, however a bischelated octahedral complexes (**Fig. 1.16**) were suggested for Ni(II) with thiocyanate ion [41].

Although bischelated and trischelated complexes of Ni, Cu and Co was obtained by the reaction of SBDTC Schiff base of acetone with the metal ions in 1:2 and 1:3 molar ratio, the bischelated neutral complexes were prepared by the reaction of the S-benzyldithiocar bazate and S-methyldithiocarbazate derivatives from acetone and the

bivalent metal ions (M = Pd or Pt) (**Fig. 1.17**) in 1:1 molar ratio. Both the complexes showed a quite similar planar fourfold environment [18] with the ligands coordinated to the M(II) ions as uninegatively charged bidentate NS chelating agents via azomethine nitrogen and the mercaptide sulfur atoms.

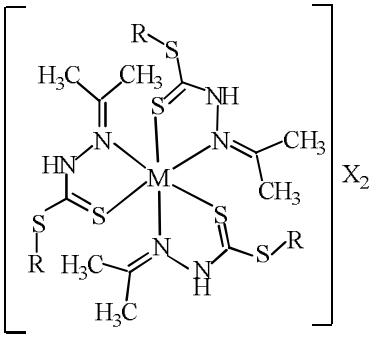

M	R	X
Ni	$-CH_2C_6H_5$	Cl^-, Br^-, NO_3^-
Cu	$-CH_2C_6H_5$	Cl^-, Br^-, NO_3^-
Co	$-CH_2C_6H_5$	Cl^-, Br^-, NO_3^-

Fig. 1.15

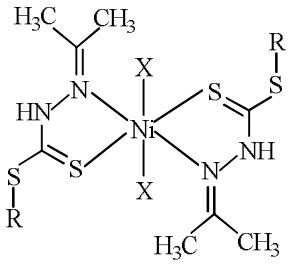

$R = -CH_2C_6H_5$; $X = CNS^-$

Fig. 1.16

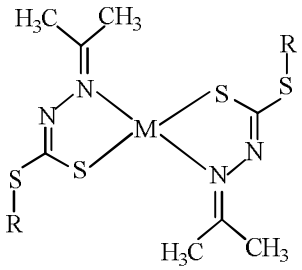

R	M
$-CH_3$	Pd(II), Pt(II)
$-CH_2C_6H_5$	Pd(II), Pt(II)

Fig. 1.17

Antimicrobial tests indicated that the Schiff bases exhibited strong activities against the pathogenic bacteria [*Bacillus subtilis* (mutant defective DNA repair), *methicillin-resistant staphylococcus aureus, B. subtilis* (wild type), and *Pseudomonas aeruginosa*] and the fungi [*Candida albicans* (CA), *Candida lipotica* (2075), *Sacaromyces cerevisiea* (20341) and *Aspergillus ochraceous* (398)]. The activities exhibited by these compounds being greater than that of the standard antibacterial and antifungal drugs, streptomycin and nystatin, respectively. The Pd(II) and Pt(II) complexes are inactive against most of these organisms but the microbe, *Pseudomonas aeruginosa* showed strong sensitivity to the Pt(II) complexes. Screening of the compounds for their cytotoxicities against T- lymphoblastic leukemia cancer cells has shown that the

acetone Schiff base of S-methyldithiocarbazate (Hasme) exhibits a weak activity, whereas the S-benzyl derivative (Hasbz) is inactive. However, the palladium(II) complexes exhibit strong cytotoxicities against this cancer cells; their activities being more than the standard anticancer drug, tamoxifen [18]. The $[Pt(asme)_2]$ exhibits a very weak cytotoxicity, whereas the $[Pt(asbz)_2]$ is inactive against the leukemic cells.

Heterocyclic ketones such as 2-acetylthiophene and 3-acetylthiophene on the other hand reacts with SBDTC to give bidentate Schiff bases that were reported to form bis-chelated neutral complexes (**Scheme 1.4**) with divalent metal ions (M = Ni, Cu, Co, Zn and Cd). In all the complexes, the ligand were suggested to act as uninegatively charged bidentate NS chelating agents [5].

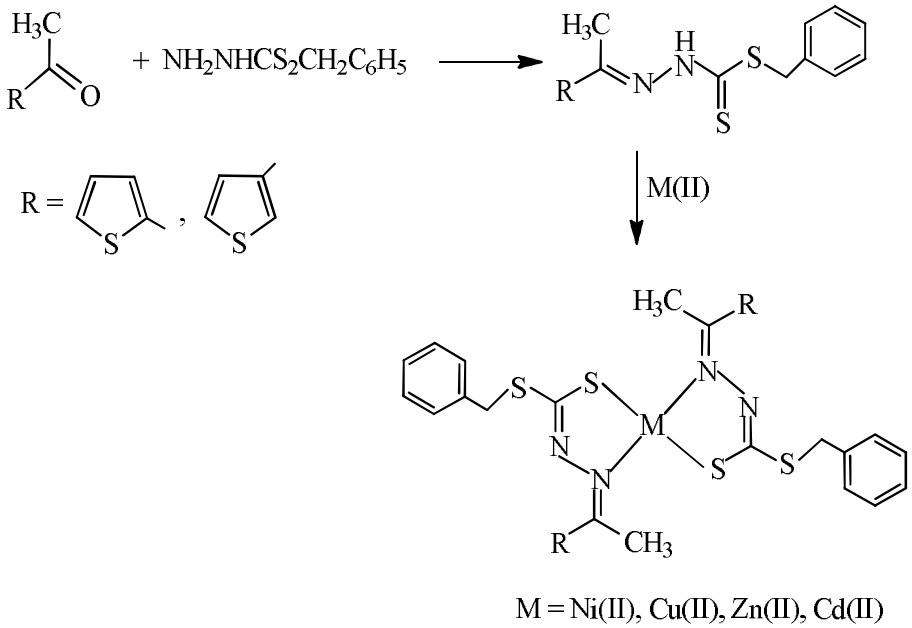

Scheme 1.4

From the biological study it was revealed that only Cu(II) complex of 2-acetyl thiophene derivative showed strong activity towards *C. lypolitica*. Both the Schiff bases, the Co(II), Cd(II) complexes of 2-acetylthiophene and Cu(II) complex of 3-acetylthiophene derivative showed weak activity against *methicillin-resistant staphylococcus aureus* (MRSA), *B. subtilis* (wild type), *Bacillus subtilis* (mutant

defective DNA repair, B28), *Pseudomonas aeruginosa* (60690), *Candida albicans* (CA), *Candida lipotica* (2075), *Sacaromyces cerevisiea* (20341) and *Aspergillus ochraceous* (398), while the others showed no activity towards the above microbes and fungi.

It was also reported that the Schiff base of 2-acetylthiophene and the Cd(II) complex of 3-acetylthiophene derivative showed significant cytotoxicity towards human mycloid leukemia (HL-60) but significantly lower than the standard drug Etoposida. The Schiff base of 2-acetylthiophene, its Cu(II), Co(II), Zn(II) and Cd(II) complexes as well as the Schiff bases of 3-acetylthiophene and its Cu(II) complex showed significant chemotherapeutic activity against human breast carcinoma with positive estrogen receptor (MFC-7) while the other compounds showed significant bioactivity towards this cell line as compared to Tamoxifen. It also revealed that the Schiff base showed higher cytotoxic activity compared to their metal complexes except for Cu(II) complex of 3-acetylthiophene. It was also deduced that the metal chelation slightly inhibit cytotoxic activity. However, neither the ligands nor the complexes exhibited cytotoxic activity against human ovarian cancer (Cavo-30), human cervical cancer (Hela) and human breast carcinoma with negative estrogen receptor (MDA-MB-231) cell lines [5].

Bidentate nitrogen-sulfur Schiff bases of SBDTC derived from 4-methoxybenzal-dehyde, 4-dimethylaminobenzaldehyde [32] and 4-nitrobenzaldehyde [42] were suggested to generate four coordinate bischelated neutral complexes with Cu(II) and Ni(II) ions (**Fig. 1.18**). The author investigated into the third order optical non- linearity of the ligands and their complexes and found that only complexes exhibited higher second order molecular hyperpolarizability. It was suggested that the presence of metal center has extended the π- electron delocalization in the complexes than the free ligands.

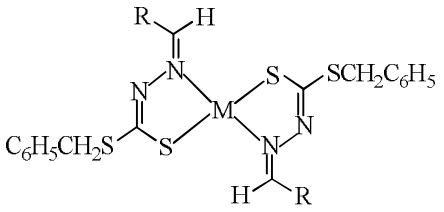

M = Cu(II); R = 4-methoxybenzyl, 4-dimethylaminobenzyl
M = Ni(II), Cu(II); R = 4-nitrobenzyl

Fig. 1.18

As shown in **Scheme 1.5** two isomeric bidentate ligands NS and NS', having nitrogen-sulfur donor atoms have been prepared by the condensation of S-benzyldithiocarbazate with 5-methyl-2-furyl-aldehyde and 2-furylmethyl ketone respectively. Reaction of these bidentate ligands with Pb(II) and Cd(II) gave complexes [43] of ML_2 and but with Co(II) gave complexes having structure of $[M(L)_2]Cl$. All the bis-chelated complexes are four coordinated in which the coordination have taken place through the thioketo sulfur and the azomethine nitrogen atoms.

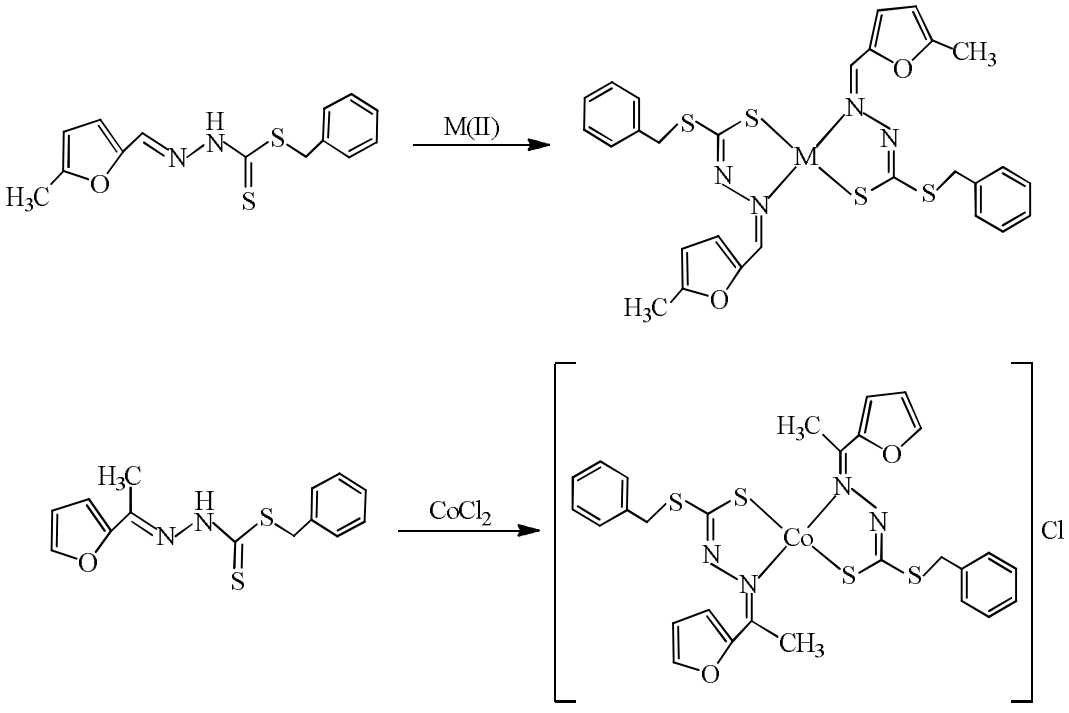

Scheme 1.5

From the study of cytotoxic activity it was revealed that the Pb(II) complex of the NS ligand was highly cytotoxic against leukemic cells (CEM-SS).

However, S-aryl/alkyldithiocarbazates with 2-acetylpyridine behaves as tridentate NNS chelating agents (**Fig. 1.19**) and forms complexes of variable coordination number with variable coordination geometry as depicted in **Scheme 1.6**, thus affecting the biological activity of the Schiff bases [16]. As shown in the **Scheme 1.6**, $CuCl_2$ gives chlorobridged dimeric complexes of 5-coordinated square pyramidal geometry (**Fig. 1.20**) with S-benzyl, S-naphthalen-2-ylmehthyl, S-4-methoxybenzyl and S-4-fluorobenzyldithiocarbazates, while it gives tetrahedral complex with S-methyldithio carbazate (**Fig. 1.21**).

In contrast, bischelated octahedral geometry (**Fig. 1.22**) was suggested for Ni(II) with S-benzyl and for Zn(II) with S-benzyl and S-naphthalen-2-ylmethyldithiocarbazate Schiff bases [16].

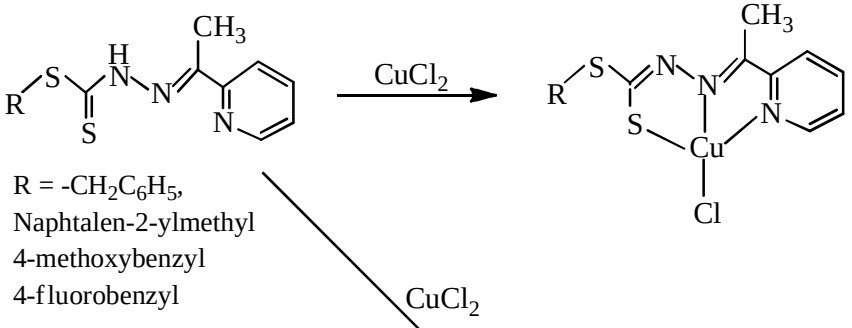

R = -$CH_2C_6H_5$,
Naphtalen-2-ylmethyl
4-methoxybenzyl
4-fluorobenzyl

Fig. 1.19

Fig. 1.21

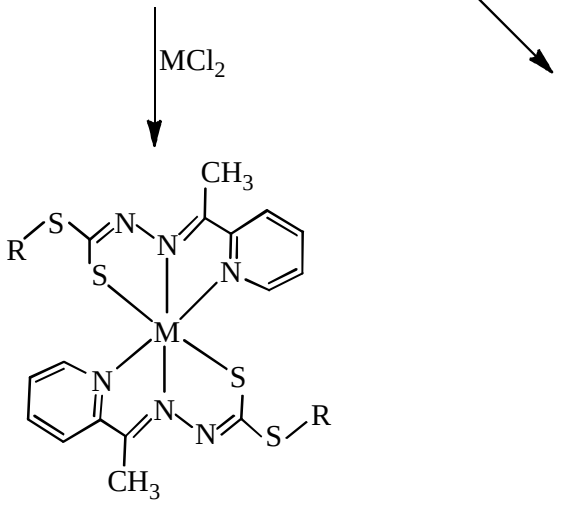

M = Zn; R = -$CH_2C_6H_5$, Naphthalen-2-ylmethyl
M = Ni; R = -$CH_2C_6H_5$

Fig. 1.22

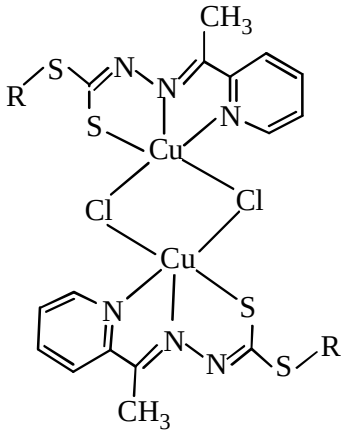

R = -$CH_2C_6H_5$, Naphtalen-2-ylmethyl,
4-methoxybenzyl, 4-fluorobenzyl

Fig. 1.20

The observation by Beshir *et al*. [16] suggested that transiod Zn(II) and dimeric Cu(II) complexes exhibited potential but similar antiinhibitory cell migraton whereas cisiod Ni(II) has no antimigratory activity at all. Their observation also suggested that the complexes with simple S-methyl, S-benzyl groups with polar substituents or carboxylated pyridine (not shown in the scheme] exhibit dramatic reduced activity. The authors also concluded that a two-ligand structure with bulky non polar S-substituents in a transiod conformation is essential for the antimigratory activity of the metal- ligand complexes.

Bidentate NS donorligands (**Fig. 1.23**), derived from 2-acetylpyridine of S-benzyldithio carbazate/S-methyldithiocarbazate [42] formed Pd(II) complexes (**Fig. 1.24**) having bonding through azomethine nitrogen and thiolate sulfur atom. The complexes were demonstrated greater antiamoebic activity against *Entamoeba histolytica* (starain HK-9) than metronidazole (Standard commercial drug).

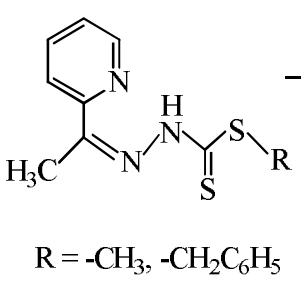

$R = -CH_3, -CH_2C_6H_5$

Fig. 1.23

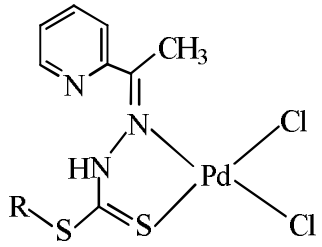

Fig. 1.24

In contrast, the Schiff base H_2SNNNS (**Fig. 1.25**), formed by condensation of 2,6-diacetyl pyridine with S-benzyldithiocarbazate (1:2), behaves as a pent dentate ligand forming a Ni(SNNNS)H_2O complex (**Fig. 1.26**) in which the ligand coordinates with the Ni(II) ions via the pyridine nitrogen atom, azomethine nitrogen atom and the thiolate sulfur atom.

The Schiff base and its Ni(II) complex were tested against four pathogenic bacteria (*Bacillus subtilis, Pseudomonas aeruginosa*, methicillin-resistant *staphylococcus aureus* and *B. subtilis* (wild type B29) and the pathogenic fungi *(Saccaharomyces ceciricae, Candida albicans, Candida lipolitica* and *Aspergillus ochraceous*). Both the compounds exhibit mild antibacterial and antifungal activities. The anticancer properties of these compounds against Human T-lymphoblastic leukemia cell line revealed that the Schiff base exhibits marked cytotoxicity against these cells, but its Ni(II) complex is inactive [44].

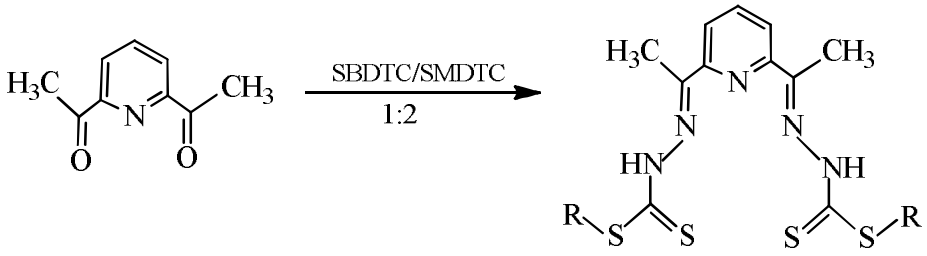

Fig. 1.25

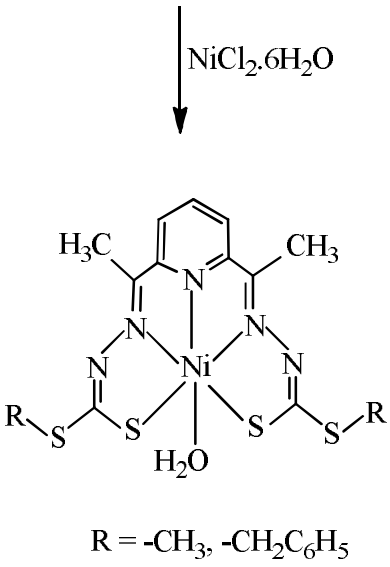

Fig. 1.26

Thahira B.S.A. Ravoof *et al.* synthesized [45] a tridentate nitrogen-sulfur Schiff base (**Fig. 1.27**), 3-methylbenzyl 2-(6-methylpyridine-2-ylmethylene) hydrazinecarbodithioate (6mpyS3M) by the condensation of 6-methylpyridine-2-aldehyde with S-3-methylbenzyl dithiocarbazate. The ligand 6mpyS3M gives octahedral complexes (**Fig. 1.28**) with Ni(ll), Cu(ll), Zn(ll) and Cd(ll).

The bioassayed of 6mpyS3M and its metal complexes against *methicillin-resistant staphylococcus aureus*(MRSA), *Pseudomonas aeruginosa* (60690), *Salmonella choleraeuis* (S.C), *Bacillus subtilis* wild type (B29) and two breast cancer cell lines MFC-7 (Human breast carcinoma with positive estrogen receptor) and MDA-MB-

231(Human breast carcinoma with negative estrogen receptor) showed that 6mpyS3M is highly active against both the cancer cell lines tested. The Cu(ll), Ni(ll) and Zn(ll) complexes were strongly active against the MFC-7 but inactive or less active against MDA-MB-231. In contrast, the Cd(II) complex was strongly active against MDA-MB-231, but inactive against the MFC-7. Only Cu(ll) and Cd(ll) complexes were active against the microbial strains tested.

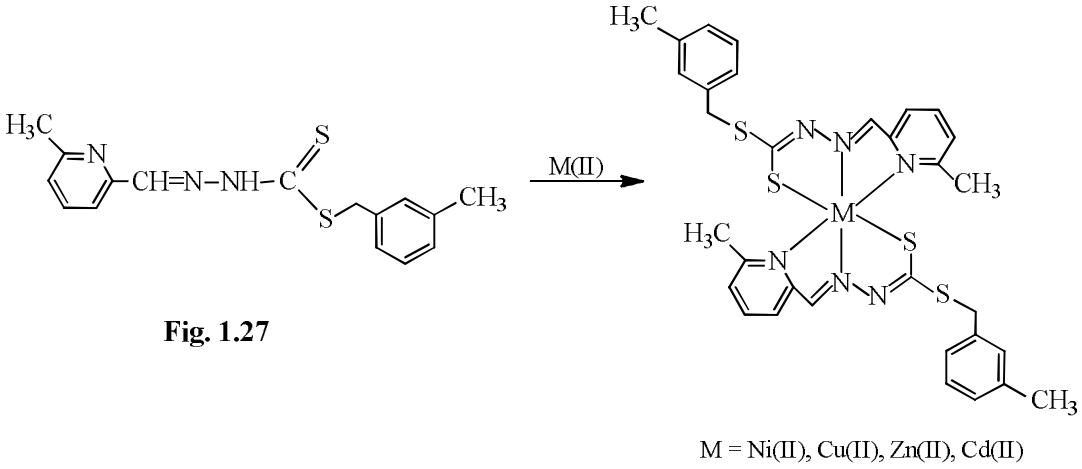

Fig. 1.27

Fig. 1.28

The Schiff base S-benzyl-β-N-(2,4-dichlorobenzylidene)dithiocarbazate, prepared by the condensation of S-benzyldithiocarbazate with 2,4-dichlorobenzaldehyde, coordinates to Zn(II) ions in an uninegatively charged manner to give the Zn(II) complex (**Fig. 1.29**) of distorted tetrahedral geometry [46].

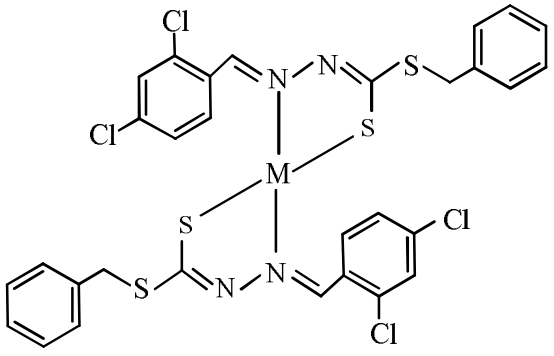

Fig. 1.29

The complex is more cytotoxic than the Schiff base ligand towards the MKN45 and HepG2 cancer cell lines. The complexation of metal ions enhances the anticancer behavior compared with the uncoordinated ligand, may be attributed to the increase conjugation R=N-N=R', in the ligand moiety on complexation. But the Schiff base and Zn(II) complex are both less effective than 5-fluorouracil, an anticancer drug.

Reaction of the S- benzyldithiocarbazate with 2-chloroacetophenone and 4-chloro acetophenone results in the formation of S-benzyl-β-N-(2-chlorophenyl)methylene dithiocarbazate (NS2) and S-benzyl-β-N-(4-chlorophenyl)methylenedithiocarbazate (NS4) isomers respectively. The ligands formed four coordinated complexes [47] with Ni(II), Cu(II), Zn(II) and Cd(II) as shown in **Fig. 1.30**.

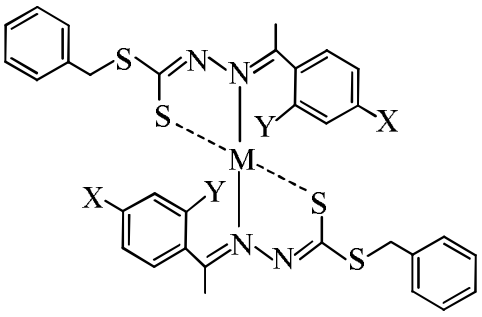

M = Ni(II), Cu(II), Zn(II), Cd(II) X = para -Cl ; Y = ortho -Cl

Fig. 1.30

A tridentate ligand was synthesized from the condensation of ferrocenoylacetone with S-benzyldithiocarbazate. Reaction of the ligand with a bivalent metal salt [$M(OAc)_2$. xH_2O, M= Mn, Ni, Cu, Zn, Hg] afforded the corresponding bischelated metal complexes [48] as shown in **Fig. 1.31** and **Fig. 1.32**, in which it acts both bidentate and tridentate behavior.

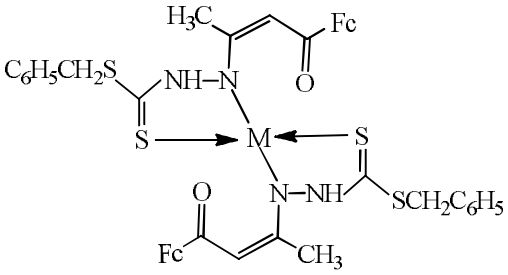

M = Ni(II), Cu(II), Zn(II), Hg(II)

Fig. 1.31

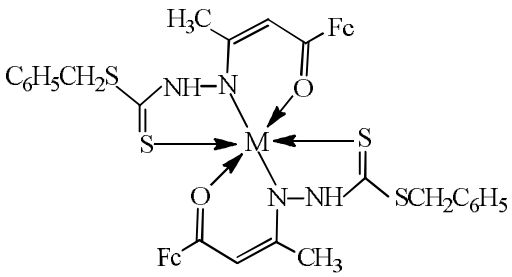

M = Mn(II), Sn(II)

Fig. 1.32

As shown in **Scheme 1.6**, unlike other dithiocarbazate compounds such as S-methyl dithiocarbazate and SBDTC, condensation of S-2picolyldithiocarbazate (S2PDTC) with pyridine-2-carboxaldehyde, 2-acetylpyrrole, 2-acetylfuran and 2-acetylthiophene also forms the expected Schiff bases NNS', NNS″, NS and NSS, which results complexes of unusual geometry [13] with Ni(II). The pyrrole derivative, a tridentate NNS″ chelating agent, giving square planar geometry (**Fig. 1.33**).

In contrast, complexes of $Ni(NNS')_2$ and $Ni(NNS)_2$ are octahedral stereochemistry (**Fig. 1.34**) in which metal coordinates to the Schiff base ligand through two azomethine nitrogen, two thiolate sulfur and two pyridyl nitrogen atom.

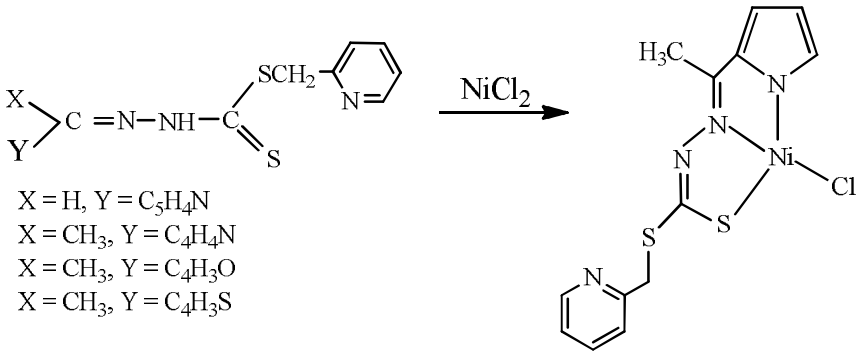

Fig. 1.33

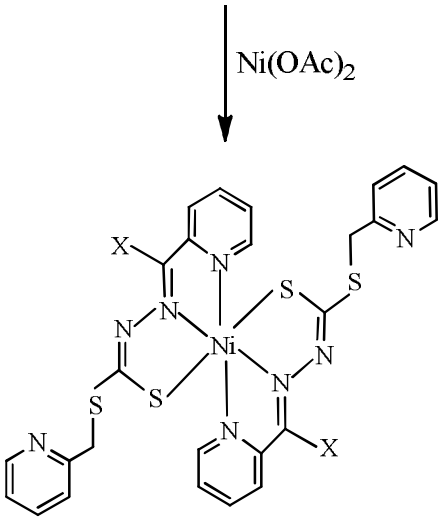

Fig. 1.34

Scheme 1.6

Course *et al.* [13] in their investigation suggested that the Schiff bases and their metal complexes showed lower antibacterial and antifungal activity than S2PDTC, SMDTC and SBDTC. However, their antibacterial activity decreases in the order: S2PDTC > SMDTC > Streptomycin > SBDTC. In contrast, the antifungal activity generally follows in the following order: SMDTC > S2PDTC > SBDTC > Nystatin. Similarly the complexes were also suggested to be inactive against CEM-SS and HT- 29 cancer cell lines, while the cytotoxic activity of Schiff base of pyridine-2-carbaldehyde was stronger against CEM-SS and HT- 29 than SBDTC but weaker than the standard Doxorubicin.

Generally the cytotoxic activity of CEM-SS cell line follows the following order: Tamoxifen < S2PDTC < SMDTC< SBDTC < Doxorubicin. Interestingly, SBDTC showed no activity against HT- 29 cell and SMDTC is stronger than S2PDCT.

As shown in **Scheme 1.7,** a tridentate Schiff base (**Fig. 1.35**) having HNNS donor sequence was prepared by the condensation of SBDTC with pyridine-2-carboxaldehyde, was shown to exhibit variable coordination behavior with Cu(II), Zn(II) and Cd(II) ions in which the Schiff base acts as uninegatively charged tridentate chelating agent [49] via the pyridine nitrogen, the azomethine nitrogen and the mercaptide sulfur atoms. The six coordinated $Zn(NNS)_2$ has a octahedral geometry (**Fig. 1.36**). The [Cu(NNS)Cl] complex was square planar (**Fig. 1.37**) while the [Cd(NNS)Br] complex is suggested to have a tetrahedral structure (**Fig. 1.38**).

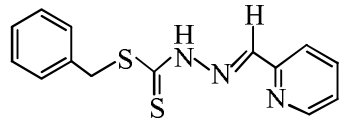

Fig. 1.35

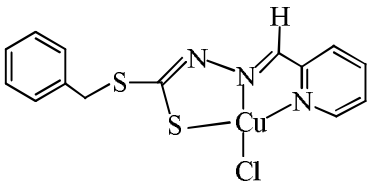

Fig. 1.37

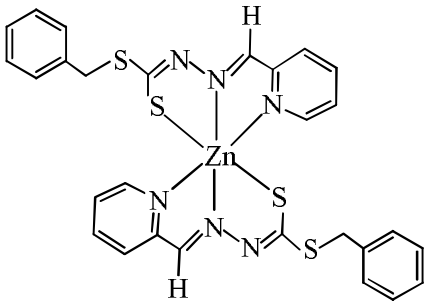

Fig. 1.36

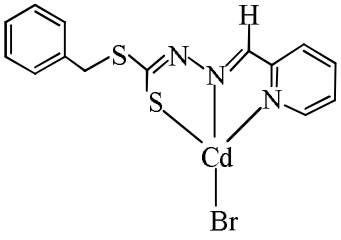

Fig. 1.38

Reaction of S-methyldithiocarbazate with 9-fluorenonane yields a bidentate Schiff base ligand. Upon coordination to the bivalent metal metal ion gives bis-chelated complexes, ML_2 [M = Ni(II), Zn(II) and Pd(II)]. Complex ZnL_2 adopts a distorted tetrahedral geometry (**Fig. 1.39**) with azomethine nitrogen atom and thiolate sulfur atom. The coordination geometry about the Pd(II) is *cis*- configuration square-planar (**Fig. 1.40**) formed by the Pd(II) atom coordinating to the NS bidentate ligand [50].

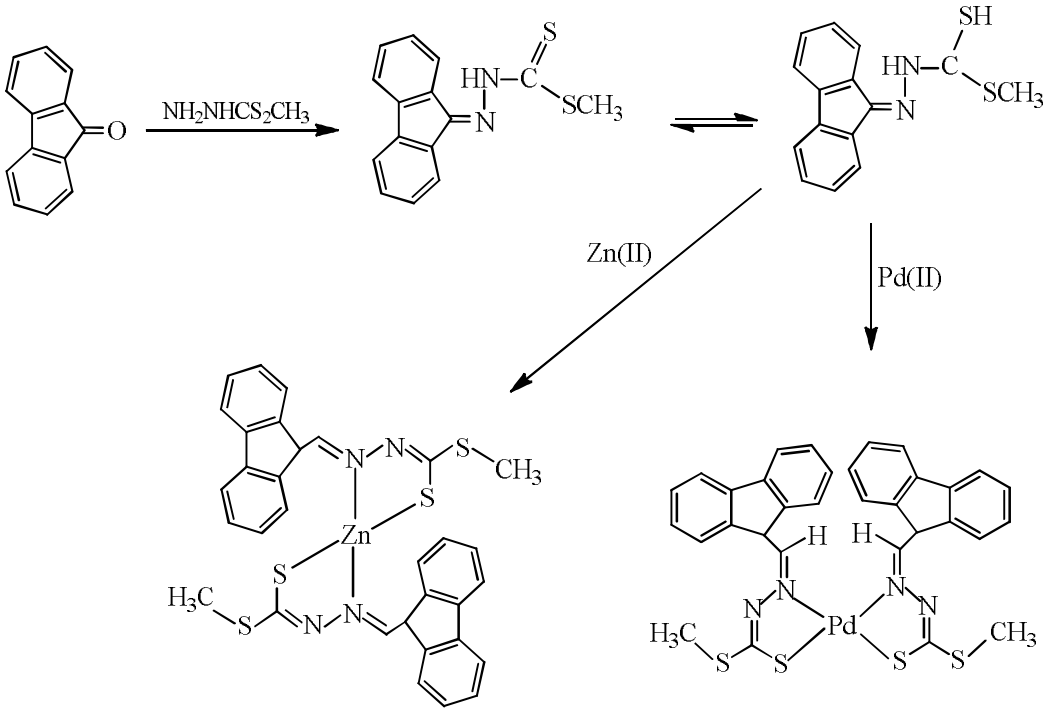

Fig. 1.39

Fig. 1.40

The reaction of S-benzyldithiocarbazate with potassiumtetrachloroplatinate (K_2PdCl_4) gives bis(S-benzyldithiocarbazato)palladium(II) complex [20] of perfectly square planar *trans*-configuration (**Fig. 1.41**) whereas, the ligand S-benzyl-N-isopropylidene-dithiocarbazate gives bis(S-benzyl-N-isopropylidenedithiocarbazato) palladium(II) complex [20] of distorted square planar *cis*-configuration (**Fig. 1.42**).

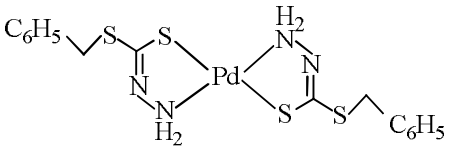

Fig. 1.41

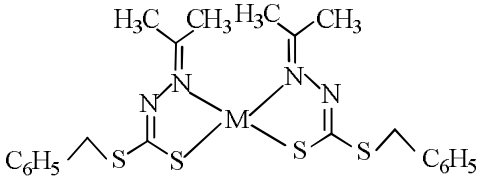

Fig. 1.42

Heterocyclic aldehydes also play an important role in the chemistry of coordination compounds. Because they undergo facile reactions with S-alkyl/aryldithiocarbazates, resulting in multidentate Schiff basees (NS, NNS, ONS, SNNS donor set). For instance, Ali *et al*. demonstrated that thiophene-2-carbaldehyde on reaction with SBDTC and SMDTC produced NS donor Schiff bases that upon coordination with bivalent metal ions [M = Ni(II), Cu(II), Pd(II) and Pt(II)] afforded bis-chelated neutral complexes (**Fig. 1.43**) in which the metal is coordinate through azomethine nitrogen and thiolate sulfur atoms [51]. They also investigated that although the Schiff bases showed strong antifungal activity against *A. alternate, C. geniculate* and *F. moliniforme* fungi, their corresponding metal chelates showed less fungitoxic effect.

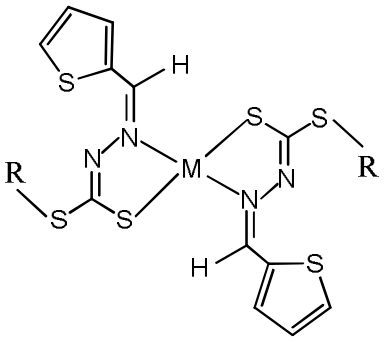

M	R
Ni	$-CH_3$, $-CH_2C_6H_5$
Cu	$-CH_3$, $-CH_2C_6H_5$
Pd	$-CH_3$, $-CH_2C_6H_5$
Pt	$-CH_3$, $-CH_2C_6H_5$

Fig. 1.43

R. Takjoo *et al.* reported a mixed ligand Palladium(II) complex [52], using bidentate NS-donor chelate and $-PPh_3$, as shown in **Fig. 1.44**.

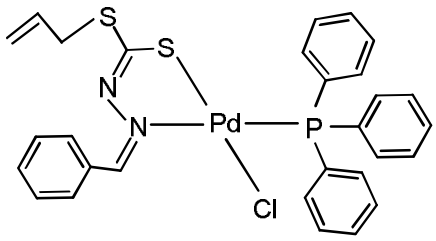

Fig. 1.44

M. Yazdanbakhsh *et al.* reported a four-coordinate distorted square planar structure of bis[S-allyl-β-N-benzylidine)dithiocarbazato]copper(II) complex [53] as shown in **Fig. 1.45**.

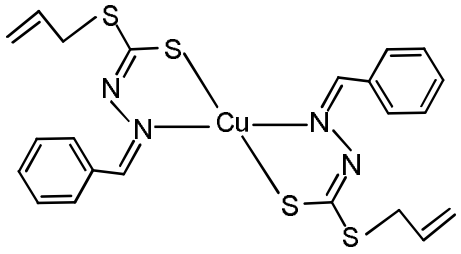

Fig. 1.45

R. Takjoo *et al.* reported four coordinated square planar bis[allyl 2-(thiophene-2-ylmethylene)hydrazinecarbodithioate]M(II) complexes [M = Ni and Cu] [54] as shown in **Fig. 1.46**.

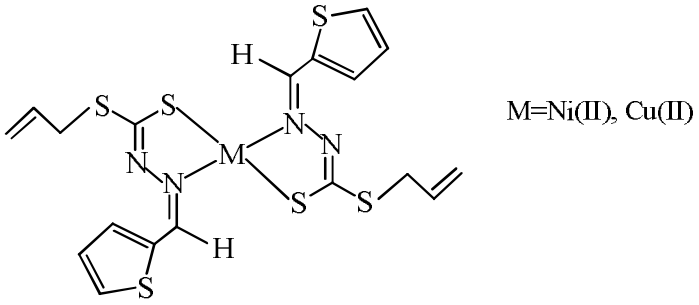

Fig. 1.46

Yazdanbakhsh *et al.* reported a square planar bis[allyl-2-(1H-pyrrol-2-ylmethylidine)-1-hydrazinecarbodithioato]Ni(II) complex [55] as shown in **Fig. 1.47**.

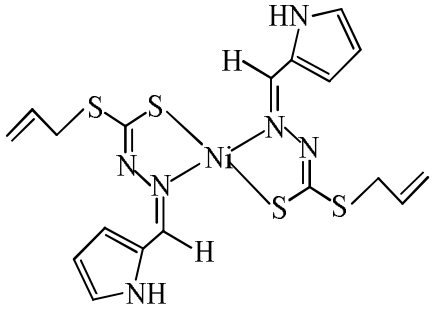

Fig. 1.47

1.6 Antibacterial activity

Antibacterial agents are categorized as narrow-, broad- or extended-spectrum agents. Narrow-spectrum agents (e.g. penicillin G) affect primarily gram-positive bacteria. Broad-spectrum antibiotics, such as tetracycline and chloramphenicol affect both gram-positive and gram-negative bacteria. An extended-spectrum antibiotic is one that, as a result of chemical modification, affects additional types of bacteria, usually gram-negative bacteria.

Whether an antimicrobial agents affects a microorganism depends on several factors. Medicinal chemists are getting better at seeking new bacterial target for attack. Rather than block the functions that bacteria perform a petri dish, chemists are learning to hit what bacteria need to do when fighting to survive and thrive in a human host. Antibacterial in use today to attack microorganisms by interfering of biosynthesis of proteins, DNA or cell wall materials [56]. The drug must be delivered to a sensitive site in each cell, such as an enzymes that is involved in the synthesis of protein or enzyme. Bacteriostatic drugs inhibit the growth and multiplication of bacteria but do not kill them. They act by interfering with enzymes systems essential to normal metabolic and growth patterns of bacteria. Bactericidal drug will destroy the bacteria [57]. However, the bacteriostatic and bactericidal activities depends upon the time of incubation and concentration of the antibiotic [57]. An observation carried out by Ali and his coworkers [7] reveals that the greater activity of the metal chelates compared to that of free ligands is attributed to the enhance conjugation of the deprotonated ligand.

1.7 Photoluminescence [58]

Photoluminescence is divided into two categories: fluorescence and phosphorescence. A pair of electrons occupying the same electronic ground state have opposite spins and are said to be in a singlet spin state (**Fig. 1.48a**). When an analyte absorbs an ultraviolet or visible photon, one of its valence electrons moves from the ground state to an excited state with a conservation of the electron's spin (**Fig. 1.48b**). Emission of a photon from the singlet excited state to the singlet ground state-or between any two energy levels with the same spin-is called fluorescence. The probability of fluorescence is very high and the average lifetime of an electron in the excited state is only 10^{-5}-10^{-8} s. Fluorescence, therefore, decays rapidly once the source of excitation is removed.

In some cases an electron in a singlet excited state is transformed to a triplet excited state (**Fig. 1.48c**) in which its spin is no longer paired with the ground state. Emission between a triplet excited state and a singlet ground state-or between any two energy levels that differ in their respective spin states-is called phosphorescence. Because the average lifetime for phosphorescence ranges from 10^{-4}-10^{4} s, phosphorescence may continue for some time after removing the excitation source.

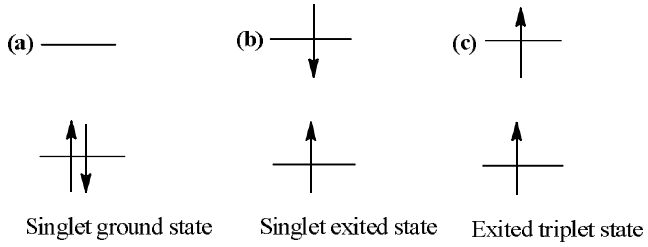

Fig. 1.48: Electron configurations for (a) a singlet ground state; (b) a singlet excited state; and (c) a triplet excited state

1.8 Electrochemical analyses [59]

Electrochemical reaction, any process either caused or accompanied by the passage of an electric current and involving in most cases the transfer of electrons between two substances-one a solid and the other a liquid.

Under ordinary conditions, the occurrence of a chemical reaction is accompanied by the liberation or absorption of heat and not of any other form of energy; but there are many chemical reactions that-when allowed to proceed in contact with two electronic conductors, separated by conducting wires-liberate what is called electrical energy, and an electric current is generated. Conversely, the energy of an electric current can be used to bring about many chemical reactions that do not occur spontaneously. A process involving the direct conversion of chemical energy when suitably organized constitutes an electrical cell. A process whereby electrical energy is converted directly into chemical energy is one of electrolysis; i.e., an electrolytic process. By virtue of their combined chemical energy, the products of an electrolytic process have a tendency to react spontaneously with one another, reproducing the substances that were reactants and were therefore consumed during the electrolysis. If this reverse reaction is allowed to occur under proper conditions, a large proportion of the electrical energy used in the electrolysis may be regenerated. This possibility is made use of in accumulators or storage cells, sets of which are known as storage batteries. The charging of an accumulator is a process of electrolysis; a chemical change is produced by the electric current passing through it. In the discharge of the cell, the reverse chemical change occurs, the accumulator acting as a cell that produces an electric current.

1.9 Aim and objective

During the past years, the synthesis of new coordination compounds containing ligands with nitrogen and sulfur donor atoms has been significantly developed. Among these materials, dithiocarbazate and its substituted compounds have been specifically considered by the researchers because these compounds display significant biological properties such as antibacterial [12], anticancer [10], antiviral [17], antitumor [18], insecticidal [20] and optoelectronic properties such as good non-linear optical (NLO) response [21]. The substitution of suitable groups with different electronic properties and bulk in the ligands can create new species having different properties. Schiff base coordination compounds have shown interesting magnetic properties, DNA hydrolytic character and fluorescence properties [2]. Many new Schiff bases and their metal complexes reported in the literature have been studied electrochemically, using various

electrodes and solvents, with the aim to understand the mechanism of their biological behavior. The majority of previous studies were based on Schiff bases of S-methyl, S-benzyl and S-acetyl dithiocarbazate and N-substituted derivatives of S-methyl dithiocarbazates, and only a few works were reported using Schiff bases of dithiocarbazate presenting a long S-alkyl chain moiety. Therefore, the aim of the present work is:

- Synthesis of new Schiff base ligands using aromatic aldehydes and ketones with S-alkyl dithiocarbazate containing long pendant chains.
- Synthesis of divalent metal complexes, Ni(II), Cu(II), Zn(II), Cd(II), Pd(II) and Pb(II) using the prepared Schiff base ligands.
- Characterization of the synthesized ligands and of corresponding complexes by analytical and spectroscopic methods such as ^{1}H and ^{13}C NMR, Mass, IR and UV-Vis spectra, magnetic moments measurements, conductance, elemental analysis, melting point measurements and X-ray single crystal structure determination.
- Study of photoluminescence properties.
- Study of electrochemical behavior.
- Study of antibacterial activities.

1.10 Scopes of the study

To achieve the objectives of this research work, the following scopes were identified:

- The Schiff bases contain hetero atoms such as nitrogen and sulfur in their structure that possess lone pair electron to coordinate with metal ions to form complexes of different geometry depending upon the structure of the Schiff bases.
- The Schiff bases can exert delocalization of electrons through resonance of π-electrons or lone pair of electrons thus affecting their biological activities.
- The organic molecules can from four, five or six membered chelate rings with metal ions that could sufficiently change their biological properties.

1.11 Significance of the study

As described above, transition metals and their complexes have evolved greatly due to their synthetic, biological potential, catalytic, unusual structural aspects, unique stereo and magneto chemistry. The ligands like thiosemicarbazones, semicarbazones, benzothiazolines, dithiocarbamates, their Schiff bases and the corresponding metal complexes play vital roles in the progress of coordination and bioinorganic chemistry. The different modes of bonding of the ligands in the metal complexes and their derivatives produce appreciable change in their biological activity. Azomethine linkage and their metal complexes are gaining importance due to their unique structural and steriochemical aspects, and their uses as models in industrial, biological, analytical and antimicrobial systems.

The participation of metal ions in many of the bond forming and bond breaking enzymatic processes of biochemistry makes it clear that individual chemical bonds in organic molecules are sometimes strengthened and other times weakened, through coordination of the molecules with metal ions. Since the carbon-nitrogen double bonds in organic Schiff bases are susceptible to both hydrolytic cleavage and to coordination with metal ions, when coordination takes place between a metal ion and an organic ligand, the properties of both are changed in a variety of ways. Many unstable organic ligands are stabilized due to complexion and stabilized towards hydrolysis. For instance, it was show that the hydrolysis of the Schiff base (-CH=N), is much more rapid than that of its metal chelates [60]. This types of enhanced stability could actually be manipulated to one's advantage to design potential biomedical drugs.

References

1. K.A. Jensen, U. Anthony, A. Holm, *Acta Chemica Scandinavica*., 23 (1969) 1916.
2. M. Montezerozohori, K. Nozarion, H.R. Ebrahimi, *J. Spec.*, vol. 2013, Article ID 718149, 1.
3. A. Mazumder, G.R. Rosair, A. Mallick, N. Chattopadhyay, S. Mitra, *Polyhedron*, 25 (2006) 1753.
4. M. Kose, G. Ceyhan, M.T. Demmirtas, I. Gonul, V. Mckee, *Spectrochimica Acta Part A: Molecular and Biomolecular Spectroscopy*, 137 (2015) 477.
5. M.-H.E. Chan, K.A. Crouse, M.I.M. Tahir, R. Rosli, N.U. -Tsafe, A.R. Cowley, *Polyhedron*, 27 (2008) 1141.
6. M.E. Hossain, M.N. Alam, J. Begum, M.A. Ali, M. Nazimuddin, F.E . Smith, R.C. Hynes, *Inorg. Chim. Acta*., 249 (1996) 207.
7. M.A. Ali, C.M. Haroon, M. Nazimuddin, S.M.M.H. Mazumder, M.T.H. Tarafder *Transition Met. Chem.*, 17 (1992) 133.
8. M.E. Hossain, M.N. Alam, M.A. Ali, M. Nazimuddin, F.E. Smith, R.C. Hynes, *Polyhedron*, 15 (1996) 973.
9. M.A. Ali, H.J.H.A. Bakar, A.H. Mirza, S.J. Smith, L.R. Gahan, P.V. Bernhardt, *Polyhedron*, 20 (2008) 71.
10. M. Mohan, M. Kumar, A. Kumar, P.H. Madhuranath, N.K. Jha, *J. Inorg. Biochem*., 33 (1988) 121.
11. M. Das, S.E. Livingstone, *Brit. J. Cancer*, 37 (1978) 466.
12. K.-B. Chew, M.T.H. Tarafder, K.A. Crouse, A.M. Ali, B.M. Yamin, H.-K. Fun, *polyhedron*, 23 (2004) 1385.
13. K.A. Crouse, K.B. Chew, M.T.H Tarafder, A. Kasbollah, A.M. Ali, B.M. Yamin, H.-K. Fun, *polyhedron*, 23 (2004) 161.
14. M.T.H. Tarafder, A. Asmadi, S.M.S. Talib, A.M. Ali, K.A. Crouse, A.M. Ali, B.M. Yamin, H.-K. Fun, *Transition Met. Chem.*, 26 (2001) 170.
15. M. Nazimuddin, M.A. Ali, F.E. Smith, M.A. Mridha, *Transition Met. Chem*., 17 (1992) 74.

16. A.B. Besir, S.K. Guchait, J.A. Gascon and G. Fenteany, *Bioinorg. Med. Chem*., 18 (2008) 498.
17. S.K.S. Hazari, J. Kopf, D. Palit, S. Rakshit, D. Rehder, *Inorg. Chim. Acta*., 362 (2009) 1343.
18. M.A. Ali, A.H. Mirza, R.J. Butcher, M.T.H. Tarafder, T.B. Keat, A.M. Ali, *J. Inorg. Biochem.,* 92 (2002) 141.
19. M.A. Ali, A.H. Mirza, R.J. Butcher, K.A. Crouse, *Transition Met. Chem*. 31 (2006) 79.
20. K. Tampouris, S. Coco, A. Yannopoulos and S. Koinis, *Polyhedron*, 26 (2007) 4269.
21. F.N.-F. How, K.A. Crouse, M.I.M. Tahir, M.T.H. Tarafder, A.R. Cowley, *Polyhedron*, 27 (2008) 3225.
22. P. Bera, C.H. Kim, S.II Seok, *Inorg. Chim. Acta*., 362 (2009) 2603.
23. M. Yazdanbakhsh, R. Takzoo, *Struct. Chem,,* 19 (2008) 895.
24. R. Takzoo, R. Centore, M. Hakimi, S.A. Beyramabadi, A. Morsali, *Inorg. Chim. Acta.,* 371 (2011) 36.
25. P. Bera , S.II Seok, *Solid State Chem.,* 183 (2010) 1872.
26. Y.H. Liu, J. Ye, X.L. Liu, R.Guo, *J. Coord. Chem.,* 62 (2009) 3488.
27. T. Curtius, K. Heidenreich, *J. Prakt. Chem.,* 52(1895) 454.
28. R. Takzoo, R. Centore, *J. Mol. Struct.,* 1031 (2013) 180.
29. S.M.M.H. Majumder, M.A. Ali, F.E. Smith, M.A.U. Mridha, *Polyhedron*, 7 (1988) 2183.
30. P.I.S. Maia, A.G.A. Fernandes, J. Jerley, N. Silva, A.D. Andricopulo, S.S. Lemos, E.S. Lang, U. Abram, V.M. Deflon, *J. Inorg. Biohem.,* 104 (2010) 1276.
31. Y.P. Tian, M.L. Zhang, Z.J. Hu, H.M. Hu, J.Y. Wu, C.Y. Duan, X.Z. You, X.Z. Zhang, *Transition Met. Chem*., 30 (2005) 778.
32. Y.P. Tian, C.Y. Duan, X.Z. You, T.C.W. Mak, Q. Luo, J.Y.Zhou,*Transition Met. Chem.,* 23 (1998) 17.
33. L.H.V. Poppel, T.L. Groy, M.T. Caudle, *Inorganic Chemistry*, 43, no.10, 3180.

34. T.B.S.A. Ravoof, K.A. Crouse, M.I.M. Tahir, A.R. Cowley, M.A. Ali, *Polyhedron*, 23 (2004) 2491.
35. P. Bera, C.-H. Kim and S. II Seok, *Solid State Sci.*, 12 (2010) 1741.
36. M.A. Ali, S.E. Livingstone, *Coord. Chem. Rev.*, 13 (1974) 101.
37. M.T.H. Tarafder, M.A. Ali, Y.W. Wong, S.H. Wong, K.A. Crouse, *Synth. React. Inorg. Met.-Org. Chem.*, 31 (2001) 115.
38. M.A. Ali, M.T.H. Tarafder, *J. Inorg. Nucl. Chem.*, 39 (1977) 1785.
39. P. Bera, C.H. Kim, S.II Seok, *Polyhedron*, 27 (2008) 3433.
40. P. Bera, C.H. Kim, S.II Seok, *Polyhedron*, 12 (2010) 532.
41. M.T.H. Tarafder, M.A.J. Miah, R.N. Bose, *J. Inorg. Nucl. Chem.*, 43 (1981) 3151.
42. C.Y. Duan, Y.P. Tian, X.Z. You, T.C.W. Mak, *Polyhedron*, 16 (1997) 4097.
43. M.T.H. Tarafder, T.-J. Khoo, K.A. Crouse, M.A. Ali, B.M. Yamin, H.-K. Fun, *polyhedron*, 21 (2002) 2691.
44. M.A. Ali, A.H. Mirza, R.J. Butcher, M.T.H. Tarafder, M.A. Ali, *Inorg. Chim. Acta.*, 320 (2001) 1.
45. T.B.S.A. Ravoof, K.A. Crouse, M.I.M. Tahir, F.N.F. How, R. Rosli, D.J. Watkins, *Transition Met. Chem.*, 35 (2010) 871.
46. X.-Y. QIU, S.-Z. Li, A.-R. Shi, Q.-Q. Li, B. Zhai, *Chinese J. Struct. Chem.*, 31 (2012) 555-561.
47. M.K.B. Break, M.I.M. Tahir, K.A. Krouse, T.-J. Khoo, *Bioinorganic Chemistry and application*, vol. 2013, Article ID 362513, 1.
48. Y.-C. Shi, H.-M.Yang, H.-B. Song, C.-G. Yan, X.-Y. Hu, *Polyhedron*, 23 (2004) 567.
49. M.T.H Tarafder, A. Kasbollah, K.A. Crouse, A.M. Ali, B.M. Yamin, H.-K. Fun, *polyhedron*, 20 (2001) 2363.
50. H.-P. Zhou, D.-M. Li, P. Wang, L.-H. Cheng, Y.-H. Gao, Y.-M. Zhu, J.-Y. Wu, Y.-P. Tian, X.-T. Tao, M.-H. Jiang, H.-K. Fun, *J. Mol. Struct.*, 826 (2007) 205.
51. M.A. Ali, A.H. Mirza, R.J. Butcher, M. Rahman, *Transition Met. Chem.*, 25 (2000) 430.

52. R. Takjoo, R. Rozita, M. Yazdanbakhsh, A.A. Kaju, Y. Chen, *Chin. J. Chem.*, 28 (2010) 221.
53. M. Yazdanbakhsh, M.M. Heravi, R. Takjoo, W. Frank, *Z. Anorg. Allg. Chem.*, 634 (2008) 972.
54. R. Takjoo, R. Centore, L. Rhyman, P. Ramasami, *J. Coord. Chem.*, 65 (2012) 1569.
55. M. Yazdanbaksh, R. Takjoo, W. Frank, A.A. kaju, *J. Coord. Chem.*, (2009) 1.
56. S.C. Stinson, *Chemical Engineering News*, 74 (1996) 75.
57. Z. Mazlina, B. Sc. Thesis, University Putra Malaysia (1999).
58. *http://www.olympusmicro.com/primer/techniques/fluorescence/fluorescenceintro.htm*
59. https://www.corrosionpedia.com/definition/3/electrochemical-reaction.
60. G.L. Eichhorn, N.D. Marchand, *J. Am. Chem. Soc.*, 78 (1956) 2688.

Methods and Materials

2.1 Physical measurements

2.1.1 Weighing

The weighing operation was performed on a ae ADAM electronic balance (Adam Equipment Company, Model: PW 214).

2.1.2 Melting point Introduction

Melting points were carried out on a melting point apparatus, Gallenkamp, England.

2.1.3 Magnetic susceptibility

For studying the electronic structure of a transition metal complex, the measurement of magnetic moment is a very useful method. It provides fundamental information about the bonding and stereochemistry of metal complexes. The magnetic properties of coordination compounds are based on the effect of ligands on the spectroscopic terms of metal ions [1]. The Gouy method is the simplest method of measuring magnetic moments. It consists of a suspension of a uniform rod in a nonhomogeneous magnetic field of about 5000 Oersteds and measuring the force exerted on it by a conventional weighing technique. The calibrants usually used are $Hg[Co(SCN)_4]$ [2] and $[Ni(en)_3S_2O_3]$ [3] which are easy to prepare, do not decompose or absorb moisture and pack well in the sample tube. Their susceptibilities at 20^oC are: 16.44×10^{-6} and 11.03×10^{-6} c.g.s units, respectively and may decrease from 0.05×10^{-6} to 0.04×10^{-6} per degree rise in temperature. All substances possess magnetic properties and are affected by the application of a magnetic field [4]. The substances may be diamagnetic when an apparent reduction in mass is caused in the applied magnetic field. The molar susceptibility, a measure of magnetic field, of a substance is an algebraic sum of the susceptibilities of the constituent atoms, ions or molecules. The susceptibility per gram atom of a paramagnetic metal ion of particular compound is determined by measuring the molar susceptibility of the compound and applying diamagnetic corrections for the other ions or molecules in the compounds. The diamagnetic corrections can be estimated by various methods [5], among which Pascal's corrections give satisfactory results for inorganic compounds.

2.1.3.1 The theory of magnetic susceptibility [4,6]

When a substance is placed in a magnetic field of intensity H gauss then the magnetic induction of the field of the substance B, is given by:

$$B = H + 4\pi I \qquad \text{Eq.1}$$

Where I is the intensity of magnetization or magnetic moment per unit volume induced by the field and the term $4\pi I$ is a contribution to B by the substance itself. Dividing eq.1 by H gives:

$$B/H = 1 + 4\pi I/H \qquad \text{Eq. 2}$$

Where, B/H represents the ratio of lines of magnetic force per unit area in the sample to the lines of force per unit area of magnetic field in vacuum and is given by magnetic susceptibility P and I/H is called the volume susceptibility of the substance and is given by the symbol χ_v. Thus eq. 2 becomes

$$P = 1 + 4\pi\chi_v \qquad \text{Eq.3}$$

If I and H are measured in the same unit, χ_v becomes dimentionless quantity. Thus P and χ_v are dimentionless quantities. Thus the volume susceptibility of a vacuum is zero, since in a vacuum B/H = 1. The volume susceptibility of a diamagnetic substance is negative while paramagnetic substances have positive susceptibilities. In most cases, a more useful quantity is the magnetic susceptibility per unit mass or mass susceptibility, χ_g and is given by

$$\chi_g = [C_{bal} \times l \times (R-R_o)]/10^9 m \qquad \text{Eq.4}$$

Where,

C_{bal} = Calibration constant of the balance = 2.086

R = Susceptibility of the glass tube with sample

R_o = Susceptibility of the empty glass tube

l = Length of the sample column (in cm)

m = Mass of the sample (in g)

The experimental mass susceptibility of the sample was then converted in to the molar susceptibility, χ_M (C.G.S unit) by the given expression:

$$\chi_M = \chi_g \times M \qquad \text{Eq.5}$$

Where, M is the proposed molar mass of the sample (g)

For compounds containing a paramagnetic ion, χ_M will be less than the susceptibility per gram atom of the paramagnetic ion, χ_L, because of the diamagnetic contribution of the other groups or ligands present. Since magnetic moments are additive, χ_L can be obtained from χ_M by the addition of appropriate corrections, called diamagnetic corrections for a variety of ions and ligands. The diamagnetic susceptibility, χ_L of the sample can be obtained as a sum of the contributions from its constituent units: atoms, ions, bonds etc. [7].

Mathematically it is written as:

$$\chi_L = \Sigma n_A \chi_A + \Sigma \lambda_A \qquad \text{Eq.6}$$

Where, χ_L is the molar susceptibility of all other constituents of the ligands (diamagnetic correction).

Corrected molar susceptibility, χ_M^{corr} was then obtained from the expression:

$$\chi_M^{corr} = \chi_M - \chi_L \qquad \text{Eq.7}$$

Finally the effective magnetic moment, μ_{eff} in B.M., of the sample was measured using the formula

$$\mu_{eff} = 2.84 (\chi_M^{corr} \times T)^{1/2} \text{ BM} \qquad \text{Eq. 8}$$

Where, T is the absolute temperature in K. Experimental value of χ_L are very small and are generally independent of both the field strength and temperature.

2.1.3.2 Types of magnetic behavior

If P <1 (i.e. χ is negative) the substance is said to be diamagnetic. It causes a reduction in the intensity of the magnetic field and inhomogeneous field moves to the region of lowest field strength. The molar susceptibility of diamagnetic substance is very small

and negative and are usually independent on field strength and temperature. Diamagnetism is a property of all matter and arises from the interaction of paired electron with the magnetic field. Diamagnetic susceptibilities of atoms in molecule are additive; and this is of particular use in estimating the diamagnetic susceptibilities of ligand atoms and counter ions in a transition metal complex [4]. Additivity of atomic susceptibility is contained in the Pascal's constant.

Paramagnetism results when p >1 (i.e. χ is positive), and it causes increase in the intensity of the field and in an inhomogeneous field it moves to the region of highest field's strength. Paramagnetic susceptibilities are positive and relatively large. They are independent on field strength but depend inversely as temperature. However, temperature independent paramagnetism (TIP) can arise in system containing unpaired electron due to the coupling of the ground states with the excited states under influence of a magnetic field. Ferromagnetism and anti-ferromagnetism are both special classes of paramagnetism. They arise from the interaction of individual paramagnetic species with one another. In anti-ferromagnetism, the magnetic vectors of the neighboring centers tend to couple anti-parallel so as to cancel one another. It reduces susceptibility and hence magnetic moment of a compound while in ferromagnetic substances the moments of separate ions tend to align themselves parallel and thus to reinforce one another. They are both temperature and field strength dependent [1].

2.1.3.3 Magnetic properties of transition metal complexes

Orbital motion of the electron generates orbital magnetic moment (μ_l) whereas spin motion of the electron generates spin magnetic moment (μ_s).

Where, l = orbital angular momentum; s = spin angular momentum

For multi-electron systems

$L = l_1 + l_2 + l_3 + \ldots\ldots\ldots\ldots$

$S = s_1 + s_2 + s_3 + \ldots\ldots\ldots\ldots$

$\mu_{l+s} = [4S(S+1)+ L(L+1)]^{1/2}$ B.M Eq. 9

For transition metal complexes, the magnetic properties arise mainly from the exposed *d*-orbitals. The *d*-orbitals are perturbed by ligands.

Therefore, the rotation of electrons about the nucleus is restricted which leads to L = 0

$\mu_s = [4S(S+1)]^{1/2}$ B.M.

S = n (1/2) = n/2; n = no of unpaired electrons

Hence

$\mu s = [4(n/2)(n/2+1)]^{1/2}$ B.M.

$= [n(n+2)]^{1/2}$ B.M. Eq. 10

This is called Spin-Only Formula which is used to calculate the spin-only magnetic moment.

Experimentally, the magnetic susceptibility was measured using the Eq. 4 on a magnetic susceptibility balance (Sherwood scientific, Cambridge, UK) at room temperature at the department of Chemistry, Rajshahi University, Rajshahi, Bangladesh. Thus the experimental magnetic moments (in B.M.) obtained by using Eq. 8 was used to calculate the number of unpaired electrons for d^n species by using eq. 10 and compared with the literature values [8] to predict the geometry around the central metal.

2.1.4 Elemental analysis

Elemental analyses were recorded on with a Yanaco JMS-D300 spectrometer, University of Toyama, Japan.

2.1.5 Conductivity

Molar conductivity measurements were carried out on a heavy-duty conductivity meter (Extech Instruments, USA, model: 407303. The conductivity meter was calibrated using KCl solution of different concentration at room temperature. The test compounds were dissolved in chloroform and in some cases in dichloromethane to prepare 10^{-5} M solution. The conductance of the compounds under investigation was calculated by deducting the conductance of the solution from the solvent.

2.2 Spectroscopic characterizations

2.2.1 Infrared spectra

IR spectra (4000-225 cm^{-1}) were obtained as KBr disc using a FT-IR 8400-Shimadzu spectrophotometer (Japan). One could identify the functional groups present in the test compounds with the aid of IR spectroscopy along with their purity.

2.2.2 Nuclear Magnetic Resonance (NMR) spectra

^{1}H NMR (400 and 500 MHz) and ^{13}C NMR (150 MHz) spectra were recorded on a JEOL JNM-A400 spectrometer in $CDCl_3$ with TMS as internal standard. The values of coupling constant (j) in Hz was calculated from the difference of chemical shift values of multiplet bands multiplying by operating frequency of the spectrometer in MHz. NMR technology gives information about the number of magnetically distinct atoms of the types being studied.

2.2.1 Mass spectra

Mass spectra were obtained on a JEOL-JMS-D300 mass spectrometer University of Toyama, Japan. This technique gives useful information on the determination of molecular weight and molecular formula of the compounds under study. The determination of molecular formula is based on the precise mass determination and isotope data ratio.

2.2.4 UV-Visible spectra

2.2.4.1 Theory underlying electronic spectroscopy

The excitation of a molecule from its electronic ground state to an electronic exited state corresponds to absorption of light in the near-infrared, visible or ultraviolet regions of the spectrum, caused by the transfer of electrons from different energy levels. For organic molecules, the electronic transitions include $\sigma \rightarrow \sigma^*$, $\sigma \rightarrow \pi^*$, $\pi \rightarrow \pi^*$, $n \rightarrow \pi^*$ and $n \rightarrow \sigma^*$, due to excitation of bonding, non-bonding (loan pair) and π bonding electrons respectively. These transitions are termed as intra ligand charge transfer transitions (ILCT). The molar absorptivity (ε) for various types of ILCT transitions observed in complexes within the range of 10^3-10^6 L $mol^{-1}cm^{-1}$ [9]. While color in

inorganic complexes is generally associated with the presence of partially filled *d* shell, there are many such compounds with d^0 or d^{10} configuration which are intensely colored. In such cases color arises at least in part as a consequence of light absorption due to transfer of an electron from an orbital primarily on the ligand, to one primarily on the metal, or vice versa. Such charge or electron transfer processes are termed as 'Ligand to Metal Charge Transfer' (LMCT) and 'Metal to Ligand Charge Transfer' (MLCT) transitions respectively. Such a process is not confined to d^0 and d^{10} species and occurs frequently in transition metal complexes. The molar absorptivities of such MLCT bands in complexes with unsaturated ligands spans from 10^2-10^3 $Lmol^{-1}cm^{-1}$ [9]. For transition metal complexes, the absorption bands in the first two of these regions (infrared and visible) are relatively weak and are associated with transitions largely localized on the metal atom. The ultraviolet bands are intense and they are associated with the transfer of an electron from one atom to another and so are called charge-transfer (CT band) bands. The spectra of transition metal complexes depend on the transition of unpaired electrons from the ground state to an exited state. These transitions are frequently referred to as *d-d* transitions because they involve the molecular orbitals that are mainly metal *d* in character (e_g and t_{2g} orbitals in octahedral and tetrahedral complexes). Transitions may occur between the split *d*-levels of the central atom, giving rise to the *d-d* or ligand field spectra. The spectra region where these bands occur spans the near infrared, visible and UV. Most of the transition metal complexes are colored due to *d-d* transitions in the visible region. The atomic overlap in metal-ligand bonds allows *d* electrons to penetrate from the central atom to the ligand, and vice versa. The transitions are affected by spacing between the e_g and t_{2g} levels, the effect of ligands on the energies of the *d* orbitals of the metal ions. Since this spacing depends on factors such as the geometry of the metal complex, the nature of the ligands present, and the oxidation state of the central metal atom, electronic spectra of complexes can provide valuable information related to bonding and structure. The molar absorption coefficient for *d-d* transitions in octahedral, tetrahedral and square planar complexes lies within the value of 1-10^3 $Lmol^{-1}$ cm^{-1} [9].

Experimentally the solution UV-visible absorption spectra were scanned on a T60 UV-visible spectrophotometer (PG Instruments, UK) at the Department of Chemistry,

Rajshahi University of Engineering & Technology, Bangladesh between 200-800 nm using 10^{-5} M solution in chloroform and for some cases in dichloromethane using a quartz cell of 1 cm path length with the help of UVWIN 5.0 software.

The value of molar extinction coefficient (ε) or logε at each absorption maxima was calculated using Beer-Lambert law: $A = \varepsilon bc$.

Where, A = observed absorbance

b = path length =1 cm

c = concentration (M or $molL^{-1}$).

2.3 X-ray crystal structure determination

X-ray diffraction provides more structural information for the inorganic chemists than any other techniques. It allows the precise measurement of bond angles and bond lengths. Although in the past, it was a time consuming and difficult process, the advent of more efficient physical method [10,11] of gathering data and doing the computations has made it relatively easy to solve most structures.

In order to solve a structure by X-ray diffraction, one generally needs a single crystal. Although powder data can provide 'fingerprint' information and, in simple cases, it is generally necessary to be able to grow crystals for more extensive analysis.

X-rays are diffracted by electrons; therefore what are located are the centers of electron clouds, mainly the core electrons. This has two important consequences. First, if there is a great disparity in atomic number between the heavy and light atoms in a molecule, it may not be possible to locate the light atom (especially if it is hydrogen), or to locate it as accurately as the heavier atom. Second, there is a small but systematic tendency for the hydrogen atom to appear to the shifted 10-20 pm toward the atom to which it is bonded [12,13]. This is because hydrogen is unique in not having a core centered on the nucleus and the bonding electrons are concentrated towards the binding atom. Because the location of an atom in an molecule as obtained by X-rays is the time average of all positions it occupied while the structure was being determined, the resultant structure is

often presented in terms of thermal ellipsoids, which are probably indicators of where the atoms are most likely to be found .

The method developed by Bragg is the foundation of almost all modern works in X-ray crystallography [14]. They used a single crystal and a monochromatic beam of X-rays and rotated the crystal until a reflection was detected. There are many different sets of planes in a crystal, so there are many angles at which reflection are observed and their intensities. Single crystal diffraction patterns are measured by using a four-circle diffractometer. The computer linked to the diffractometer determines the unit cells dimensions and the angular setting of the diffractometer's four circles that are needed to observe any particular intensity peak in the diffraction pattern. The computer controls the settings, and moves the crystal and the detector for each one in turn. At each setting, the diffraction intensity is measured and background intensities are assessed by making measurements at slightly different settings. Computing techniques are available that lead not only to automating indexing but also to the automated determination of the shape, symmetry and the size of the unit cell.

The X-ray crystal structure analyses of the three compounds reported in chapter 3 were carried out at 100 K and 173 K on a Rigaku R-AXIS RAPID diffractometer equipped with CCD and Cu-Kα radiation (λ = 1.54187 Å) at Center for Environmental Conservation and Research Safety, University of Toyama, Japan. Cell refinement, indexing and scaling of the data sets were done by using Crystal Structure Rigaku programs [15]. An empirical absorption correction was applied for all the three compounds. All the structures were solved by using SIR92 [16] and subsequent Fourier analyses [17] and refined by the full-matrix least-squares method based on F^2 with all observed reflections [17]. The H atoms were fixed at geometrical positions except that of nitrogen N(2) in **1** which was located on the Fourier map and refined. The ORTEP drawings were done by using the WinGX System, Ver 1.80.05 [18].

Diffraction data for other two compounds reported in chapter 4 were collected on a Rigaku R-AXIS RAPID diffractometer equipped with CCD (University of Toyama, Japan). Both the experiments were performed at 173 K with Mo-Kα radiation (λ =

0.71075 Å). Cell refinement, indexing and scaling of the data set were carried out using Crystal Structure package [15]. The structures were solved by direct methods [16] and subsequent Fourier analyses and refined by the full-matrix least-squares method based on F^2 with all observed reflections [17]. An absorption correction was applied to both data sets [19]. The contribution of H atoms at geometrical calculated positions was introduced in the final cycles of refinement. Figures were done with Ortep3 for Windows [20].

2.4 Fluorescence [21]

Fluorescence is a member of the ubiquitous luminescence family of processes in which susceptible molecules emit light from electronically excited states created by either a physical (for example, absorption of light), mechanical (friction), or chemical mechanism. Generation of luminescence through excitation of a molecule by ultraviolet or visible light photons is a phenomenon termed photoluminescence, which is formally divided into two categories, fluorescence and phosphorescence, depending upon the electronic configuration of the excited state and the emission pathway. Fluorescence is the property of some atoms and molecules to absorb light at a particular wavelength and to subsequently emit light of longer wavelength after a brief interval, termed the fluorescence lifetime. The process of phosphorescence occurs in a manner similar to fluorescence, but with a much longer excited state lifetime. Compounds emitting fluorescence are called fluourophores or fluorochromes. When a fluorophore absorbs light, energy is taken up for the excitation of electrons to higher energy states. The process of absorption is rapid and is immediately followed by a return to lower energy states, which is accompanied by an emission of light, observed as fluorescence. Absorption and emission of light of various fluorophores may take place at different regions of the light spectrum.

Fluorescence rarely results from absorption of UV-radiation of wavelengths shorter than 250 nm because this type of radiation is sufficiently energetic to cause deactivation of the excited state by predissociation or dissociation. Most organic molecules have at least some bonds that can be ruptured by energies of this strength. Fluorescence commonly occurs from a transition from the lowest vibrational level of

the first excited electronic state to the one of the vibrational levels of the electronic ground state.

As shown in **Fig. 2.1**, a photon of excitation light is absorbed by an electron of a fluorescent particle, which raises the energy level of the electron to an excited state. During this short excitation period, some of the energy is dissipated by molecular collisions or transferred to a proximal molecule, and then the remaining energy is emitted as a photon to relax the electron back to the ground state. Because the emitted photon usually carries less energy and therefore has a longer wavelength than the excitation photon, the emitted fluorescence can be distinguished from the excitation light. The excitation and photon emission from a fluorophore is cyclical, and until the fluorophore is irreversibly damaged, it can be repeatedly excited. Because fluorophores can therefore emit numerous photons through this cycle of excitation and emission, fluorescent molecules are used for a broad range of research applications.

Experimentally, fluorescence spectra of the compounds were recorded on a Shimadzu RF-5301 PC spectrofluorophotometer using 10^{-5} M solution in chloroform/ dichloromethane at room temperature.

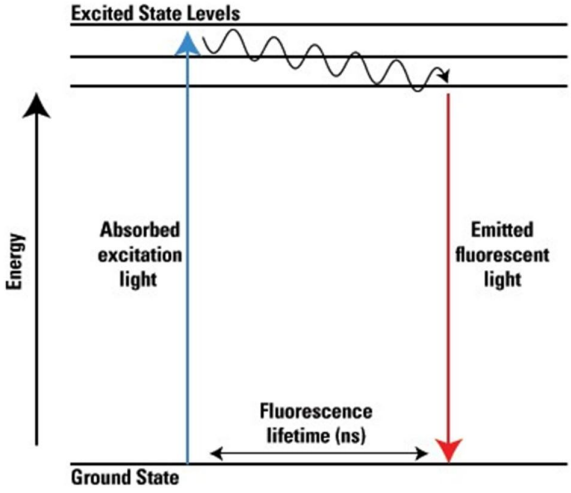

Fig. 2.1: Jablonski energy diagram of fluorescence

2.5 Antibacterial activity

The prime objective of performing the antibacterial screening is to determine the susceptibility of the pathogenic microorganisms to test compound, which in turn is used in the section of the compound in a therapeutic agent. In general, antibacterial screening *in vitro* is undertaken in the following two types:

Primary Assay

It is essentially a qualitative or semi-qualitative test that indicates the sensitivity or resistance of microorganisms to the test compounds. However, this technique cannot be used to distinguish between bacteriostatic and bactericidal agents. The primary assay can be performed *in vitro* by disc diffusion assay method [22] which includes:

(a) Plate diffusion test, and

(b) Streak test.

The plate diffusion test utilizes different concentrations of a test compound absorbed on sterile filter paper discs on the same plate whereas the streak test permits the determination of the antibacterial effect of a test compound on several microorganisms simultaneously and is suitable for the estimation of the spectrum of the activity. However, the plate diffusion test is commonly used.

Secondary assay

It quantities the relative potency, such as Minimum Inhibitory Concentration (MIC), the lowest concentration of an antimicrobial agent required to inhibit the growth of the microorganisms *in vitro*

2.5.1 Apparatus and reagents

(i) Test compounds

(ii) Standard disc (kanamycin)

(iii) Chloroform, DMSO,

(iv) Alcohols (95%)

(v) Filter paper disc (sterilized),

(vi) Petri dishes

(vii) Inoculating loop

(ix) Sterile cotton

(x) Sterile forceps

(xi) Test tube.

(xii) Micropipette

(xiii) Nose masks and hand gloves

(xiv) Spirit burner and match box

(xv) Rectified spirit

(xvi) Nutrient agar (DIFCO)

(xvii) Laminar air flow unit

(xviii) Incubator

(xix) Refrigerator

(xx) Autoclave

Bacterial strain taken for the study

Five Pathogenic bacteria were selected for the test, three of which are gram positive and the remaining were gram negative. These organism of pure culture were primarily collected from the department of Microbiology, university of Dhaka and were further cultured at the Molecular biology Laboratory, Institute of Biological Science, Rajshahi University, Rajshahi-6205.

List of the pathogenic bacteria

Gram positive bacteria

(i) Staphylococcus aureus

(ii) Bacillus subtilis

(ii) Klebsiella sp.

Gram negative bacteria

(i) Escherichia coli

(ii) Pseudomonas aeruginosa

Sterilization procedures

The antibacterial screening was carried out in a laminar air flow unit and all types of precautions were highly maintained to avoid any type of contamination during the test. UV light was switched on for half an hour before working in the laminar hood to avoid any accidental contamination. Petri dishes and other glass wares were sterilized in the autoclave at 121 ^{0}C temperature and a pressure of 15 Ibs/ sq. inch for 15 minutes. Micropipette tips culture media, cotton, forceps, blank disks etc. were also sterilized.

Culture media

For demonstrating the antibacterial and subculture of the test organisms nutrient agar media (DIFCO) was used.

Preparation of nutrient agar media

The instant nutrient agar (DIFCO) medium was used weighed and then reconstuted with distilled water in a conical flask according to specification. If it was then heated in water bath to dissolve the agar until a transparent solution was obtained.

Preparation of fresh culture of the pathogenic organisms

The nutrient agar medium was prepared and dispersed in a number of clean test tubes to prepare slants (5 ml in each test tubes). This test tubes were plugged with cotton and sterilized in an autoclave at 121^{0}C and 15 Ibs/ sq. inch for 15 minutes. After sterilization, the test tubes were kept in an inclined position for solidification. This where then incubated at 37.5 ^{0}C to ensure sterilization. The test organisms were

transferred to the agar slants from the supplied pure cultures with the help of an inoculating loop in an aseptic condition. Burning the loop after its transfer of microorganisms to avoid contamination very carefully. The inoculated where then incubated at 37.5 ^{0}C for 24 hours to assure the growth of test organism. These fresh cultures were used for the sensitivity tests.

Preparation of test plates

The test plates were prepared according to the following procedures:

(i) The nutrient agar medium prepared in the previous section was poured in 15 ml quantity in each clean test tubes and plugged with cotton.

(ii) The test tubes and a number of petri dishes were sterilized in an autoclave at 121^{0}C and 15 Ibs/ sq. inch pressure for 15 minutes and were transferred into laminar airflow and the allowed to cool to about 45 ^{0}C to 50 ^{0}C.

(iii) The test organisms were transferred from the fresh subculture to the test tube contain- ning 15 ml autoclaved medium with the help of incubating loop in an aseptic condition. Then the test tube was shaken by rotation to get a uniform suspension of the organism.

(iv) The bacterial suspensions were immediately transferred to the sterile petri dishes in an aseptic area. The petri dishes were rotated several times, first clockwise and then anticlockwise to assure homogenous distribution of the test organisms. The media were poured into petri dishes in such a way to give a uniform depth of approximately 4 mm.

(v) Finally, after medium was cooled to room temperature in laminar airflow unit, it was stored in a refrigerator (4 ^{0}C).

Preparation of the stock solution and sample disc

The stock solution was prepared by dissolving 2.0 mg of sample in 0.15 ml of the desired solvent. This means that 1.0 µl of the stock solution contains 13.0 µg of the test sample.

Preparation of discs containing samples

For the preparation of discs containing the test compound, following procedures were utilized:

(a) Sample discs

Sterilized filter paper discs (5 mm in a diameter) were taken by the forceps in the plates. From the stock solution a disc of 400 µg/disc was prepared by soaking 30 µl of stock solution in a filter paper disc. The test solutions were applied on the discs with the help of a micropipette in an aseptic condition. These discs were left for a few minutes in an aseptic condition for complete removal of solvent.

(b) Standard discs

These were used to compare the antibacterial activity of the test material. In the present study, readymade Kanamycin were used as standard disc for comparison.

Placement of the discs and incubation

(i) By means of a pair sterile forceps, the dried disc and standard disc were placed gently on the solidified agar plates seeded with the test organism to ensure contact with the medium.

(ii) The plates were then kept in a refrigerator for 4 ^{0}C for 4 hours in order to provide sufficient time to diffuse the antibiotics into the medium.

(iii) Finally, the plates were incubated at 37.5 ^{0}C for 24 hours in an incubator.

Precaution

(i) The discs were placed in such a way that they were not closer than 15 mm to the edge of the plate and far enough apart to prevent overlapping the zones of inhibition.

(ii) After incubation, the antibacterial activities of the test samples were determined by measuring the diameter of inhibitory zones in terms of mm with a transparent scale.

2.6 Cyclic Voltammetry

Cyclic voltammetry (CV) is perhaps the most effective and versatile electro analytical technique that may provide the information of the thermodynamics of redox processes, adsorption processes and the kinetics of electron transfer reactions. It enables the electrode potential to be rapidly scanned in search of redox couples [23]. Once located, a couple can then be characterized from the potentials of peaks on the cyclic voltammogram and from changes caused by variation of the scan rate.

In cyclic voltammetry, the electrode potential ramps linearly versus time. This ramping is known as the experiment's scan rate (V/s). The potential is measured between the reference electrode and the working electrode and the current is measured between the working electrode and the counter electrode. This data is then plotted as current (i) vs. potential (E). The forward scan produces a current peak for any analytes that can be reduced (or oxidized, depending on the initial scan direction) through the range of the potential scanned. The current will 60 increase as the potential reaches the reduction potential of the analyte, but then falls off as the concentration of the analyte is depleted close to the electrode surface. If the redox couple is reversible then when the applied potential is reversed, it will reach the potential that will reoxidize the product formed in the first reduction reaction, and produce a current of reverse polarity from the forward scan. This oxidation peak will usually have a similar shape to the reduction peak. As a result, information about the redox potential and electrochemical reaction rates of the compounds is obtained. For instance if the electronic transfer at the surface is fast and the current is limited by the diffusion of species to the electrode surface, then the current peak will be proportional to the square root of the scan rate.

The important parameters of cyclic voltammetry are the magnitude of the peak currents, i_{pa} and i_{pc}, and the potentials at which peaks occur, E_{pa} and E_{pc}. Reversible peaks have a distinct absolute potential difference between the reduction (E_{pc}) and oxidation peak (E_{pa}). In an ideal system $|E_{pc}-E_{pa}|$ would be 59 mV for a 1 electron process and 30 mV for a 2 electron process [24]. In addition the ratio of the currents passed at reduction (i_{pc}) and end oxidation (i_{pa}) is near unity ($i_{pa}/i_{pc}=1$) for a reversible

peaks. When such reversible peaks are observed thermodynamic information in the form of half-cell potential $E^0_{1/2}$ can be determined. When waves are semi-reversible such as when i_{pa}/i_{pc} is less than or greater than 1, it can be possible to determine even more information especially kinetic processes like following chemical reaction. When waves are non-reversible it is impossible to determine what their thermodynamic $E^0_{1/2}$ is with cyclic voltammetry.

The cyclic voltammetry was run on on a CHI602 E electrochemical analyzer. Pt disk electrode (ϕ = 2mm), platinum wire and Ag/AgCl (sat. KCl) were used as working, counter and reference electrodes respectively. Sample solutions were 10^{-3} M of each complex in spectroscopic grade $CHCl_3$ containing 0.1 M tetra-n butylammonium tetrafluoroborate as the supporting electrolyte.

2.7 Reagents and chemicals

Name of Reagents/Chemicals	Company name
Hydrazine hydrate (99%)	Fluka Chemica, USA
1-bromohexane	Fluka Chemica, USA
Potassium hydroxide	Merck, India
Carbon disulfide	Merck, India
Potassium bromide	Fluka Chemica, USA
Nickel(II) acetate tetrahydrate	Fluka Chemica, USA
Copper acetate(II) monohydrate	Fluka Chemica, USA
Palladium(II) chloride	Fluka Chemica, USA
Zinc(II) acetate dihydrate	BDH, England
Cadmium(II)acetate trihydrate,	BDH, England
Lead(II)acetate trihydrate,	BDH, England
4-methylbenzaldehyde	BDH, England
4-methoxybenzaldehyde	BDH, England
Thiophene-2carbaldehyde	BDH, England
Chloroform	Scharlue
Acetonitrile	Fisher

Dichloromethane	Scharlue
Dimethyl sulfoxide	Fisher
Dimethylformamide	Fisher
Methanol	Merck, India
Ethanol	Merck, India

References

1. R.S. Drago, Physical Methods in Chemistry, W.D. Saunders Company, Philadelphia (1977).
2. B.N. Figgis, Nyholm, *J. Chem. Soc.*, (1958) 4190.
3. N.F. Curtis, *J. Chem. Soc.*, (1961) 3147.
4. F.E. Mabbs, D.J. Machin, Magnetism and Transition Metal Complexes, Chapman Hall, London (1973).
5. C.J. O'Connor, Magnetochemistry-advances in theory and experimentation, Prog ress in Inorganic Chemistry, 29 (1982) 2003.
6. A. Earnshaw, Introduction to Magnetic Chemistry, Academic press, London (1968).
7. R.L. Carlin Magnetochemistry, Springer-Verlag, New York (1986).
8. K. Burger, Coordination Chemistry: Experimental Methods, Butterworth, London (1973).
9. A.B.P. Lever, Inorganic Electronic Spectroscopy, 2nd edition; Elsevier: New York (1986).
10. R.S. Drago, Physical Methods for Chemists, 2nd edition, Saunders, Philadelphia (1992).
11. E.A.V. Ebsworth, D.W.H. Rankin, S. Cradock, Structural Methods in Inorganic Chemistry, 2nd edition, Blackwell: Oxford (1991).
12. P. Coppens, Experimental Electron Densities and Chemical Bonding, Angewandte Chemie International Edition in English, 16 (1977) 32.
13. T.S. Cameron, P.K. Bakshi, B. Boreca, M.T.H. Liu, *J. Am. Chem. Soc.,* 114 (1992) 1889.
14. W.L. Bragg, The Crystalline State, Macmillan, New York (1993).
15. Rigaku (2010). Crystal Structure. Version 4.0. Rigaku Corporation, Tokyo, Japan.
16. A. Altomare, G. Cascarano, C. Giacovazzo, A. Guagliardi, M. Burla, G. Polidori, M. Camalli, *J. Appl. Cryst.*, 27 (1994) 435.
17. G.M. Sheldrick, *Acta Crystallogr., Sect. A*, 64 (2008) 112.
18. L.J. Farrugia, *J. Appl. Crystallogr.*, 32 (1999) 837.
19. Rigaku (1995). ABSCOR. Rigaku Corporation, Tokyo, Japan.

20. L. J. Farrugia, *J. Appl. Crystallogr.*, 30 (1997) 565.
21. http://www.olympusmicro.com/primer/techniques/fluorescence/fluorescenceintro.htm.
22. A.W. Bauer, W.M.M. Kirby. J.C. Sherris, M. Turck, Antibiotic Susceptibility Testing by a Standardized Single Disc Method, *Am. J. Clin. Pathol.*, 45 (1966) 493.
23. A.J. Bard, L.R. Faulkner, Electrochemical Methods: Fundamentals and Applications, John Wiley and Sons, New York (2000).
24. R.S. Nicholson, I. Shain, Theory of Stationary Electrode Polarography: single scan and cyclic methods applied to reversible, irreversible, and kinetic systems, Anal. Chem. 36 (1964) 706.

Synthesis, characterization, X-ray crystal structure, photoluminescence and electrochemistry of the N, S Schiff base ligand derived from 4-methylbenzaldehyde and S-hexyldithiocarbazate and of its bivalent metal complexes

3.1 Introduction

Transition metal complexes derived from Schiff bases have occupied a central role in the development of coordination chemistry. Hydrazine carbodithioate species typically act as bidentate ligands, formed *in situ* during complexation, and coordinate through the β-nitrogen and the thiolate sulfur donors. In fact, the presence of N and S atoms enable these ligands to react with both transition and main group metal ions yielding air stable and intensely colored metal complexes, some of which have been shown to exhibit interesting physico-chemical properties [1,2]. Schiff bases derived from S-alkyl/aryl dithiocarbazate and their complexes exhibit promising potential applications such as antibacterial, antifungal, anticancer, antitumor, wound healing, cell motility and as antioxidant activities [2]. In addition, the reaction of S-alkyl/aryl dithiocarbazate with different aldehydes and ketones leads to ligands with modified donor properties, bringing about intriguing coordination and geometrical variation in metal complexes thus affecting their bioactivities [3-5]. It is well known that coordination of metals to Schiff base ligands may enhance their biological activities. Many new Schiff bases and their metal complexes reported in the literature have been studied electrochemically, using various electrodes and solvents, with a view to understand the mechanism of their biological study [6].

Schiff bases derived from a large number of carbonyl compounds and dithiocarbazates have been used, however, the studies on their optical properties, such as fluorescence, are rare [7]. The variety of possible Schiff-base metal complexes with a wide choice of ligands, and coordination environments, has prompted us to undertake research in this area. The majority of previous studies were based on Schiff bases of S-methyl, S-benzyl and S-acetyl dithiocarbazate and N-substituted derivatives of S-methyl dithiocarbazates, and only a few works were reported using Schiff bases of dithiocarbazate derived from long chain S-alkyl moiety. Therefore, the objectives of

the present work is the preparation of a bidentate Schiff base derived from S-hexyldithiocarbazate and 4-methylbenzaldehyde and the study of coordination chemistry with some bivalent metal ions. The X-ray single crystal structures of the ligand and its Ni(II) and Pd(II) complexes have been determined. The fluorescence properties of all the compounds and the electrochemical activity of only the Cu(II) complex have also been studied.

3.2 Preparation of S-hexyl 3-(4-methylbenzylidene)dithiocarbazate, 1

To an ethanolic solution of KOH (2.81 g, 0.05 mol) hydrazine hydrate (2.50 g, 0.05 mol, 99%) was added and the mixture was stirred at 0 ^{o}C. To this solution carbon disulfide (3.81 g, 0.05 mol) was added dropwise with constant stirring for one hour. Then 1-bromohexane (8.25 g, 0.05 mol) was added dropwise with vigorous stirring at 0 ^{o}C for an additional hour. Finally, 4-methylbenzaldehyde (6.00 g, 0.05 mol) in ethanol was added and the mixture refluxed for 30 min. The mixture was filtered while hot and then the filtrate was cooled to 0 ^{o}C giving a precipitate of the Schiff base product (**Scheme 3.2**). It was recrystallized from ethanol at room temperature and dried in a vacuum desiccator over anhydrous $CaCl_2$. Colorless crystals, suitable for X-ray diffraction, of the title compound were obtained by slow evaporation of a solution in ethanol/acetonitrile (2:1) after 23 days. The physical and spectroscopic data of the Schiff base ligand **1** is as follows:

Colorless crystal, Yield: 75 %; m. p. (83-85) ^{o}C. *Anal. Calc.* for $C_{15}H_{22}N_2S_2$: C, 61.18; H, 7.53; N, 9.51; S, 21.78 % ; Found: C, 61.25; H, 7.54; N, 9.52; S, 21.80 %.

Selected IR data (KBr dics, cm^{-1}): ν(N-H) 3101m, ν(C-H, alkyl) 2929m, ν(C=N) 1619s, ν(C=S) 1101s, ν(N-N) 1026s, ν(CSS) 871m.

^{1}H NMR (500 MHz, $CDCl_3$, ppm) δ: 11.01(s,1H, NH), 7.93(s, 1H, CH=N), 7.62(d, 2H, C-4,6, J=8.00 MHz), 7.21(d, 2H, C-3,7, J=8.00 MHz)), 3.31(t, 2H, -SCH_2), 2.42(s, 3H, C-1), 1.76(p, 2H, C-11), 1.47(p, 2H, C-12), 1.34(m, 4H, C-13,14), 0.91(t, 3H, C-15).

^{13}C NMR (125 MHz, $CDCl_3$, ppm) δ: 199.33(C=S), 162.04(CH=N), 141.84(C-5), 129.66(C-4,6), 128.69(C-2), 127.99(C-3,7), 34.68-(C-1), 31.53(C-10), 28.85(C-11), 28.67(C-12), 22.66(C-13), 21.74(C-14), 14.17(C-15).

UV-Vis spectrum [$CHCl_3$, λ_{max} nm (log ε, L mol^{-1} cm^{-1})]: 241(4.05), 262(4.0), 325(4.30), 338(4.32).

HRMS(FAB) Calc. for $C_{15}H_{22}N_2S_2$ (M+1): 295.1224; Found(M+1): 295.1302.

3.3 Synthesis of bis[S-hexyl 3-(4-methylbenzylidene)dithiocarbazato-κ^2N^3,S]M(II) complexes 2-7

A solution of $Ni(CH_3COO)_2.4H_2O$ (0.06 g, 0.25 mmol, 8 mL methanol) was added to a solution of the ligand S-hexyl 3-(4-methylbenzylidene)dithiocarbazate (0.15 g, 0.5 mmol, 10 mL methanol). The resulting mixture was stirred at room temperature for four hours. A dark reddish brown precipitate was formed, filtered off, washed with methanol and dried in vacuo over anhydrous $CaCl_2$. Dark reddish brown single crystals, suitable for X-ray diffraction, of the compound **2** were obtained by slow evaporation from a mixture of chloroform and acetonitrile (1:1) after 7 days.

The Cu(II), Zn(II), Cd(II), Pd(II) and Pb(II) complexes **3-7** were prepared following the same procedure as described for complex **2** by using $Cu(CH_3COO)_2.H_2O$, $Zn(CH_3COO)_2.2H_2O$, $Cd(CH_3COO)_2.3H_2O$, $PdCl_2$ and $Pb(CH_3COO)_2.3H_2O$, respectively (**Scheme 3.2**). The product was recrystallized by a mixture of chloroform and acetonitrile (5:1). Orange red single crystals, suitable for X-ray diffraction, of compound **6** were obtained by slow evaporation from a mixture of chloroform and acetonitrile (2:1) after 5 days. The physical and spectroscopic data of the compounds **2-7** are given below:

3.3.1 Bis[S-hexyl 3-(4-methylbenzylidene)dithiocarbazato-κ^2N^3,S]nickel(II), 2

Dark reddish brown, Yield: 65 %; m.p. (100-102 ^oC). *Anal. Calc.* for $C_{30}H_{42}N_4NiS_4$: C, 55.81; H, 6.56; N, 8.68; S, 19.86 % ; Found: C, 55.83; H, 6.57; N, 8.68; S, 19.87 %. Selected IR data (KBr dics, cm^{-1}): ν(C-H, alkyl) 2914m, ν(C=N) 1604s, ν(N-N) 1030s, ν(CSS) 803m, ν(M-N) 516, ν(M-S) 405.

^1H NMR (500 MHz, $CDCl_3$, ppm) δ: 7.67(s, 2H, CH=N), 7.88(d, 4H, C-4,6, J=6.50 MHz), 7.19(d, 4H, C-3,7, J=6.50 MHz), 3.12(t, 4H, $-SCH_2$), 2.38(s, 6H, C-1), 1.74(p, 4H, C-11), 1.43(p, 4H, C-12) 1.30(m, 8H, C-13,14), 0.88(t, 6H, C-15).

UV-Vis spectrum [$CHCl_3$, λ_{max} nm (log ε, L mol^{-1} cm^{-1})]: 241(4.33), 291(4.47), 338(4.57), 382(4.17), 443(3.91).

HRMS(FAB) Calc. for $C_{30}H_{42}N_4NiS_4$ (M+1): 645.1646; Found(M+1): 645.1728.

Molar conductivity (1.0×10^{-5} M; $CHCl_3$, $\Omega^{-1}cm^2mol^{-1}$): 0.00; μ_{eff} = Diamagnetic.

3.3.2 Bis[S-hexyl 3-(4-methylbenzylidene)dithiocarbazato-κ^2N^3,S]copper(II), 3

Brick red, Yield: 61 %; m. p. (102-105 ^oC (d). *Anal. Calc.* for $C_{30}H_{42}N_4CuS_4$: C, 55.39; H, 6.51; N, 8.61; S, 19.71 % ; Found: C, 55.41; H, 6.52; N, 8.61; S, 19.72 %.

Selected IR data (KBr dics, cm^{-1}): ν(C-H, alkyl) 2926m, ν(C=N) 1583s, ν(N-N) 1031s, ν(CSS) 804m, ν(M-N) 525, ν(M-S) 400.

UV-Vis spectrum [$CHCl_3$, λ_{max} nm (log ε, L mol^{-1} cm^{-1})]: 244(4.10), 271(4.16), 324(4.56), 376(4.09), 443(3.29), 517(2.95).

HRMS(FAB) Calc. for $C_{30}H_{42}N_4CuS_4$ (M+1): 650.1588; Found(M+1): 650.1664.

Molar conductivity (1.0×10^{-5} M; $CHCl_3$, $\Omega^{-1}cm^2mol^{-1}$): 0.00; μ_{eff} = 1.82 B.M.

3.3.3 Bis[S-hexyl 3-(4-methylbenzylidene)dithiocarbazato-κ^2N^3,S]zinc(II), 4

Pale yellow, Yield: 55 %; m.p. (125 -127 ^oC). *Anal. Calc.* for $C_{30}H_{42}N_4ZnS_4$: C, 55.24; H, 6.49; N, 8.59; S, 19.66 %; Found: C, 55.27; H, 6.50; N, 8.60; S, 19.68 % .

Selected IR data (KBr dics, cm^{-1}): ν(C-H, alkyl) 2924m, ν(C=N) 1601s, ν(N-N) 1041s, ν(CSS) 811m, ν(M-N) 481, ν(M-S) 399.

^1H NMR (500 MHz, $CDCl_3$, ppm) δ: 7.67(s, 2H, CH=N), 8.12(d, 4H, C-4,6, J=7.50 MHz), 7.21(d, 4H, C-3,7, J=7.50 MHz), 3.24(t, 4H, $-SCH_2$), 2.40(s, 6H, C-1), 1.80(p, 4H, C-11), 1.47(p, 4H, C-12), 1.33(m, 8H, C-13,14), 0.88(t, 6H, C-15).

^{13}C NMR (125 MHz, $CDCl_3$, ppm) δ: 184.77(C=S), 163.06(CH=N), 143.43(C-5), 133.48(C-4,6), 129.40(C-3,7), 128.61(C-2), 32.96(C-1), 31.56(C-10), 29.37(C-11), 28.77(C-12), 22.74(C-13), 21.94(C-14), 14.20(C-15).

UV-Vis spectrum [$CHCl_3$, λ_{max} nm (log ε, L mol^{-1} cm^{-1})]: 238(4.12), 267(4.23), 322(4.39), 355(4.35), 435(4.57).

HRMS(FAB) Calc. for $C_{30}H_{42}N_4ZnS_4$ (M+1): 651.1584; Found(M+1): 651.1659.

Molar conductivity (1.0×10^{-5} M; $CHCl_3$, $\Omega^{-1}cm^2mol^{-1}$): 0.00; μ_{eff} = Diamagnetic.

3.3.4 Bis[S-hexyl 3-(4-methylbenzylidene)dithiocarbazato-κ^2N^3,S]cadmium(II), 5

Yellow, Yield: 48 %; m.p. (136 -138 ^oC). *Anal. Calc.* for $C_{30}H_{42}N_4CdS_4$: C, 51.52; H, 6.05; N, 8.01; S, 18.34 %. Found: C, 51.55; H, 6.06; N, 8.01; S, 18.36 %.

Selected IR data (KBr dics, cm^{-1}): ν(C-H,alkyl) 2918m, ν(C=N) 1590s, ν(N-N) 1034s, ν(CSS) 810m, ν(M-N) 537, ν(M-S) 474.

^1H NMR (500 MHz, $CDCl_3$, ppm) δ: 7.79(s, 2H, CH=N), 7.95(d, 4H, C-4,6, J=8.0 MHz), 7.20(d, 4H, C-3,7, J=8.0 MHz), 3.01(t, 4H, $-SCH_2$), 2.36(s, 6H, C-1), 1.70(p, 4H, C-11), 1.61(p, 4H, C-12), 1.27(m, 8H, C-13,14), 0.87(t, 6H, C-15).

^{13}C NMR (125 MHz, $CDCl_3$, ppm) δ: 176.19(C=S), 162.26(CH=N), 142.51(C-5), 130.35(C-4,6), 128.29 (C-3,7), 129.32(C-2), 35.64(C-1), 32.54(C-10), 31.52(C-11), 29.65(C-12), 22.69(C-13), 21.74(C-14), 14.17(C-15).

UV-Vis spectrum [$CHCl_3$, λ_{max} nm (log ε, L mol^{-1} cm^{-1})]: 244(4.15), 338(4.85).

HRMS(FAB) Calc. for $C_{30}H_{42}N_4CdS_4$ (M+1): 701.1326; Found(M+1): 701.1411.

Molar conductivity (1.0×10^{-5} M; $CHCl_3$, $\Omega^{-1}cm^2mol^{-1}$): 0.00; μ_{eff} = Diamagnetic.

3.3.5 Bis[S-hexyl 3-(4-methylbenzylidene)dithiocarbazato-κ^2N^3,S]palladium(II), 6

Orange red, Yield: 64 %; m.p. (159 -161 ^oC). *Anal. Calc.* for $C_{30}H_{42}N_4PdS_4$: C, 51.97; H, 6.11; N, 8.08; S, 18.50 % ; Found: C, 51.99; H, 6.11; N, 8.09; S, 18.51 %.

Selected IR data (KBr dics, cm^{-1}): ν(C-H, alkyl) 2926m, ν(C=N) 1596s, ν(N-N) 1031s, ν(CSS) 813m, ν(M-N) 506, ν(M-S) 404.

^1H NMR (500 MHz, $CDCl_3$, ppm) δ: 7.62(s, 2H, CH=N), 7.53(d, 4H, C-4,6, J=7.50 MHz), 7.14(d, 4H, C-3,7, J=8.00 MHz), 3.06(t, 4H, $-SCH_2$), 2.41(s, 6H, C-1), 1.74(p, 4H, C-11), 1.44(p, 4H, C-12), 1.33(m, 8H, C-13,14), 0.88(t, 6H, C-15).

^{13}C NMR (125 MHz, $CDCl_3$, ppm) δ: 179.53(C=S), 161.71(CH=N), 143.16(C-5), 131.55(C-4,6), 129.35(C-2), 128.54(C-3,7), 35.16(C-1), 31.52(C-10), 29.54(C-11), 28.62(C-12), 22.69(C-13), 21.95(C-14), 14.20(C-15).

UV-Vis spectrum [$CHCl_3$, λ_{max} nm (log ε, L mol^{-1} cm^{-1})]: 247(4.57), 305(4.62), 367(4.22).

HRMS(FAB) Calc. for $C_{30}H_{42}N_4PdS_4$ (M+1): 693.1327; found(M+1): 693.1404.

Molar conductivity (1.0×10^{-5} M; $CHCl_3$, $\Omega^{-1}cm^2mol^{-1}$): 0.00; μ_{eff} = Diamagnetic.

3.3.6 Bis[S-hexyl 3-(4-methylbenzylidene)dithiocarbazato-κ^2N^3,S]lead(II), 7

Pale yellow, Yield: 55 % ; m.p. (140 -142 ^oC). *Anal. Calc.* for $C_{30}H_{42}N_4PbS_4$: C, 45.37; H, 5.33; N, 7.06; S,16.15 %; Found: C, 45.40; H, 5.34; N, 7.08; S,16.17 %.

Selected IR data (KBr dics, cm^{-1}): ν(C-H, alkyl) 2924m, ν(C=N) 1604s, ν(N-N) 1033s, ν(CSS) 817m, ν(M-N) 509, ν(M-S) 407.

^1H NMR (500 MHz, $CDCl_3$, ppm) δ: 8.08(s, 2H, CH=N), 7.58(d, 4H, C-4,6, J=8.0 MHz), 7.12(d, 4H, C-3,7, J=8.0 MHz), 2.93(t, 4H, $-SCH_2$), 2.41(s, 6H, C-1), 1.71(p, 4H, C-11), 1.41(p, 4H, C-12), 1.29(m, 8H, C-13,14), 0.87(t, 6H, C-15).

^{13}C NMR (125 MHz, $CDCl_3$, ppm): 176.19(C=S), 162.26(CH=N), 142.51(C-5), 130.35(C-4,6), 129.96(C-2), 128.29(C-3,7), 35.38(C-1), 34.16(C-10), 31.55(C-11), 28.80(C-12), 22.75(C-13), 21.77(C-14), 14.22(C-15).

UV-Vis spectrum[$CHCl_3$, λ_{max} nm (log ε, L mol^{-1} cm^{-1})]: 244(4.17), 338(4.90).

HRMS(FAB) Calc. for $C_{30}H_{42}N_4PbS_4$ (M+1): 795.2059; Found(M+1): 795.2125.

Molar conductivity (1.0×10^{-5} M; $CHCl_3$, $\Omega^{-1}cm^2mol^{-1}$): 0.00; μ_{eff} = Diamagnetic.

3.4 Results and discussion

3.4.1 S-hexyl 3-(4-methylbenzylidene)dithiocarbazate, 1

The reaction of 4-methylbenzaldehyde with S-hexyldithiocarbazate afforded the Schiff base ligand **1**. The IR spectra of **1** (**Section 3.2**) showed a medium band at 3101 cm^{-1} for ν(N-H) and two strong bands at 1619 and 1101 cm^{-1} are assigned to the ν(C=N) and ν(C=S) stretching vibrations, respectively [8,9]. However, the ligand does not exhibit any ν(S-H) band around 2700 cm^{-1}, indicating that in solid state it maintains the thione functional group [8,10]. The ν(N=N) is observed in the free ligand at 1026 cm^{-1} [2]. The ligand also exhibited a medium band at 871 cm^{-1} for the ν(CSS) stretching mode [11].

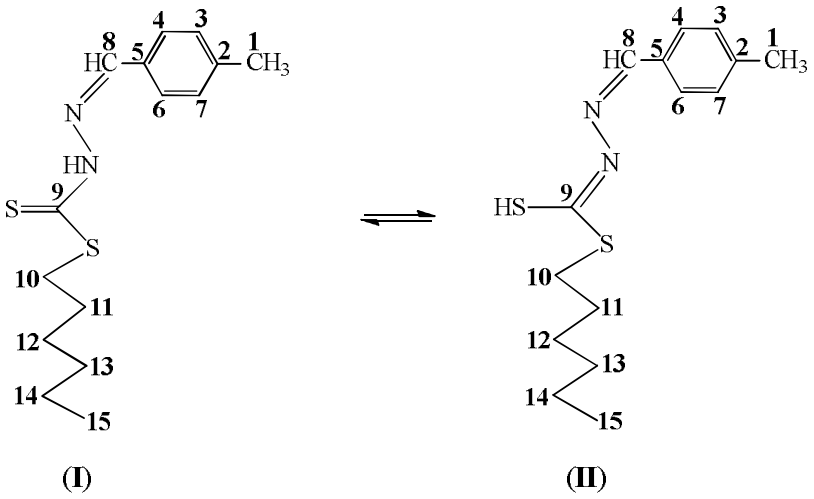

Scheme 3.1: Thione (I) and thiol (II) tautomeric forms of HL **(1)**

The ^{1}H NMR of ligand **1** (**Section 3.2**) showed a broad singlet at 11.01 ppm assigned to the (N-H) proton [9]. Usually these species may exist in solution as an equilibrium mixture between the thione and thiol tautomeric forms. It is worth noting that the ligand **1** does not display any signal for the SH proton (~ 4.0 ppm), indicating the absence of the thiol form [8,12].

The ligand **1** exhibited a singlet at 7.93 ppm for the azomethine (CH=N) proton [11]. For the ligand the signals due to the aromatic ring protons appeared as two doublets referred to (C-4,6) and (C-3,7) at 7.62 and 7.21 ppm respectively. The ligand showed one triplet at 3.31 ppm for the -SCH_2 proton (C-10) [13,14] and one singlet at 2.42 ppm for the -CH_3 (C-1) protons [13**,** 15, 16]. Two pentaplets and one multiplet are also showed at 1.76 (C-11), 1.47 (C-12) and 1.34 (C-13,14) ppm, respectively for ligand as well as another singlet at 0.91 ppm for -CH_3(C-15) protons of hexyl (-C_6H_{13}) chain.

The ^{13}C NMR signals of the ligand **1** (**Section 3.2**) are observed at 199.33 and 162.04 ppm for (C=S) and (CH=N) carbons, respectively [13,17,18]. In the ligand the aromatic carbons are observed at 141.84(C-5), 129.66(C-4,6), 128.69(C-2), 127.99(C-3,7) ppm [13]; the methyl carbon(C-1) at 34.68 ppm [16] and the alkyl carbons fall at 31.53(C-10), 28.85(C-11), 28.67(C-12), 22.66(C-13), 21.74(C-14), 14.17(C-15) ppm.

The mass spectral data by FAB method of the compound **1** (**Section 3.2**) has been given in above, in its High Resolution Mass Spectrum (HRMS) showed peak at m/z of 295.1302 which consisted with the proposed formula.

The solution UV-Vis spectrum of compound **1** (**Section 3.2**) showed bands at 241 and 262 nm, assigned to the $\pi \rightarrow \pi^*$ transitions for the aromatic ring and azomethine (CH=N) moiety, respectively [18]. Another two bands at 325 and 338 nm are assigned to $\pi \rightarrow \pi^*$ and $n \rightarrow \pi^*$ transitions of the dithiocarbazate group [17,18].

3.4.2 Bis[S-hexyl 3-(4-methylbenzylidene)dithiocarbazato-κ^2N^3,S]M(II) complexes 2-7

Reaction of the ligand **1** with divalent metal ions M(II) [M = Ni, Cu, Zn, Cd, Pd and Pb] in a 2:1 molar ratio in methanol, accompanied by mono-deprotonation, resulted in the formation of bischelated complexes. The *Lasign's* test (halogen test) indicated the absence of chloride ions in the Pd(II) complex **6**, suggesting the uni-negative bidentate complexation of the Schiff bases. All the compounds were soluble in non-coordinating organic solvents such as $CHCl_3$, CH_2Cl_2, DMSO and DMF. The room temperature molar conductance values of the complexes (10^{-5} M solution in $CHCl_3$) indicated their non-electrolytic nature [8].

In the infrared spectra of complexes **2-7** (as shown in **Section 3.3**) the band at around 3101 cm^{-1} is absent, indicating the deprotonation of the NH proton and that the coordination of anionic ligand have taken place in the enol form [8,12,19]. Correspondingly the absence of the ν(C=S) band in the complexes is an unauthentic evidence for the formation of complexes via the enol group [12,19]. In the complexes the ν(C=N) band appeared at (1604-1583 cm^{-1}), which falls at lower frequency with respect to the ligand, is an evidence for the coordination of the ligand to the metal atom through the azomethine nitrogen [12]. The shift of the ν(N-N) band of the free ligand to higher frquency in the spectra of the complexes supports the suggestion of azomethine nitrogen bonding to the metal ions [2,9,10]. The stretching frequency of ν(CSS) in the complexes decreases (817-803 cm^{-1}) as compared to that observed in the ligand, indicating that complexation have taken place through thiolate sulphur atom [4, 11].

Furthermore, the presence of two new bands at (537-506 cm^{-1}) and (474-399 cm^{-1}) assigned for ν(M-N) and ν(M-S) respectively, is also an indication of the bonding of metal through azomethine nitrogen and thiolate sulfur donor [20].

The absence of NH signal in the ^{1}H NMR spectra for complexes **2-7** (**Section 3.3**) indicates the complexation via deprotonation of this group [17]. Both in solid state and in solution, the Schiff bases remain in their thione form, but in the presence of metal(II) ions, the ligand is deprotonated and coordinates the metal *via* the enol form forming stable complexes, ML_2 (where HL corresponds to the neutral form of the Schiff base ligand). The ready conversion of the Schiff base from the thione to the thiol form in the presence of metal ions, followed by deprotonation and coordination to the metal, may be attributed to the extra stability gained through the π-electron delocalization along the -C-N-N-C-S- chains of the dithiocarbazate moieties. The thione-to-thiol evolution in the presence of metal ions has been found regularly to happen to Schiff bases derived from S-alkyl/S-aryl dithiocarbazates [21].

In the ^{1}H NMR spectra of complexes **2-7** (**Section 3.3**) the azomethine proton appeared at higher field (7.62-7.79 ppm) in the complexes as compared to the free ligand **1** (7.93 ppm), due to the coordination of azomethine nitrogen [11,17,18, 22]. The signals due to the aromatic ring protons appeared as two doublets for (C-4,6) and (C-3,7) at 7.62 and 7.21 ppm respectively, in the ligand are shifted to (7.53-8.12 ppm) and (7.13-7.20 ppm) in the complexes. Another singlet at 3.31 ppm for $-SCH_2$ proton exhibited by the ligand was shifted to (3.01-3.12 ppm) in the complexes [13,14]. Moreover, the triplet at 2.42 ppm for the $-CH_3$ protons in the ligand also shifted upfield (2.36 -2.41) ppm as a result of complexation [13,15,16]. No significant change was observed for the proton attached at C-1 up to C-6 of the alkyl moiety in the complexes. However, the ^{1}H NMR spectra for Cu(II) complex **3** was not helpful for the identification of the functional group having the metal ion a paramagnetic electron configuration [15].

The ^{13}C NMR data in solution confirm the structure of the complexes as observed in solid state by X-ray diffraction.

The mass spectral data by FAB method of the compound **2-7** have been given in **Section 3.3**. The molecular ion peaks of Ni(II), Cu(II), Zn(II), Cd(II), Pd(II) and Pb(II) complexes **2-7** are at m/z 645.1728, 650.1664, 651.1659, 701.1411, 693.1404 and 795.2125, respectively as confirmed by HRMS, suggested the formation of bis-chelated complexes of the Schiff base ligand **1.**

In the UV-Vis spectra of the Ni(II), Cu(II), Zn(II) and Pd(II) complexes (**Section 3.3**) the thioamide n → π* intra–ligand bands are shifted to high energy (blue shift) upon coordination of the thiol sulphur to the metal [22]. The band in the region (443-435 nm) can be assigned to the S → M LMCT charge transfer. The appearance of this LMCT band in Ni(II), Cu(II) and Zn(II) complexes is also strong evidence that metal is coordinated to sulfur through the thiol sulfur [6,23].

The diamagnetic nature of the Ni(II) and Pd(II), consistent with the d^8 configuration, suggested a square planar geometry [18,22], although d^8 metal ions in this coordination environment are expected to exhibit three bands corresponding to the $^1A_{1g} \rightarrow {}^1A_{2g}$, $^1A_{1g} \rightarrow {}^1B_{1g}$ and $^1A_{1g} \rightarrow {}^1E_{1g}$ transitions [18,22]. However, such transitions are usually not observed since the strong S → *M* LMCT bands of ligands containing chalcogen donor atoms mask the expected *d-d* bands [18,22].

The diamagnetic Zn(II) and Cd(II) complexes, consistent with a d^{10} metal ion configuration, do not show *d-d* transition suggested tetrahedral geometry [18]. Also the diamagnetic Pb(II) complex exhibits a tetrahedral geometry [24]. The spectrum of Cu(II) complex showed a very broad weak band at 517 nm is assigned to the $^2B_1 \rightarrow {}^2A_1$ transition, diagnostic of square planar geometry [17]. The Cu(II) complex has magnetic moment of 1.82 B.M. corresponding to a single electron spin [17].

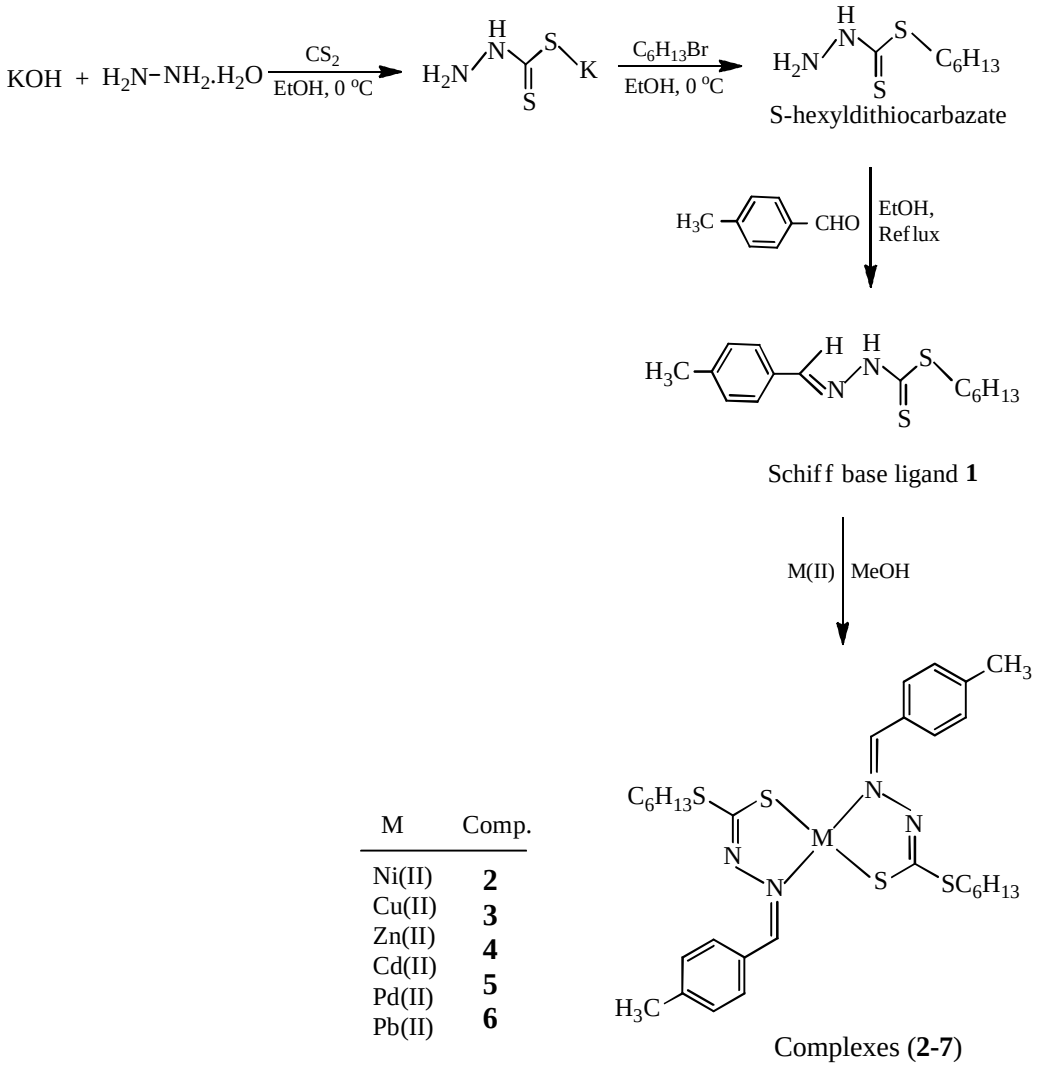

M	Comp.
Ni(II)	**2**
Cu(II)	**3**
Zn(II)	**4**
Cd(II)	**5**
Pd(II)	**6**

Scheme 3.2: Synthetic route for the preparation of ligand **1** and the metal complexes **2-7**

3.5 X-ray data collection and crystal structure determination

Crystal structure analyses of the compounds reported were carried out at 100 K for **1** and **2** and 173 K for **6** on a Rigaku R-AXIS RAPID diffractometer equipped with CCD and Cu-Kα radiation (λ = 1.54187 Å). Cell refinement, indexing and scaling of the data sets were done by using Crystal Structure Rigaku programs [25]. An empirical absorption correction was applied [transmission factors of (0.615, 0.811), (0.615, 0.932) and (0.280, 0.456) for **1**, **2** and **6**, respectively. All the structures were solved by using SIR92 [26] and subsequent Fourier analyses [27] and refined by the full-matrix least-squares method based on F^2 with all observed reflections [27]. The H atoms were fixed at geometrical positions except that of nitrogen N(2) in **1** which was located on the Fourier map and refined.

The ORTEP drawings were done by using the WinGX System, Ver 1.80.05 [28]. Crystal data and details of refinements are given in **Table 3.1**.

3.5.1 Crystal structure description of ligand and of NiL_2 and PdL_2 complexes

The molecular and crystal structures of Schiff base ligand S-hexyl 3-(4-methylbenzy lidene)dithiocarbazate (HL), its NiL_2 and PdL_2 complex were determined by single crystal X-ray diffraction method.

The ORTEP drawing of the ligand **1**, which crystallizes in triclinic system space group $P\bar{1}$, is shown in **Fig. 3.1**. The dithiocarbazate group adopts an E configuration with respect to the C=N bond of the benzylidene moiety. The *β*-nitrogen and the thioketo sulphur are *trans* located with respect to the C(9)-N(2) bond. The molecule is in its thione tautomeric and the co-planarity of atoms (with the exception of the S-hexyl chain) indicates an electron delocalization within it. **Table 3.3** lists a selection of bond distances and angles which are compared to the correspondent geometrical parameters measured in the nickel complex.

Upon coordination some salient features are observed with respect to the free ligand **1**, and the most significant are an elongation of the C(9)-S(1) bond length 1.720(4) and 1.777(17) Å in **2** and **6** respectively, that must be compared to of 1.670(3) Å measured

in HL, thus validating the coordination with deprotonated thiolate sulfur atom. Correspondingly the N(2)-C(9) bond length, of 1.335(3) Å, shortens to 1.270(6) and 1.282(15) Å in the **2** and **6** complex, respectively while the N(1)-N(2) bond length of 1.375(3) Å in HL is slightly elongated in the complexes (1.426(5) and 1.404(17) Å, **Table 3.2**).

The crystal packing evidences the ligand molecules piled along axis *a* and connected in pair by N2-H…S1 hydrogen bonds (H…S = 2.56 Å, N…S = 3.3760(1) Å, O–H…S angle = 168°) as shown in **Fig. 3.2**. On the other hand no appreciable π–π interaction among aromatic rings is present in the crystal packing. It is obvious that the free ligand requires a rotation about the C9-N2 by 180° in order to allow the N,S chelating behavior towards the metal.

The corresponding bis-chelated Ni(II) complex **2** crystallizes in triclinic system, space group $P\bar{1}$. **Fig. 3.3** depicts an ORTEP drawing of the metal complex while a selection of coordination bond lengths and angles is reported in **Table 3.3**. The metal is located on a crystallographic inversion center and the two Schiff bases, in their deprotonated imino thiolate form chelate the metal centre via the azomethine nitrogen N(1) and thiolate sulfur S(1) atoms in a trans-planar configuration as imposed by the crystal symmetry. The complex has coplanar geometry with the exception of the hexyl chains that are pendant from the bischelated moiety. In the NiL_2 complex, the Ni–S(1) and Ni-N(1) bond distances are of 2.1777(11) and 1.933(4) Å, respectively, with a S(1)-Ni-N(1') chelating angle of 86.06(10)°. These geometrical parameters agree with those reported for other nickel complexes showing no significant changes (or within their esd's) either when ligands assume a trans [17,18,29] or a cis configuration [9,30].

The complexes stack at a distance of 4.6738(3) Å (axis *a*), which exclude any significant interactions between the aromatic rings.

The bis-chelated Pd(II) complex **6** crystallizes in monoclinic system, space group *C*2. **Fig. 3.5** depicts an ORTEP drawing of the metal complex while a selection of coordination bond lengths and angles is reported in **Table 3.3**. The metal is located on a crystallographic two-fold and the two Schiff bases, in their deprotonated imino thiolate form chelate the metal centre via the azomithine nitrogen N(1) and thiolate sulfur S(1) atoms in a cis-planar configuration as imposed by the crystal symmetry (bond angles S(1)-Pd-S(1') = 87.3(2)°, N(1)-Pd-N(1') = 107.1(6)°). The complex does not exhibit a coplanar arrangement as that observed for the nickel derivative, but the square planar coordination geometry is slightly tetrahedrally distorted (displacement of N and S donors of $\pm$0.13 Å from the coordination mean plane). The centroid-to-centroid distance between the rings of the methylbenzy lidene moieties are at 4.114 Å, indicating an intramolecular π-π stacking interaction. The Pd-S(1) and Pd-N(1) coordination bond distances are of 2.264(4) and 2.154(12) Å, respectively, with a S(1)-Pd-N(1) chelating angle of 83.2(3)°. These values are in agreement with those observed in similar Pd-bis(dithiocarbazato) complexes either in *cis* [31-36] and *trans* configuration [31,37-39]. These different configurations seem addresses by the packing forces and by the substituents present on the Schiff base ligand.

In addition the configuration of dithiocarbazate group about the imine bond N1=C8 is E in the Pd(II) complex **6** and Z in Ni(II) complex **2**. In fact the torsion angle N2–N1–C8 –C5 in 6 is 172.1(14)°, different from that observed in the nickel derivative **2** of 1.2(7)°. This allows an approach between the rings of the methylbenzylidene moieties, with a centroid-to-centroid distance of 4.114(8) Å, indicating a very weak π-π interaction.

The crystal packing of **6** shows a wavy arrangement of complexes (**Fig. 3.6**). In **Fig. 3.7** it is depicted a comparison between the complexes showing the different conformation and orientation assumed by the ligands with respect the square planar coordination plane in the Ni(II) and Pd(II) complex.

Table 3.1 Crystallographic data and details of refinement for compounds **1, 2** and **6**.

	1	**2**	**6**
Empirical formula	$C_{15}H_{22}N_2S_2$	$C_{30}H_{42}N_4NiS_4$	$C_{30}H_{42}N_4PdS_4$
Fw	294.47	645.63	693.33
Crystal system	Triclinic	Triclinic	Monoclinic
Space group	$P\bar{1}$	$P\bar{1}$	$C2$
a, Å	4.79244(9)	4.6738(3)	18.3559(11)
b, Å	11.3790(2)	10.5132(5)	9.6747(6)
c, Å	14.5382(3)	16.4789(8)	10.3368(7)
α, deg	100.1666(7)	86.522(3)	
β, deg	91.2117(7)	84.850(3)	116.810(3)
γ, deg	94.6754(7)	79.057(3)	
V, Å^3	777.26(3)	790.99(7)	1638.36(17)
Z	2	2	2
Dcalcd,g cm^{-3}	1.258	1.355	1.405
μ(Cu-Kα), mm^{-1}	2.996	3.545	7.134
F(000)	316	342	720
θ max, deg	68.20	68.22	66.98
No. of reflections collected	8970	5923	9607
No. of independent reflections	2802	2834	2891
R_{int}	0.0519	0.0744	0.1201
No. of reflections ($I > 2\sigma(I)$)	2162	2030	2160
Refined parameters	176	178	177
goodness-of-fit (F^2)	1.043	1.083	1.033
R1 ($I>2\sigma(I)$) [a]	0.0463	0.0718	0.091
wR2 (all data) [a]	0.1285	0.2207	0.2430
Residuals, e/Å^3	0.430, –0.260	0.990, –0.360	2.090, –1.310

[a] $R1 = \Sigma \big| |Fo| - |Fc| \big| / \Sigma |Fo|$, $wR2 = [\Sigma w (Fo^2 - Fc^2)^2 / \Sigma w (Fo^2)^2]^{1/2}$

Table 3.2: Selected bond lengths (Å) and angles (°) of **1** and of the coordinated ligand in the complex **2** and **6**

	1	**2**	**6**
S(1)-C(9)	1.670(3)	1.720(4)	1.777(17)
S(2)-C(9)	1.759(3)	1.756(4)	1.747(16)
N(1)-N(2)	1.375(3)	1.426(5)	1.404(17)
N(1)-C(8)	1.277(3)	1.296(6)	1.208(16)
N(2)-C(9)	1.335(3)	1.270(6)	1.282(15)
N(2)-N(1)-C(8)	115.97(18)	113.9(3)	114.2(12)
N(1)-N(2)-C(9)	120.61(18)	111.9(3)	115.8(16)
S(1)-C(9)-S(2)	126.25(13)	113.9(3)	109.6(9)
S(1)-C(9)-N(2)	120.30(17)	125.9(3)	125.6(15)
S(2)-C(9)-N(2)	113.44(17)	120.2(3)	124.7(15)

Table 3.3: Coordination bond lengths (Å) and angles (°) of **2** and **6**

	2		**6**
Ni-S(1)	2.1777(11)	Pd-S(1)	2.264(4)
Ni-N(1)	1.933(4)	Pd-N(1)	2.154(12)
S(1)-Ni-N(1')	86.06(10)	S(1)-Pd-S(1')	87.3(2)
S(1)-Ni-N(1)	93.94(10)	N(1)-Pd-N(1')	107.1(6)
S(1)-Ni-S(1')	180.0	S(1)-Pd-N(1)	83.2(3)
N(1)-Ni-N(1')	180.0	S(1)-Pd-N(1')	168.1(3)

Primed atoms at -x, -y, -z (for Ni complex) and 1-x, y, -z (for Pd complex)

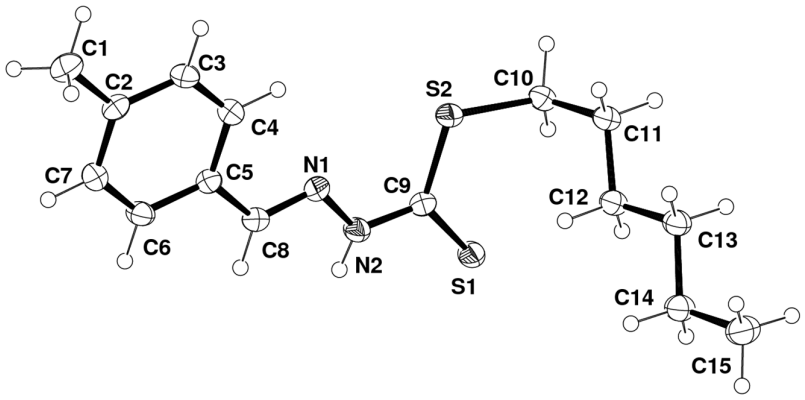

Fig. 3.1: ORTEP drawing (ellipsoid probability at 50 %) of ligand **1**.

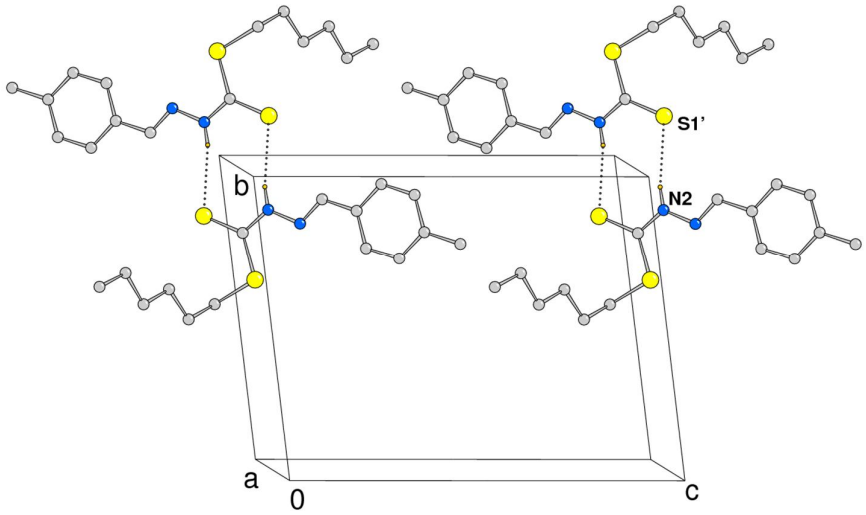

Fig. 3.2: Crystal packing of the Schiff base ligand **1** showing pair of molecules connected by N-H…S interactions (Hydrogen atoms omitted for clarity except those involved in H bonds).

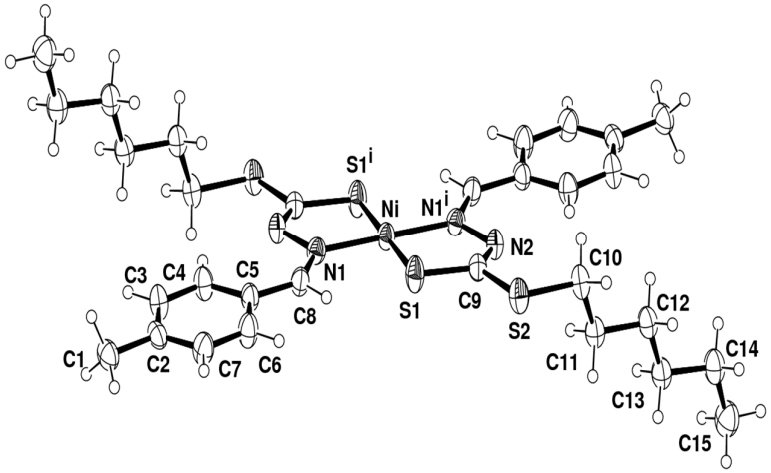

Fig. 3.3: ORTEP drawing (ellipsoid probability at 50%) of the centrosymmetric NiL_2 complex, **2**.

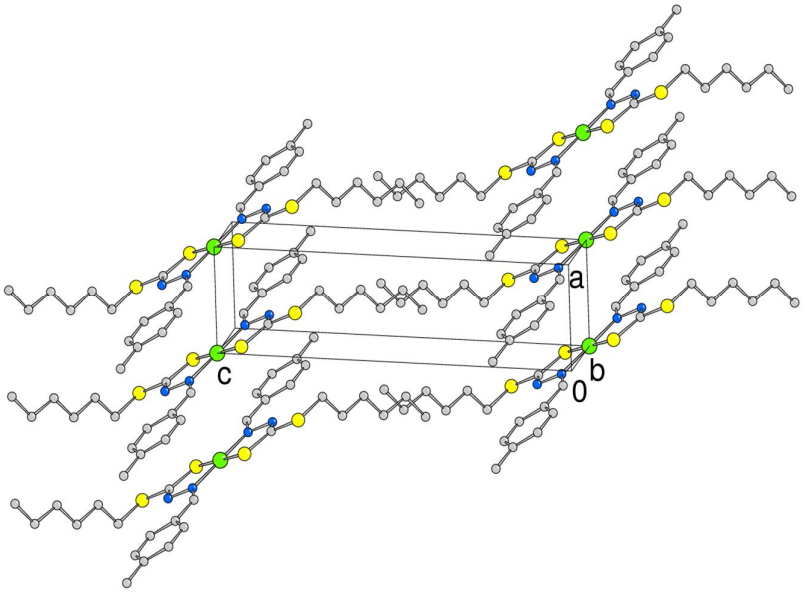

Fig. 3.4: Crystal packing of the NiL_2 complex **2** (Hydrogen atoms omitted for clarity).

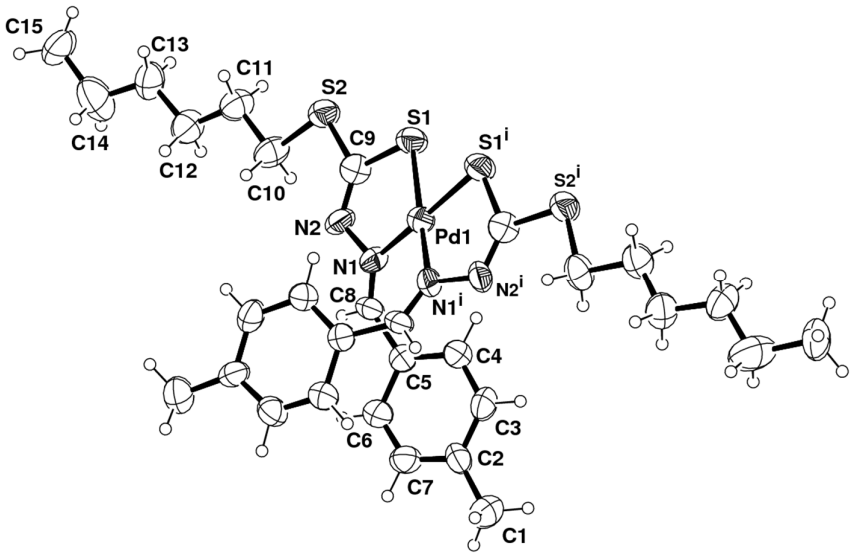

Fig. 3.5: ORTEP drawing (40% ellipsoid probability) of PdL_2 complex, **6**

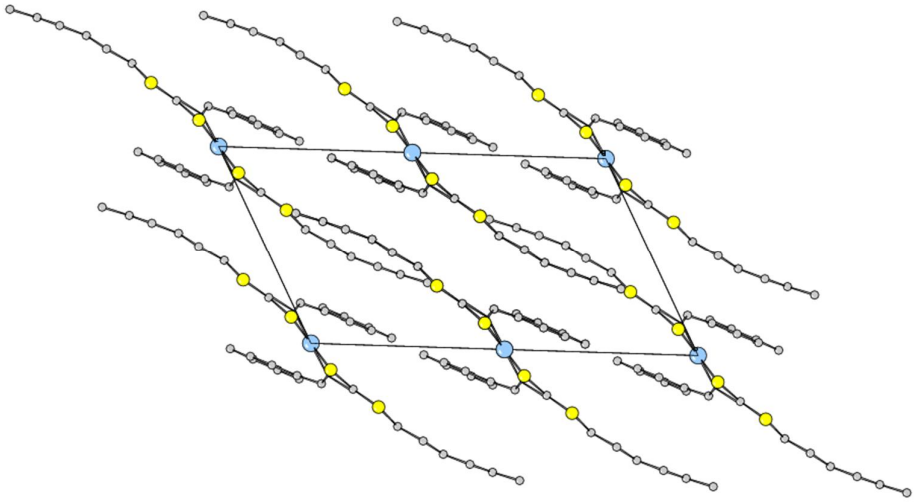

Fig. 3.6: Crystal packing viewed down axis *b* of PdL_2 complex, **6**
(Hydrogen atoms omitted for clarity except those involved in H bonds).

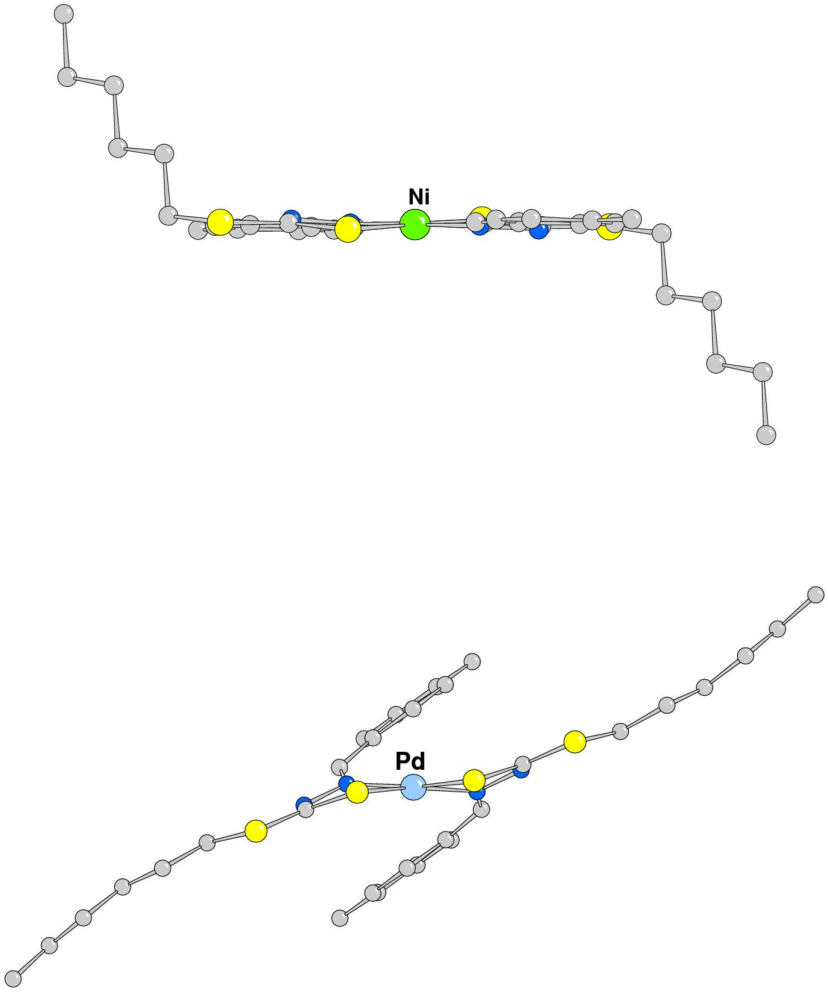

Fig. 3.7: The different conformation assumed by the ligands with respect the square planar coordination plane in the NiL_2 (**2**) and PdL_2 (**6**) complexes.

3.6 Fluorescence spectral study

The photoluminescence properties of Schiff base ligand **1** and its metal complexes **2-7** were studied at room temperature in $CHCl_3$. Upon excitation at 338 nm, the emission spectrum of the ligand shows three emission peaks at λ_{max}= 406, 430 and 452 nm (**Table 3.4** and **Fig. 3.8**). Excitation of the metal complexes at 305-376 nm gives an emission at 396-460 nm (each complex contains 3 emission peaks within this range).

The emission spectral shape of all the complexes closely resembled that of the ligand (**Fig. 3.8**).

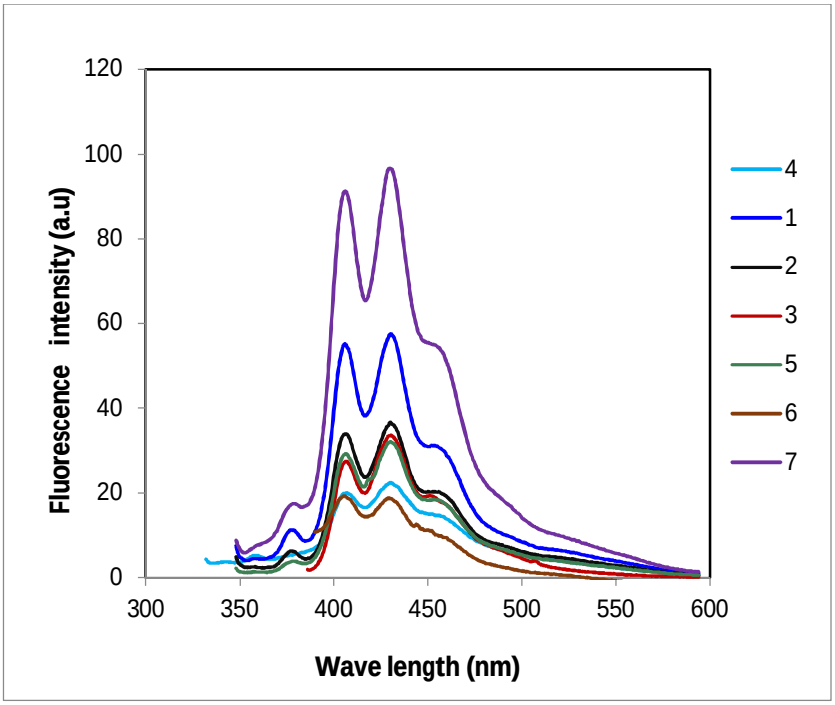

Fig. 3.8: Emission spectra of compounds **1-7** of 10^{-5} M solution in $CHCl_3$ at room temperature

It is evident from **Fig. 3.8** that the fluorescence emission intensity of the ligand decreases dramatically depending on the complex **2-6** formation with the metal ions with the exception of complex **7**. Metal ions can enhance or quench the fluorescence emission of some Schiff base ligands containing an aromatic ring. The decrease of emission intensities is due to the formation of coordination complexes of the S and N atom in the ligand with the metal ion. These coordination complexes make the energy transfer from the excited state of the ligand to the metal ions causing decreases of the fluorescence intensity [40]. For this reason the intensity of complexes **2-6** is decreased. Quenching of fluorescence of a ligand by transition metal ions during complexation is a rather common phenomenon which is explained by processes such as magnetic perturbation, redox activity, and electronic energy transfer [7,23,40,41].

Enhancement of fluorescence through complexation is, however, of much interest as it opens up the opportunity for photochemical applications of these complexes. In the absence of metal ions the fluorescence of the ligand is probably quenched by the occurrence of a photo induced electron transfer (PET) process due to the presence of lone pair of electrons of the donor atoms. Such a pet process is prevented by the complexation of ligand with the metal ions; thus the fluorescence intensity may be greately enhanced by the coordination of the metals. The chelation of the ligand to the metal increases the rigidity of the ligand and thus reduces the loss of energy by thermal vibration decay [42].

Table 3.4: Excitation wavelength dependent emissions of compounds **1-7**

Compound	Excitation wavelength (nm)	Peak wavelength of emission (nm)
1	338	406, 430, 452
2	338	406, 430, 453
3	376	407, 430, 460
4	355	396, 441
5	376	406, 430, 453
6	305	340, 405, 429
7	338	406,430,459

3.7 Electrochemical studies

The potential scanning of the Cu(II) compound **3** was performed using a Pt disk electrode (ϕ=2mm) in presence of tetra-n butylammonium tetrafluoroborate supporting electrolyte at scan rate of 25 mVs^{-1}. From the voltammogram shown in **Fig. 3.9**, the common diagnostic criteria for that redox reaction, namely the peak potential difference (E_{pa}-E_{pc}) about 230 mV and I_{pc}/Ipa = 3.5 indicate that the redox reaction of compound **3** is an apparently quasi-reversible, one electron redox process in under the experimental condition. During cathodic scan at -0.39V, Cu(II) is reduced to Cu(I) providing highly intense wave , however, when the potential scanning is reverted from -0.6V, an anodic wave is developed giving maximum intensity at -0.16V where Cu(I) is

oxidized to Cu(II) species. It was seen that even at faster scan rates (ν > 100 mVs^{-1}), I_{pc}/I_{pa} ratio was not significantly altered. This observation suggests that reduced form of the Cu(II) complex is probably unstable at the cathodic potential and undergo some irreversible chemical or structural changes.

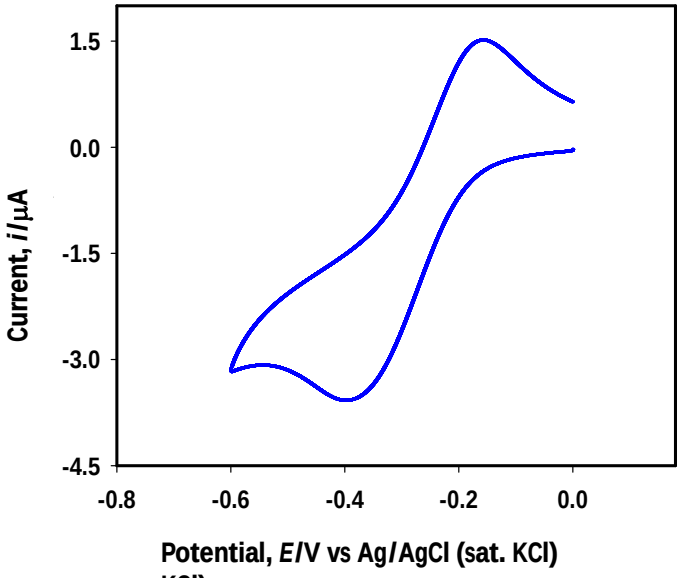

Fig. 3.9: Cyclic voltammetry of Cu(II) complex **3** at a scan rate using a Pt disk electrode in presence of $[(n\text{-But})_4N]BF_4$ as supporting electrolyte in $CHCl_3$. Scanning was performed against Ag/AgCl (sat. KCl) reference electrode.

In order to ensure electron transfer properties, Electrochemical Impedance Spectral (EIS) measurements were next performed at -0.45V within the frequency range of 0.01 kHz to 100 kHz. **Fig. 3.12** shows the Nyquist plots and corresponding Bode module and Bode phase are displayed in **Fig. 3.11** and **3.12**, respectively. The higher frequency impedance indicates solution resistance (R_s) and the impedance, due to higher AC frequency, corresponds the resistance due to electron transfer (R_{et}). A rise of the impedance after the arc of the semicircle (at lower AC frequency region) indicates a diffusion process. According to **Fig. 3.10**, it is clear that the $[(n\text{-But})_4N]BF_4$ supporting electrolyte imparted higher electron transfer resistance both in the imaginary and in the real parts of the EIS spectra. When spectrum was recorded in the presence of Cu(II)

complex **3**, an arc was evolved. By considering the diameter of the arc (associated to the real part of the semicircle) it was confirmed that an ease of electron transfer from the electrode surface to the redox center of the metal complex was occurred, where the value of R_{et} was ca. 100 kΩ.

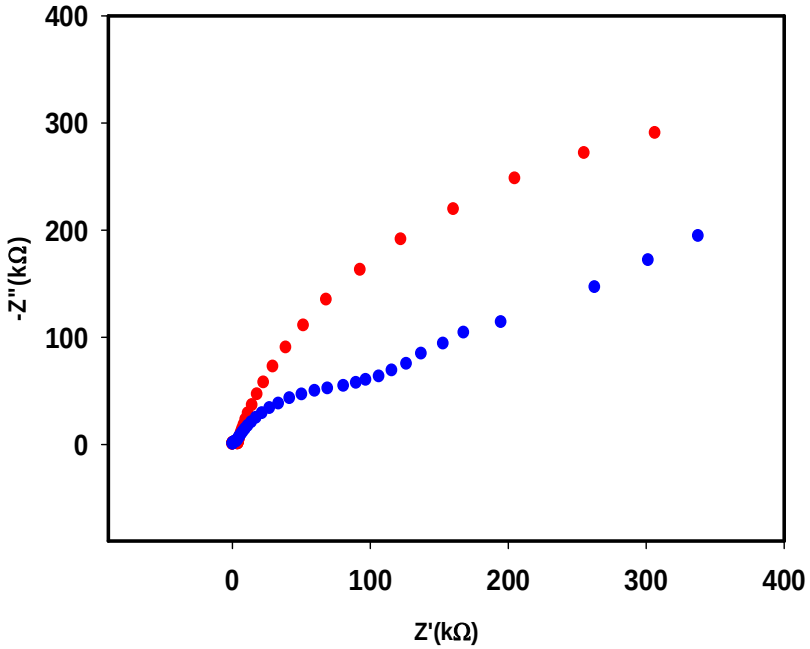

Fig. 3.10: Impedance spectra of Cu(II) complex **3** (blue dots) and $[(n\text{-But})_4N]BF_4$ (red dots).

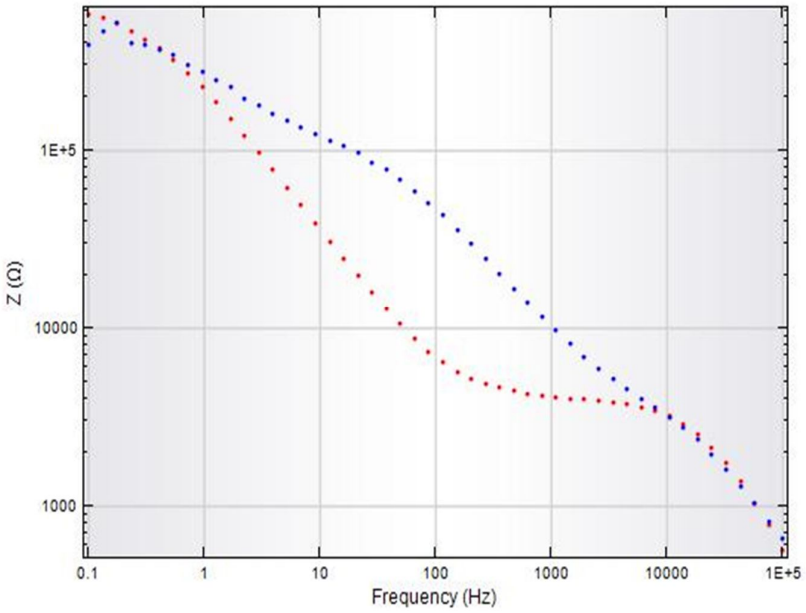

Fig. 3.11: Bode module of the Impedance spectra

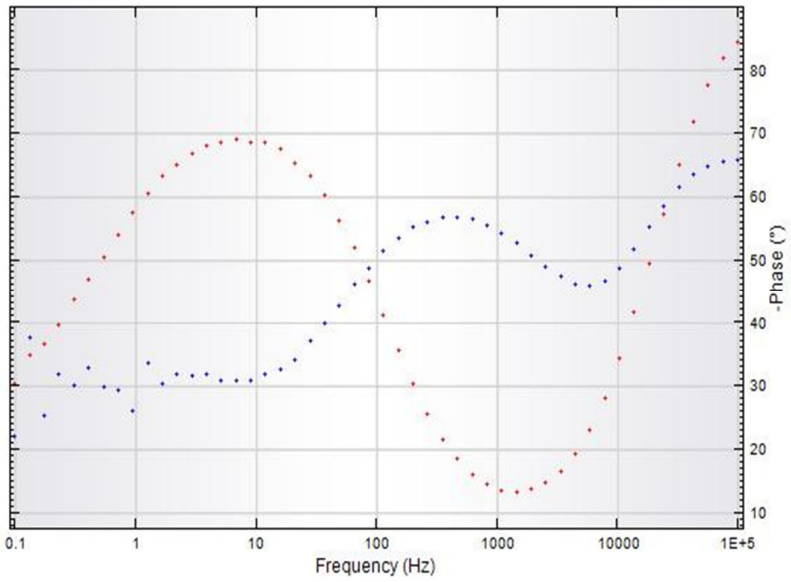

Fig. 3.12: Bode phase of the Impedance spectra.

References

1. M.A. Ali, A.H. Mirza, R.J. Fereday, R.J. Butcher, J.M. Fuller, S.C. Drew, L.R. Gahan, G.R. Hanson, B. Moubaraki, K.S. Murray, *Inorg. Chim. Acta.*, 358 (2005) 3937.
2. M.A. Ali, H.J.H. Abu Bakar, A.H. Mirza, S.J. Smith, L.R. Gahan, P.V. Bernhardt, *Polyhedron*, 27 (2008) 71.
3. A.B. Besir, S.K. Guchhait, J.A. Gascon, G. Fenteany, *Bioinorganic and Medicinal Chemistry Letters*, 18 (2008) 498.
4. R. Takjoo, R. Centore, M. Hakimi, S.A. Beyramabadi, A. Morsali, *Inorg. Chim. Acta.*, 371 (2011) 36.
5. N.K. Singh, S.K. Kushawaha, M.K. Bharty, R. Dulary, R. J Butcher, *J. Mol. Struct*., 936 (2009) 257.
6. M.A. Ali, A.L. Tan, A.H. Mirza, J.H. Santos, A.H.B.H. Abdullah, *Transition Met. Chem.*, 37 (2012) 651.
7. A. Majumder, G.M. Rosair, A. Mallick, N. Chattopadhyay, S. Mitra, *Polyhedron*, 25 (2006) 1753.
8. K.A. Crouse, K.-B. Chew, M.T.H Tarafder, A. Kasbollah, A.M. Ali, B.M. Yamin, H-K. Fun, *Polyhedron*, 23 (2004) 161.
9. M.H.E. Chan, K.A. Crouse, M.I.M. Tahir, R. Rosli, N. Umar-Tsafe, A.R. Cowley, *Polyhedron*, 27 (2008) 1141.
10. S. Roy, T.N. Mandal, A.K. Barik, S. Pal, S. Gupta, R.J. Butcher, M. Nethaji, S. Kar, *Polyhedron*, 27 (2008) 593.
11. R. Takjoo, R. Centore, L. Rhyman, P. Ramasami, *J. Coord. Chem*., 65 (2012) 1569.
12. K.B. Chew, M.T.H. Tarafder, K.A. Crouse, A.M. Ali, B.M. Yamin, H.-K. Fun, *Polyhedron*, 23 (2004) 1385.
13. T.B.S.A. Ravoof, K.A. Crouse, M.I.M. Tahir, F.N.F. How, R. Rosli, D.J. Watkins, *Transition Met. Chem.*, 35 (2010) 871.
14. Y.-P. Tian, C.-Y. Duan, Z.-L. Lu, X.-Z. You, *Transition Met. Chem.*, 21 (1996) 254.
15. Y.-J. Jang, U.K. Lee, B.-K. Koo, *Bull. Korean Chem. Soc*. 26 (2011) 925.

16. J.S. Kumaran, S. Priya, N. Jayachandramoni, S. Mahalakshmi, *J. Chem.* vol 2013, Article ID260358, 1.
17. M.A.A.A. Islam, M.C. Sheikh, M.S. Alam, E. Zangrando, M.A. Alam, M.T.H. Tarafder, R. Miyatake, *Transition Met. Chem.*, 39 (2014) 141.
18. M.A.A.A. Islam, M.T.H. Tarafder, M.C. Sheikh, M.A. Alam, E. Zangrando, *Transition Met. Chem.*, 36 (2011) 531.
19. R. Takjoo, R. Takjoo, M. Yazdanbakhsh, A.A. Kaju, C. Yaguang, *Chin. J. Chem.*, 28 (2010) 221.
20. M.T.H. Tarafder, M. Rahim, *Indian J. Chem.*, 28A (1989) 1105.
21. M.A. Ali, A. H. Mirza, M. Haniti S. A. Hamid, P. V. Bernhardt, *Polyhedron*, 24 (2005) 383.
22. M. Yazdanbaksh, R. Takzoo, W. Frank and A. A. kaju, *J. Coord. Chem.*, (2009) 1.
23. E.S. Aazam, A.F.EL Husseiny, H.M.A. Amri, *Arabian J. Chem.*, 5 (2012) 45.
24. S.A. Shaker, H.A. Mohammd, A.A. Salih, *Australian Journal of Basic and Applied Sciences*, 4 (2010) 5178.
25. Rigaku (2010). CrystalStructure. Version 4.0. Rigaku Corporation, Tokyo, Japan.
26. A. Altomare, G. Cascarano, C. Giacovazzo, A. Guagliardi, M. Burla, G. Polidori, M. Camalli, *J. Appl. Cryst.*, 27 (1994) 435.
27. G.M. Sheldrick, *Acta Crystallogr. Sect. A*, 64 (2008) 112.
28. L. J. Farrugia, *J. Appl. Crystallogr.*, 32 (1999) 837.
29. M.L. Zhang, Y.P. Tian, , X.J. Zhang, J.Y. Wu, S.Y. Zhang, D. Wang, M.H. Jiang, S. Chantrapromma, H.-K. Fun, *Transition Met. Chem.*, 29 (2004) 596.
30. S.L. Li, J.Y. Wu, Y.P. Tian, Y.W. Tang, M.H. Jiang, H.-K. Fun, S. Chantrapromma, *Opt Mater*, 28 (2006) 897.
31. K. Tampouris, S. Coco, A. Yannopoulos, S. Koinis, *Polyhedron*, 26 (2007) 4269.
32. T. Glowiak, T. Ciszewska, *Acta Crystallogr., Sect.* B, 38 (1982) 1735.
33. M.A. Ali, A.H. Mirza, R.J. Butcher, M.T.H. Tarafder, T.B. Keat, A.M. Ali, *J. Inorg. Biochem.*, 92 (2002) 141.

34. H.-P. Zhou, D.-M. Li, P. Wang, L.-H. Cheng, Y.-H. Gao, Y.-M. Zhu, J.-Y. Wu, Y.-P.Tian, X.-T. Tao, M.-H.Jiang, H.-K. Fun, *J. Mol. Struct.,* 826 (2007) 205.
35. Z.-D. Liu, X.-J. Zhang, J.-Y. Wu, F.-Y. Hao, H.-P. Zhou, Y.-P. Tian, *Polyhedron,* 30 (2011) 279.
36. C.-Y. Duan, Y.-P. Tian, Z.-H. Liu, X.-Z. You, T.C.W.Mak, *J. Organomet. Chem.,* 570 (1998) 155.
37. H. Khaledi, H.M. Ali, *Acta Crystallogr., Sect.E,* 67 (2011) m84.
38. H. Khaledi, H.M. Ali *Acta Crystallogr., Sect.E,* 67 (2011) m230.
39. M.T.H. Tarafder, M.A.A.A. Islam, M.B.H. Howlader, N.Guidolin, E. Zangrando *Acta Crystallogr., Sect.C*, 66 (2010) m363.
40. Z. Önal, H. Zengin, M. Sönmez, *Turk. J. Chem.*, 35 (2011) 905-914.
41. C. Anitha, C.D. Sheela, P. Tharmaraj, R. Shanmugakala, *International J. Inorg. Chem.*, 2013, Article ID 436275, 1.
42. S. Konar, A. Jana, K. Das, *Polyhedron,* 30, (2011) 2801.

Synthesis, characterization, photoluminescence and electrochemical studies of Ni(II), Cu(II), Zn(II), Cd(II) and Pd(II) complexes of the bidentate S-hexyl-β-N-(2-thienyl)methylenedithiocarbazate ligand

4.1 Introduction

Schiff bases derived from the reaction of *S*-alkyl- and *S*-aryldithiocarbazate with heterocyclic aldehydes and ketones have been extensively studied over the last decades [1-5]. The attention on these compounds arose mainly due to their capability of chelating of metal ions in a variety of coordination modes. In most of the cases, complexations involve the imine nitrogen and the thioamide sulfur atoms to form five membered rings with the metal atoms. The resulting metal complexes have been shown to exhibit interesting biological and physico-chemical properties. Schiff bases are potential anticancer drugs and when administered as their metal complexes, the anticancer activity of these complexes is enhanced in comparison to the free ligand [6]. In fact bischelated nickel(II) and copper(II) complexes with similar ligands showed to exhibit antibacterial [7–10], antifungal [8], and cytotoxic activities [8,9].

The majority of previous studies were based on Schiff bases of S-methyl, S-benzyl and S-acetyl dithiocarbazate and *N*-substituted derivatives of *S*-methyl dithiocarbazates, and only a few papers were reported using Schiff bases of dithiocarbazate derived from long S-alkyl chain moiety. As part of our ongoing work on the coordination chemistry of such complexes, we describe here the preparation and characterization of a bidentate Schiff base derived from SHDTC and thiophene-2 carbaldehyde and the study of the coordination chemistry with some bivalent metal ions. The X-ray single crystal structures of the Ni(II) and Cu(II) complexes have also been determined. Moreover, the electrochemical behavior of Cu(II) complex and photoluminescence properties of all the compounds in chloroform were examined.

4.2 Synthesis of S-hexyl-3-(2-thienylidene)dithiocarbazate, 8

To an ethanolic solution of KOH (2.81 g, 0.05 mol) hydrazine hydrate (2.50 g, 0.05 mol, 99%) was added and the mixture was stirred at 0^oC. To this solution carbon disulfide (3.81 g, 0.05 mol) was added drop wise with constant stirring for one hour. Then 1-bromohexane (8.25 g, 0.05 mol) was added drop wise with vigorous stirring at 0°C for an additional hour. Finally, 2-thiophenecarboxaldehyde (5.61 g, 0.05 mol) in ethanol was added and the mixture refluxed for 30 min. The mixture was filtered while hot and then the filtrate was cooled to 0^oC giving a precipitate of the Schiff base product (**Scheme 4.2**). It was recrystallized from ethanol at room temperature and dried in a vacuum desiccator over anhydrous $CaCl_2$. The physical and spectroscopic data of the ligand **8** is as follows:

Yellow crystalline, Yield: 78 %; m. p. (78-80 °C). *Anal. Calc.* for $C_{12}H_{18}N_2S_3$: C, 50.31; H, 6.33; N, 9.78; S, 33.57 %. Found: C, 50.35; H, 6.34; N, 9.80; S, 33.58 %.

Selected IR data (KBr dics, cm^{-1}): ν(N-H) 3099m, ν(C-H, alkyl) 2921m, ν(C=N) 1590s, ν(C=S) 1102s, ν(N-N) 1038s, ν(CSS) 820m.

^1H NMR (400 MHz, $CDCl_3$, ppm) δ: 10.18(s, 1H, NH), 8.02(s, 1H, CH=N), 7.44(d, 1H, C-1), 7.34(d, 1H, C-3), 7.07(t, 1H, C-2), 3.28(t, 2H, $-SCH_2$), 1.75(p, 2H, C-8), 1.47(p, 2H, C-9), 1.33(m , 4H, C-10,11), 0.90(t, 3H, C-12).

^{13}C NMR (150 MHz, $CDCl_3$, ppm) δ: 199.10(C=S), 155.79(CH=N), 140.05(C-4), 131.60(C-1), 129.66(C-3), 127.79(C-2), 34.60(C-7), 31.40(C-8), 28.73(C-9), 28.54(C-10), 22.53(C-11), 14.05(C-12).

UV-Vis spectrum [$CHCl_3$, λ_{max} nm (log ε, L mol^{-1} cm^{-1})]: 235(4.12), 296(3.94) 335 (4.22), 352(4.27).

HRMS (FAB) Calc. for $C_{12}H_{18}N_2S_3$ (M+1): 287.0632; Found (M+1): 287.0708.

4.3 Synthesis of bis[S-hexyl-3-(2-thienylidene)dithiocarbazato-κ^2N^3,S]M(II), 9-13

A solution of $Ni(CH_3COO)_2.4H_2O$ (0.12 g, 0.5 mmol, 10 mL methanol) was added to a solution of the ligand HL, (0.29 g, 1.0 mmol, 20 mL methanol). The resulting mixture was stirred at room temperature for four hours. A dark reddish brown precipitate was formed, filtered off, washed with methanol and dried in vacuo over anhydrous $CaCl_2$.

Dark reddish brown single crystals, suitable for X-ray diffraction, of compound **9** were obtained by slow evaporation from a mixture of chloroform and acetonitrile (4:1).

The Cu(II), Zn(II), Cd(II) and Pd(II) complexes **10-13** were prepared following the same procedure as described for complex **9** by using $Cu(CH_3COO)_2.H_2O$, $Zn(CH_3COO)_2.2H_2O$, $Cd(CH_3COO)_2.3H_2O$ and $PdCl_2$, respectively, except for Pd(II) complex **13** that was prepared by refluxing. The products were recrystallized by a mixture of chloroform and acetonitrile (4:1). Reddish brown single crystals, suitable for X-ray diffraction, of compound **10** were obtained by slow evaporation from a mixture of chloroform and acetonitrile (4:1). The physical and spectroscopic data of compounds **9-13** are given as follows:

4.3.1 Bis[S-hexyl-3-(2-thienylidene)dithiocarbazato-κ^2N^3,S]nickel(II), 9

Dark reddish brown, Yield: 68 %; m. p. (133-135 °C). *Anal. Calc.* for $C_{24}H_{34}N_4NiS_6$: C, 45.78; H, 5.44; N, 8.90; S, 30.55 %. Found: C, 45.81; H, 5.45; N, 8.90; S, 30.57 %.

Selected IR data (KBr dics, cm^{-1}): ν(C-H, alkyl) 2920m, ν(C=N) 1577s, ν(N-N) 1033s, ν(CSS) 833m.

^1H NMR (400 MHz, $CDCl_3$, ppm); δ: 8.00(s, 2H, CH=N), 7.72(d, 2H, C-1), 7.46(d, 2H, C-3), 7.10(t, 2H, C-2), 3.27(t, 4H, $-SCH_2$), 1.75(p, 4H, C-8), 1.46(p, 4H, C-9), 1.30(m, 8H, C-10,11), 0.89(t, 6H, C-12).

UV-Vis spectrum [$CHCl_3$, λ_{max} nm (logε, L mol^{-1} cm^{-1})]: 235(4.34), 284(4.34), 331(4.33), 398(4.24), 472(3.95), 641(2.16).

HRMS (FAB) Calc. for $C_{24}H_{34}N_4NiS_6$ (M+1): 629.0461; Found (M+1): 629.0536.

Molar conductivity (1.0×10^{-5} M; $CHCl_3$, $\Omega^{-1}cm^2mol^{-1}$): 0.00; μ_{eff} = Diamagnetic.

4.3.2 Bis[S-hexyl-3-(2-thienylidene)dithiocarbazato-κ^2N^3,S]copper(II), 10

Reddish brown, Yield: 68 %; m. p. (118-120 °C). *Anal. Calc.* for $C_{24}H_{34}N_4CuS_6$: C, 45.43; H, 5.40; N, 8.83; S, 30.32 %. Found: C, 45.45; H, 5.41; N, 8.84; S, 30.34 %.

Selected IR data (KBr dics, cm^{-1}): ν(C-H, alkyl) 2920m, ν(C=N) 1582s, ν(N-N) 1031s, ν(CSS) 825m.

UV-Vis spectrum [$CHCl_3$, λ_{max} nm (log ε, L mol^{-1} cm^{-1})]: 235(4.41), 298(4.39), 338(4.55), 378(4.64), 439(3.84), 670(2.84).

HRMS (FAB) Calc. for $C_{24}H_{34}N_4CuS_6$ (M+1): 634.0404; Found (M+1): 634.0494.
Molar conductivity (1.0×10^{-5} M; $CHCl_3$, $\Omega^{-1}cm^2mol^{-1}$): 0.00; μ_{eff} = 1.81 B.M.

4.3.3 Bis[S-hexyl-3-(2-thienylidene)dithiocarbazato-κ^2N^3,S]zinc(II), 11

White, Yield: 56 %; m. p. (128-130 °C). *Anal. Calc.* for $C_{24}H_{34}N_4ZnS_6$: C, 45.30; H, 5.39; N, 8.81; S, 30.23 %. Found: C, 45.32; H, 5.39; N, 8.82; S, 30.24 %.
Selected IR data (KBr dics, cm^{-1}): ν(C-H, alkyl) 2925m, ν(C=N) 1599s, ν(N-N) 1039s, ν(CSS) 822m.
^{1}H NMR (400 MHz, $CDCl_3$, ppm): δ: 8.02(s, 2H, CH=N), 7.80(d, 2H, C-1), 7.58(d, 2H, C-3), 7.16(t, 2H, C-2), 3.27(t, 4H, -SCH_2), 1.75(p, 4H, C-8), 1.46(p, 4H, C-9), 1.33(m, 8H, C-10,11), 0.89(t, 6H, C-12).
UV-Vis spectrum [$CHCl_3$, λ_{max} nm (log ε, L mol^{-1} cm^{-1})]: 236(4.41), 277(4.35), 353(4.61), 439(3.82).
HRMS (FAB) Calc. for $C_{24}H_{34}N_4ZnS_6$ (M+1): 635.0399; Found (M+1): 635.0469.
Molar conductivity (1.0×10^{-5} M; $CHCl_3$, $\Omega^{-1}cm^2mol^{-1}$): 0.00; μ_{eff} = Diamagnetic.

4.3.4 Bis[S-hexyl-3-(2-thienylidene)dithiocarbazato-κ^2N^3,S]cadmium(II), 12

White, Yield: 54%; m. p. (160-162 °C). *Anal. Calc.* for $C_{24}H_{34}N_4CdS_6$: C, 42.18; H, 5.02; N, 8.20 ; S, 28.15 %. Found: C, 42.23; H, 5.03; N, 8.23; S, 28.19 %.
Selected IR data (KBr dics, cm^{-1}): ν(C-H, alkyl) 2926 m, ν(C=N) 1583s, ν(N-N) 1031s, ν(CSS) 816 m.
^{1}H NMR (400 MHz, $CDCl_3$, ppm): δ: 8.08(s, 2H, CH=N), 7.56(d, 2H, C-1), 7.42(d, 2H, C-3), 7.04(t, 2H, C-2), 3.18(t, 4H, -SCH_2), 1.65(p, 4H, C-8), 1.37(p, 4H, C-9), 1.25(m, 8H, C-10,11), 0.88(t, 6H, C-12).
UV-Vis spectrum [$CHCl_3$, λ_{max} nm (log ε, L mol^{-1} cm^{-1})]: 235(4.38), 276(4.32), 353(4.66), 439(3.78).
HRMS (FAB) Calc. for $C_{24}H_{34}N_4CdS_6$ (M+1): 685.0141; Found (M+1): 685.0211.
Molar conductivity (1.0×10^{-5} M; $CHCl_3$, $\Omega^{-1}cm^2mol^{-1}$): 0.00; μ_{eff} = Diamagnetic.

4.3.5 Bis[S-hexyl-3-(2-thienylidene)dithiocarbazato-κ^2N^3,S]palladium(II), 13

Orange red, Yield: 63 %; m. p. (153-155 °C). *Anal. Calc.* for $C_{24}H_{34}N_4PdS_6$: C, 42.56; H, 5.06; N, 8.27 ; S, 28.40 %. Found: C, 42.59 ; H, 5.07; N, 8.28; S, 28.42 %.

Selected IR data (KBr dics, cm^{-1}): ν(C-H, alkyl) 2924 m, ν(C=N) 1583s, ν(N-N) 1029s, ν(CSS) 832m.

^{1}H NMR (400 MHz, $CDCl_3$, ppm): 8.12(s, 2H, CH=N), 7.75(d, 2H, C-1), 7.52(d, 2H, C-3), 7.13(t, 2H, C-2), 3.30(t, 4H, -SCH_2), 1.78(p, 4H, C-8), 1.46(p, 4H, C-9), 1.32(m, 8H, C-10,11), 0.88(t, 6H, C-12).

UV-Vis spectrum [$CHCl_3$, λ_{max} nm (log ε, L mol^{-1} cm^{-1})]: 247(4.38), 296(4.43), 346(4.36), 414(4.22).

HRMS (FAB) Calc. for $C_{24}H_{34}N_4PdS_6$ (M+1): 677.0143; Found (M+1): 677.0217.

Molar conductivity (1.0×10^{-5} M; $CHCl_3$, $\Omega^{-1}cm^2mol^{-1}$): 0.00; μ_{eff} = Diamagnetic.

4.4 X-ray data collection and structure determination

Diffraction data for compounds **9-10** were collected on a Rigaku R-AXIS RAPID diffractometer equipped with CCD (University of Toyama, Japan). Both the experiments were performed at 173 K with Mo-Kα radiation (λ = 0.71075 Å). Cell refinement, indexing and scaling of the data set were carried out using Crystal Structure package [11]. The structures were solved by direct methods [12] and subsequent Fourier analyses and refined by the full-matrix least-squares method based on F^2 with all observed reflections [13]. An absorption correction was applied to both data sets [14]. The contribution of H atoms at geometrical calculated positions was introduced in the final cycles of refinement. Figures were done with Ortep3 for Windows [15]. Pertinent crystallographic data and refinement details are summarized in **Table 4.1**.

4.5 Results and discussion

4.5.1 Physical characterization

The reaction of 2-thiophenecarboxaldehyde with S-hexyldithiocarbazate afforded the Schiff base ligand **8** (as described in the experimental section). Reaction of the ligand with divalent metal ions M(II) [M = Ni, Cu, Zn, Cd and Pd] in a 2:1 molar ratio, resulted in the formation of bischelated complexes. The *Lasign's* test (halogen test) indicated the absence of chloride ions in the Pd(II) complex **13**, suggesting the uni-negative bidentate complexation of the Schiff base. The yield, color, melting point, magnetic susceptibility and the spectroscopic data for the characterization of the

compounds are given in the experimental section. All analytical and spectroscopic data are in good agreement with their proposed structures. All the compounds are stable in air and are fairly soluble in organic solvents such as $CHCl_3$, CH_2Cl_2, DMSO and DMF. The room temperature molar conductance values of the complexes (10^{-5} M solution in $CHCl_3$) indicated their non-electrolytic nature [1].

The IR spectra of **8** (as shown in **Section 4.2**) showed a medium band at 3099 cm^{-1} for ν(N-H), which is absent in complexes **9-13,** indicating the deprotonation of the imine NH proton and that the coordination of anionic ligand have taken place in the enol form [3,16]. Two strong bands at 1590 and 1102 cm^{-1} are assigned to the ν(C=N) and ν(C=S) stretching vibrations, respectively [5,17]. However, the ligand does not exhibit any ν(S-H) band around 2700 cm^{-1}, indicating that in solid state it maintains the thione functional group [16,17]. The absence of the ν(C=S) band in the complexes is an unauthentic evidence for the formation of complexes via the enol group [3,18]. In the complexes the ν(C=N) band appeared at (1599-1577 cm^{-1}), indicating the coordination of the ligand to the metal atom through the azomethine nitrogen [19]. The ν(N=N) band, observed in the free ligand at 1038 cm^{-1}, is shifted to (1029-1039 cm^{-1}) in the spectra of the complexes supports the suggestion of azomethine nitrogen bonding to the metal ions [1,5,16]. The stretching frequency of ν(CSS) in the complexes decreases (833-816 cm^{-1}) as compared to that observed in the ligand, pointing to sulfur of thiol as a coordination site [20].

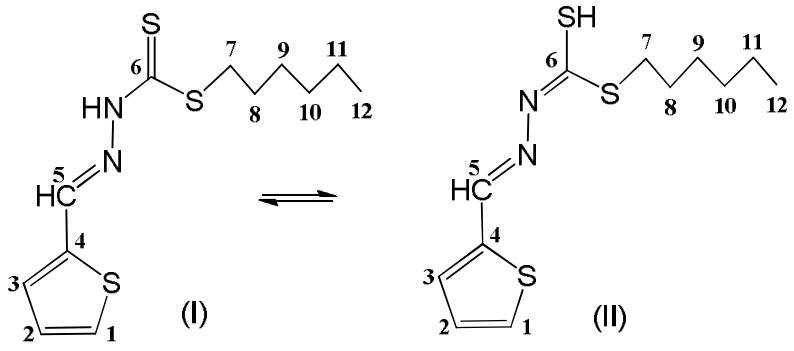

Scheme 4.1: Thione (I) and thiol (II) tautomeric forms of HL, **8**.

4.5.2 NMR

The ^{1}H NMR of the ligand **8** (**Section 4.2**) showed a broad singlet at 10.18 ppm assigned to the (N-H) proton [5]. Usually these species may exist in solution as an equilibrium mixture between the thione and thiol tautomeric forms. It is worth noting that ligand **8** does not display any signal for the SH proton (~ 4.0 ppm), indicating the absence of the thiol form [3,17]. The lack of the NH signal in the ^{1}H NMR spectra (**Section 4.3**) for complexes **9-13** indicates that the complexation occurs via deprotonation of this group [21], as confirmed by the X-ray crystallographic study.

Both in solid state and in solution, the Schiff base remains in the thione form, but in the presence of metal(II) ions, the ligand undergoes deprotonation and coordinates the metal *via* the enol tautomer forming stable bischelated ML_2 complexes (HL corresponds to the neutral form of the Schiff base ligand). The ready conversion of the Schiff base from the thione to the thiol form in the presence of metal ions, followed by deprotonation and coordination to the metal, may be attributed to the extra stability gained through the π-electron delocalization along the -C-N-N-C-S- chains of the dithiocarbazate moiety. The thione-to-thiol tautomerization in the presence of metal ions has been regularly found to happen in Schiff bases derived from S-alkyl/S-aryl dithiocarbazates [22].

The azomethine (CH=N) proton $C^{5}H$ observed as a singlet at 8.02 ppm in HL, shifted after complexation, indicating coordination through the azomethine nitrogen [20,21,23]. The signals due to the thiophene ring protons appeared as two doublets for $C^{1}H$ and $C^{3}H$ and a triplet for $C^{2}H$ at 7.44, 7.34 and 7.04 ppm respectively, in the ligand [20]. The signals at 3.28, 1.75, 1.47, 1.33 and 0.90 ppm for the protons referred to -SCH_2, C-8, C-9, C-10,11 and C-12, respectively, and all show slight variation upon complexation [20]. The ^{1}H NMR spectra of Cu(II) complex **10** was useless for the identification of the functional group having the metal ion a paramagnetic electron configuration [24].

The ^{13}C NMR signals of the ligand **8** are observed at 199.10 and 155.79 ppm for (C=S) and (CH=N) carbons, respectively [21,23]. In the ligand the heterocyclic carbons are

observed at 140.05(C-4), 131.60(C-1), 129.66(C-3), 127.79(C-2) ppm, whereas the alkyl carbons fall at 34.60(C-7), 31.40(C-8), 28.73(C-9), 28.54(C-10), 22.53(C-11) and 14.05(C-12) ppm.

4.5.3 Mass

The mass spectral data by FAB method of compounds **8-13** have been given above. The Schiff base, **8** in its High Resolution Mass Spectrum (HRMS) showed peak at m/z of 287.0708, which is consistent with the proposed formula. The molecular ions of Ni(II), Cu(II), Zn(II), Cd(II) and Pd(II) complexes at m/z 629.0536, 634.0494, 635.0469, 685.0211 and 677.0217, respectively as confirmed by HRMS, suggested the formation of bischelated complexes of the Schiff base **8**.

4.5.4 UV-Vis spectra

The solution UV-vis spectrum of ligand **8** showed bands at 235, 296, 335 and 352 nm, assigned to the ($\pi \rightarrow \pi^*$, aromatic), ($\pi \rightarrow \pi^*$, CH=N), ($\pi \rightarrow \pi^*$, dithiocarbazate moiety) and ($n \rightarrow \pi^*$, dithiocarbazate moiety), respectively [25,26]. The complexes exhibited intra-ligand transitions in the range (235-247), (276-298) and (346-398) nm, for the $\pi \rightarrow \pi^*$ (aromatic), $\pi \rightarrow \pi^*$(CH=N) and $n \rightarrow \pi^*$ (C=S) transitions, respectively [25,27]. The complexes showed a medium intensity band at 414-472 nm for the $S \rightarrow M$ charge transfer transition, indicating the coordination of the Schiff base to the metal atom via the thiolate sulfur [27,28]. The Ni(II) and Cu(II) complexes showed a very broad weak d-d band at 641 and 670 nm, respectively, diagnostic of square planar geometry [21,29]. The Cu(II) complex has magnetic moment of 1.81 B.M. corresponding to a single electron spin [30].

The diamagnetic nature of the Pd(II) complex, consistent with the d^8 configuration, suggested a square planar geometry [30], although d^8 metal ions in this coordination environment are expected to exhibit three bands associated to the $^1A_{1g} \rightarrow {}^1A_{2g}$, $^1A_{1g} \rightarrow {}^1B_{1g}$, and $^1A_{1g} \rightarrow {}^1E_{1g}$ transitions. However, such transitions are usually not observed since the strong $S \rightarrow M$ LMCT bands of ligands containing chalcogen donor atoms mask the expected *d-d* bands. The diamagnetic Zn(II) and Cd(II) complexes, consistent

with a d^{10} metal ion configuration, do not show *d-d* transition, diagnostic of square planar geometry [23].

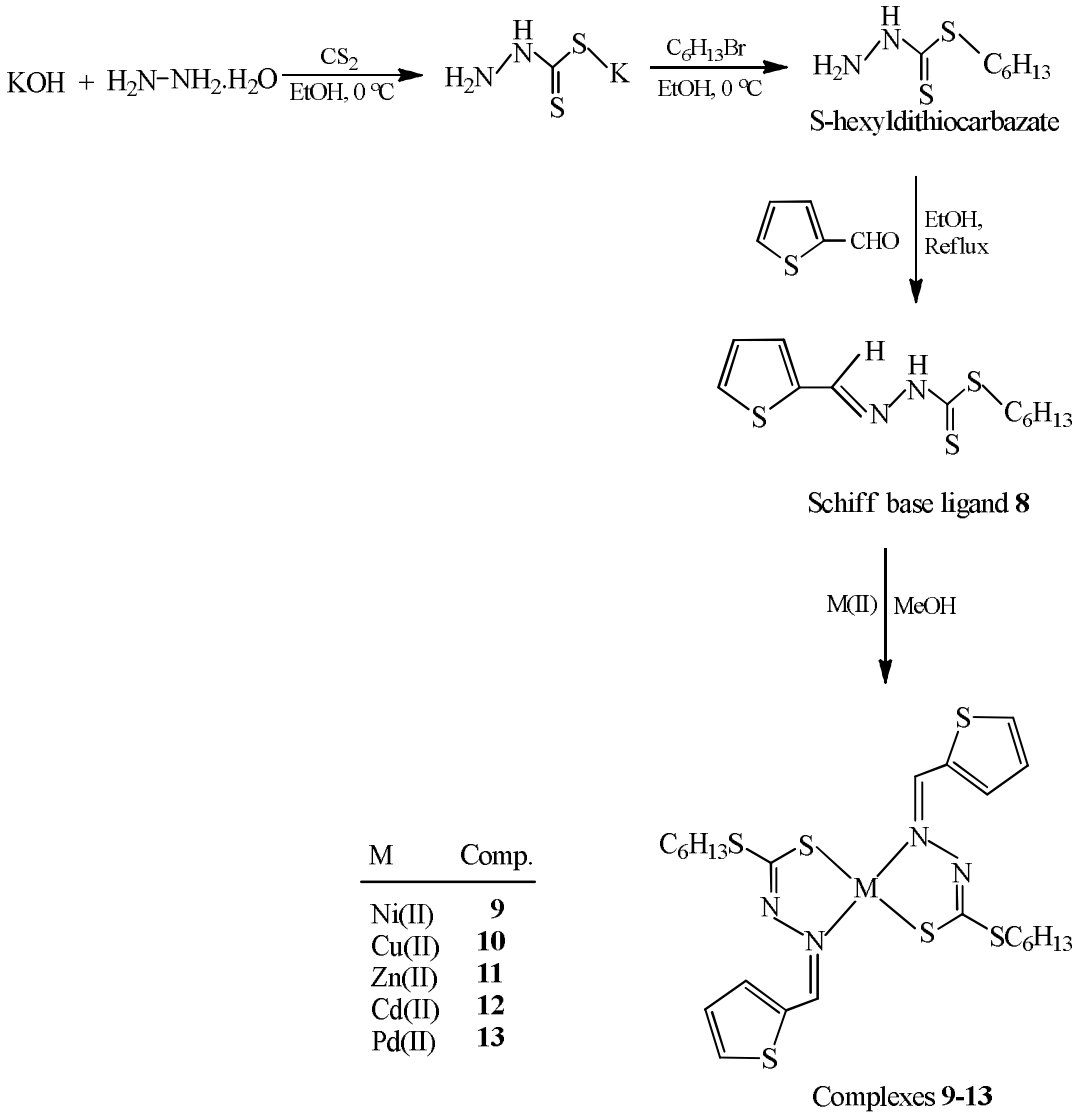

Scheme 4.2: Synthetic route for the preparation of ligand **8** and the metal complexes **9-13**

4.6 Structural description of NiL_2, 9 and CuL_2, 10 complexes

The X-ray structural analysis of the bischelated nickel(II) and copper(II) complexes indicates that the crystals are isomorphous and isostructural crystallizing in monoclinic system, space group $P2_1/c$. **Fig. 4.1** depicts an ORTEP drawing of the nickel derivative with atom numbering scheme, that of copper is reported as supplementary (**Fig. 4.3**). The coordination bond lengths and angles for the two complexes are reported in **Table 4.2**.

The complexes shows that the two Schiff bases, in their deprotonated imino thiolate form, chelate the metal centre via the azomethine nitrogen N(1) and thiolate sulfur S(2) atoms in a trans-planar configuration exhibiting a pseudo centrosymmetric arrangement. The molecular structure of uncoordinated similar ligands [31-32] shows the dithiocarbazate group adopting an E configuration with respect to the C=N bond. The β-nitrogen and the thioketo sulfur are trans located with respect to the C(6)-N bond (as depicted in **Scheme 4.1**). Thus the deprotonated ligand requires a rotation about the C(6)-N by 180° in order to allow the N,S chelating behavior towards the metal. Upon coordination the ligand shows some geometrical variations with respect to the free species, and the most significant are an elongation of the thioketo C(6)-S bond length, which validates the coordination with deprotonated thiolate sulfur atom, a decrease of the N-C(5) bond length, and a associated increase of the N-N bond, as previously described [33] (the numbering scheme here indicated refers to **Scheme 4. 1**).

In the NiL_2 complex, the Ni-S and Ni-N the bond distances are of 2.1785(4), 2.1812(4) and 1.9112(12), 1.9177(12) Å, respectively, and S-Ni-N chelating bond angles average to 85.88(4)°. The corresponding figures in the CuL_2 derivative are 2.2591(4), 2.2637(4) and 1.9988(12), 2.0047(12) Å, respectively, with a S-Cu-N chelating angle of 84.57(3)° (mean value). The observed differences in the bond lengths are to be ascribed to the different metal ionic radius. These geometrical parameters do not deviate significantly from the values recently reported for the nickel and copper complexes having the ligands in *cis* configuration [33]. However in the cited paper an analysis on almost seventy structures of nickel and copper complexes, differentiated for *trans* and *cis* configuration, clearly indicated longer M–S bond distances in case of trans arrangement of ligands both for Ni and Cu square planar complexes, while no significant difference

was observed in M–N distances. It is worth noting that in the present complexes both the M–S and M–N bond distances are within the range of the derivatives having a *trans* configuration.

The hexyl chains have, as expected, carbon atoms in all anti conformation, being recognized as an energy minimum. It is worth noting that the crystal packing (**Fig. 4.2**) evidences the complexes arranged in such a way that the alkyl chains point towards the center of the unit cell giving rise to a hydrophobic area.

Table 4.1: Crystallographic data and details of refinement for complexes **9**-**10**

	9	**10**
Empirical formula	$C_{24}H_{34}N_4CuS_6$	$C_{24}H_{34}N_4NiS_6$
Formula mass	634.47	629.62
System	Monoclinic	
Space group	*P* 2_1/c	
a (Å)	13.9228(3)	13.9738(3)
b (Å)	10.33945(19)	10.31877(19)
c (Å)	20.6389(4)	20.4549(4)
β (°)	103.1778(7)	102.4271(7)
V (Å^3)	2892.82(10)	2880.34(10)
Z	4	4
D_{calc} (Mg/m^3)	1.457	1.452
μ (mm^{-1})	1.209	1.130
F(000)	1324	1320
θ max (°)	27.45	27.46
No. of reflections collected	28302	25909
no. of independent reflections	6605	6587
*R*int	0.0357	0.0404
no. of reflns ($I > 2\sigma(I)$)	6248	6242
Parameters refined	318	318
*R*1 (($I > 2\sigma(I)$) [a]	0.0254	0.0261
*wR*2 [a]	0.0689	0.0684
Residuals (e/Å^3)	0.450, –0.300	0.450, –0.380

[a] $R1 = \Sigma \; ||Fo| - |Fc|| \; / \; \Sigma |Fo|$, $wR2 = [\Sigma \, w (Fo^2 - Fc^2)^2 / \Sigma w (Fo^2)^2]^{1/2}$

Table 4.2: Coordination bond lengths (Å) and angles (°) for metal complexes **9** and **10**.

	9 (M = Ni)	**10** (M = Cu)
M-N(1)	1.9112(12)	1.9988(12)
M-N(3)	1.9177(12)	2.0047(12)
M-S(2)	2.1785(4)	2.2591(4)
M-S(5)	2.1812(4)	2.2637(4)
S(2)-M-S(5)	173.288(13)	169.960(14)
S(2)-M-N(1)	85.74(3)	84.59(3)
S(2)-M-N(3)	94.61(4)	96.18(3)
S(5)-M-N(1)	93.71(3)	95.31(3)
S(5)-M-N(3)	86.03(4)	84.55(3)
N(1)-M-N(3)	179.08(5)	176.37(5)

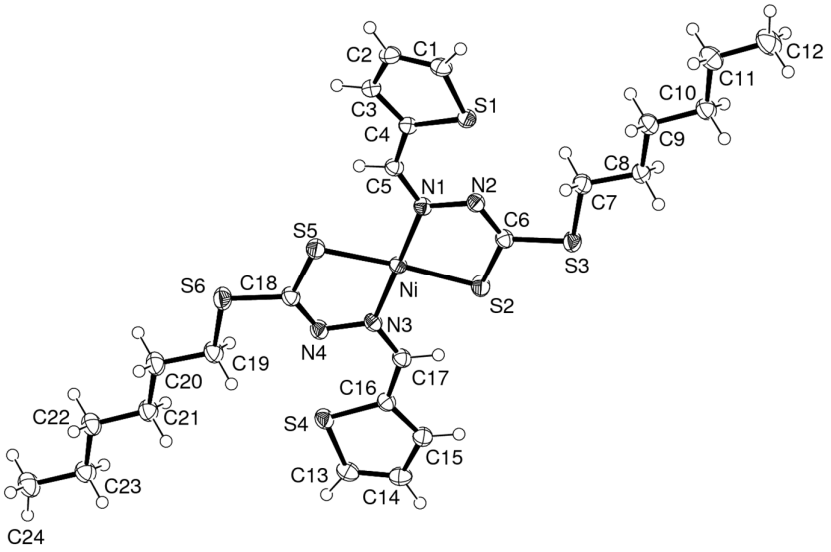

Fig. 4.1: ORTEP drawing (ellipsoid probability at 50%) of NiL_2, **9**

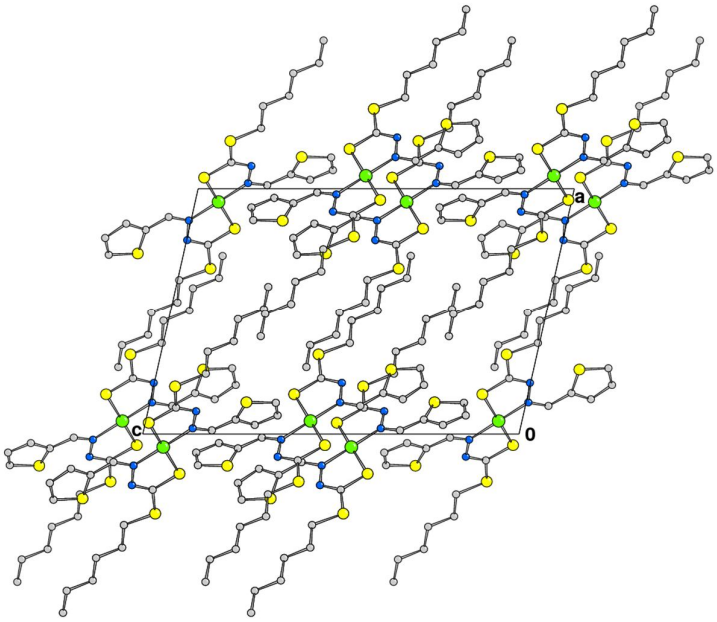

Fig. 4.2: Crystal packing viewed down axis *b* of the NiL_2, **9**
(the same arrangement is observed in the copper derivative;
H atoms not shown for clarity).

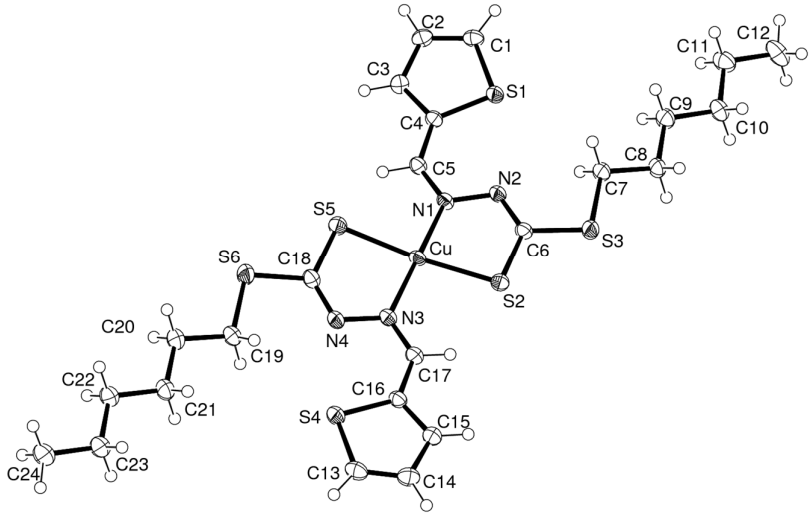

Fig. 4.3: ORTEP drawing (ellipsoid probability at 50%) of CuL_2, **10**

4.7 Fluorescence Studies

The photoluminescence properties of Schiff base ligand **8** and its metal complexes **9-13** were studied of 10^{-5} M solution in $CHCl_3$ at room temperature. Upon excitation at 352 nm, the emission spectrum of ligand **8** shows three emission peaks at λ_{max} = 406, 430 and 456 nm (**Table 4.3** and **Fig. 4.4**). Excitation of the metal complexes at 284-380 nm gives an emission at 318-456 nm. The emission spectral shape of complexes **10-13** closely resembled that of the ligand, with a significant difference in position of emission maximum [6] for complex **9**. In the absence of metal ions the fluorescence of the ligand is probably quenched by the occurrence of a photo induced electron transfer (PET) process due to the presence of lone pair of electrons in the ligand [34].

It is evident Form **Fig. 4.4** that the fluorescence emission intensity of the ligand decreases dramatically depending on the complex formation with the metal ions. The decrease of emission intensities is due to the formation of coordination complexes of the S and N atom in the ligand with the metal ion. These coordination complexes make the energy transfer from the excited state of the ligand to the metal ions causing decreases of the fluorescence intensity [35]. For this reason the intensity of complexes **9-13** is decreased. Quenching of fluorescence of a ligand by transition metal ions during complexation is a rather common phenomenon which is explained by processes such as magnetic perturbation, redox activity, and electronic energy transfer [6,28,35,36].

Table 4.3: Excitation wavelength dependent emissions of compounds **8-13**

Compound	Excitation wavelength (nm)	Peak wavelength of emission (nm)
8	352	406, 430, 456
9	284	318, 328, 405, 431
10	380	407, 430,452
11	353	407, 431,456
12	353	407, 430,453
13	346	406, 432, 455

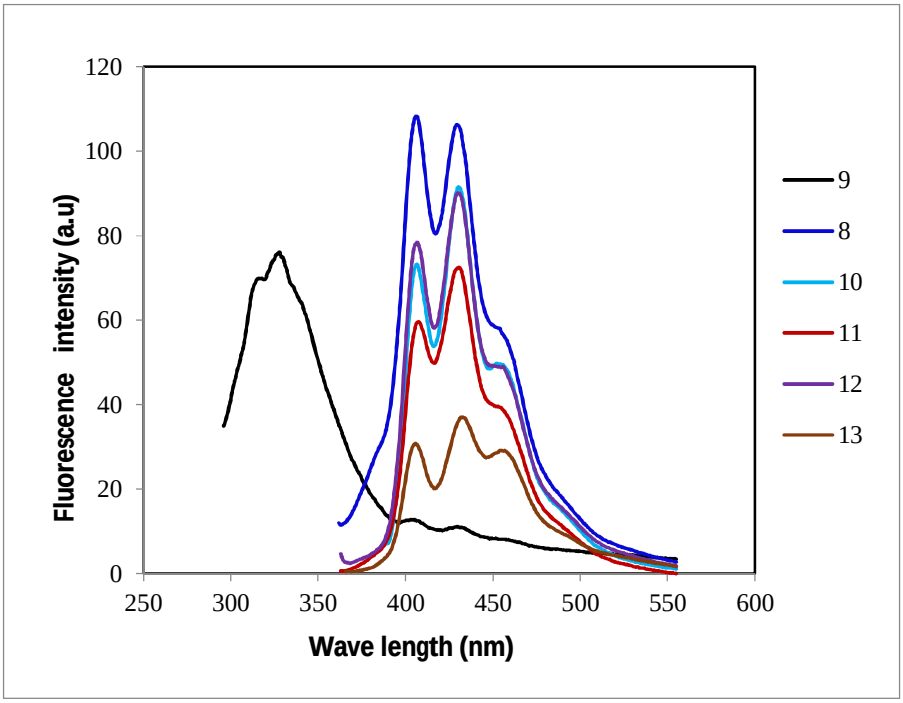

Fig. 4.4: Emission spectra of compounds **8-13** of 10^{-5} M solution in $CHCl_3$ at room temperature.

4.8 Electrochemical study

The potential scanning of the copper(II) complex **10** was performed using a Pt disk electrode (ϕ = 2mm) in presence of tetra-n butylammonium tetrafluoroborate as supporting electrolyte at scan rate of 25 mVs-1. From the voltammogram shown in **Fig. 4.5**, the common diagnostic criteria for that redox reaction, namely the peak potential difference (E_{pa} - E_{pc}) about 120 mV and I_{pc}/I_{pa} = 3.98 indicate that the redox reaction of compound **10** is an apparently quasi-reversible, one electron redox process in under the experimental condition.

During cathodic scan at -0.27V, Cu(II) is reduced to Cu(I) providing highly intense wave and when the potential scanning is reverted from -0.5V, an anodic wave is developed giving maximum intensity at -0.15V where Cu(I) is oxidized to Cu(II) species. However, even at faster scan rates (ν > 100 mVs^{-1}), I_{pc}/I_{pa} ratio was not

significantly altered. This observation suggests that reduced form of the metal complex is probably unstable and undergo some irreversible chemical or structural changes. Redox couples are detected to be at -0.27 and −0.15 V (E^o = −0.21V) with respect to Ag/AgCl (sat. KCl). However, the cathodic wave is nearly four times more intense than the anodic part.

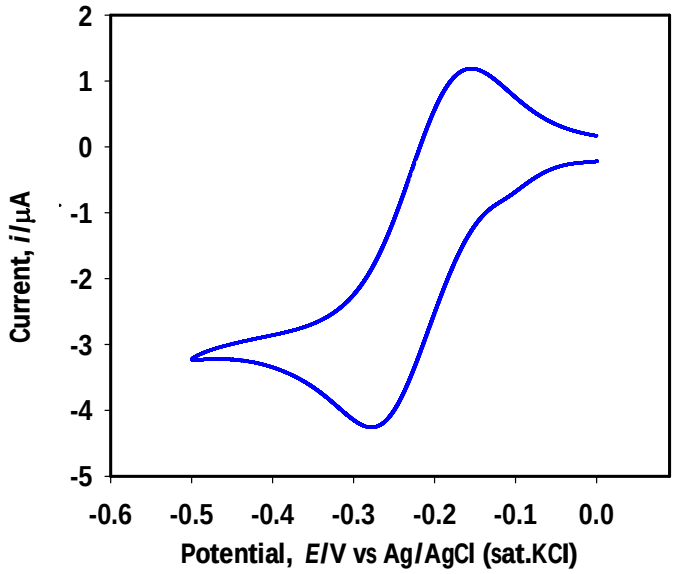

Fig. 4.5: Cyclic voltammetry of Cu(II) complex **10** at a scan rate using a Pt disk electrode in presence of $[(n\text{-But})_4N]BF_4$ as supporting electrolyte in $CHCl_3$. Scanning was performed against Ag/AgCl (sat. KCl) reference electrode.

References

1. M.A. Ali, H.J.H. Abu Bakar, A.H. Mirza, S.J. Smith, L.R. Gahan, P.V. Bernhardt, *Polyhedron*, 28 (2008) 71.
2. S. Roy, T.N. Mandal, A.K. Barik, S. Pal, S. Gupta, A. Hazra, R.J. Butcher, A.D. Hunter, M. Zeller, S.K. Kar, *Polyhedron*, 26 (2007) 2603.
3. K.B. Chew, M.T.H. Tarafder, K.A. Crouse, A.M. Ali, B.M. Yamin, H.-K. Fun, *Polyhedron*, 23 (2004) 1385.
4. M.A. Ali, A.H. Mirza, R.J. Fereday, R.J. Butcher, J.M. Fuller, S.C. Drew, L.R. Gahan, G.R. Hanson, B. Moubaraki, K.S. Murray, *Inorg. Chim. Acta.*, 358 (2005) 3937.
5. M.H.E. Chan, K.A. Crouse, M.I.M. Tahir, R. Rosli, N. Umar-Tsafe, A.R. Cowley, *Polyhedron*, 27 (2008) 1141.
6. A. Majumder, G. M. Rosair, A. Mallick, N. Chattopadhyay, S. Mitra, *Polyhedron*, 25 (2006) 1753.
7. F.N.-F. How, K.A. Crouse, M.I.M. Tahir, M.T.H. Tarafder, A.R. Cowley, *Polyhedron*, 27 (2008) 3325.
8. T.B.S.A. Ravoof, K.A. Crouse, M.I.M. Tahir, A.R. Cowley, M.A. Ali, *Polyhedron*, 26 (2007) 1159.
9. A. Garoufis, S.K. Hadjikakou, N. Hadjiliadis, *Coord. Chem. Rev.*, 253 (2009) 1384.
10. M.L. Low, L. Maigre, P. Dorlet, R. Guillot, J.-M. Pagès, K.A. Crouse, C. Policar, N. Delsuc, *Bioconjugate Chem.*, 25 (2014) 2269.
11. Rigaku (2010). Crystal Structure. Version 4.0. Rigaku Corporation, Tokyo, Japan.
12. A. Altomare, G. Cascarano, C. Giacovazzo, A. Guagliardi, M. Burla, G. Polidori, M. Camalli, *J. Appl. Cryst.*, 27 (1994) 435.
13. G.M. Sheldrick, *Acta Cryst.*, A64 (2008) 112.
14. Rigaku (1995). ABSCOR. Rigaku Corporation, Tokyo, Japan.
15. L. J. Farrugia, *J. Appl. Crystallogr.*, 30 (1997) 565.
16. K.A. Crouse, K.-B. Chew, M.T.H Tarafder, A. Kasbollah, A.M. Ali, B.M. Yamin, H-K. Fun, *Polyhedron*, 23 (2004) 161.

17. S. Roy, T.N. Mandal, A.K. Barik, S. Gupta, R.J. Butcher, M. Nethaji, S.K. Kar, *Polyhedron*, 27 (2008) 593.
18. R. Takjoo, R. Takjoo, M. Yazdanbakhsh, A.A. Kaju, C. Yaguang, *Chin. J. Chem*., 28 (2010) 221.
19. M. Yazdanbaksh, R. Takzoo, W. Frank, A.A. Kaju, *J. Coord. Chem*., 62 (2009) 3651.
20. R. Takjoo, R. Centore, L. Rhyman, P. Ramasami, *J. Coord. Chem.*, 65 (2012) 1569.
21. M.A.A.A. Islam, M.C. Sheikh, M.S. Alam, E. Zangrando, M.A. Alam, M.T.H. Tarafder, R. Miyatake, *Transition Met. Chem.*, 39 (2014) 141.
22. M.A. Ali, A.H. Mirza, M. Haniti, S.A. Hamid, P.V. Bernhardt, *Polyhedron*, 24 (2005) 383.
23. M.A.A.A. Islam, M.T.H. Tarafder, M.C. Sheikh, M.A. Alam, E. Zangrando, *Transition Met. Chem.*, 36 (2011) 531.
24. Y.-J. Jang, U.K. Lee, B.-K. Koo, *Bull. Korean Chem. Soc*. 26 (2011) 925-929.
25. M.A. Ali, A.H. Mirza, R.J. Butcher, K.A. Crouse, *Transition Met. Chem.*, 31 (2006) 79.
26. Lever ABP (1984) Inorganic Electronic Spectroscopy. Elsevier, New York.
27. T.B.S.A. Ravoof, K.A. Crouse, M.I.M. Tahir, F.N.F. How, R. Rosli, D.J. Watkins, *Transition Met. Chem.*, 35 (2010) 871.
28. E.S. Aazam, A.F.EL Husseiny, H.M.A. Amri, *Arabian J. Chem.*, 5 (2012) 45.
29. R. Takzoo, R. Centore, M. Hakimi, S.A. Beyramabadiand, A. Morsali, *Inorg. Chim. Acta.*, 371 (2011) 36.
30. K. Mahajan, N. Fahmi, R.V. Singh, *Ind. J. Chem*., 46A (2007) 1221.
31. M.S. Begum, M.B.H. Howlader, R. Miyatake, E. Zangrando, M.C. Sheikh, *Acta Cryst*., E71 (2015) o199.
32. M.S. Begum, E. Zangrando, M.C. Sheikh, R. Miyatake, M.M. Hossain, *Acta Cryst*., E71 (2015) o265.
33. E. Zangrando, M.T. Islam, M.A.A.A. Islam, M.C. Sheikh, M.T.H. Tarafder, R. Miyatake, R. Zahan, M.A. Hossain, *Inorg. Chim. Acta.*, 427 (2015) 278.
34. S. Konar, A. Jana, K. Das, *Polyhedron*, 30 (2011) 2801.

35. Z. Önal, H. Zengin, M. Sönmez, *Turk. J. Chem.*, 35 (2011) 905.
36. C. Anitha, C.D. Sheela, P. Tharmaraj, R. Shanmugakala, *International J. Inorg. Chem.*, (2013) Article ID 436275, 1.

Synthesis, spectroscopic characterization, photoluminescence and antibacterial activities of some bivalent metal complexes of N,S donor ligand containing dithiocarbazate moiety. X-ray crystal structure of S-hexyl 3-(4-methoxybenzylidene)dithiocarbazate

5.1 Introduction

During the past years, the synthesis of new coordination compounds containing nitrogen and sulfur donor atoms has been significantly developed. Among these mateials, dithiocarbazate compounds have been studied, mainly due to their potential anticancer [1], antibacterial [2,3], antifungal [4], antitumor [5,6], insecticidal [7] and optoelectronic properties such as god non-linear optical response [8]. Actually, dithiocarbazates constitute one of the most important classes of mixed hard-soft nitrogen-sulfur donor ligands [9]. A change in the substitution pattern of these compounds can create new ligands with different properties. In dithiocarbazate compounds, owing to the thione-thiol tautomer, N and S donor atoms are connected to the metal atom with the formation of five- or six- membered rings. The presence of additional donor atoms in suitable position in the compounds can increase the coordination ability of the ligand giving rise to different coordination geometries [10]. The efficiency of the Schiff bases as therapeutic agents has often been enhanced upon coordination with metals [1]. The bis[S-benzyl-β-N-(2,4-dichlorobenzylidene)dithio-carbazato]Zn(II) complex [11] is more cytotoxic than the Schiff base ligand towards the MKN45 and HepG2 cancer cell lines. The complexation of metal ions enhances the anticancer behavior compared with the uncoordinated ligand, may be attributed to the increase conjugation R=N-N=R', in the ligand moiety on complexation. The distorted square-pyramidal [Cu(S-benzyl-β-N-(2-acetylpyrid-2-yl) methylenedithiocarbazato) (sac) (H_2O)] complex is highly active against the leukemic cell line (HL-60) and found to exhibit strong cytotoxicity [12] against the ovarian cancer cell line (Caov-3).

As part of our general study of metal complexes of Schiff base ligands of S-hexyl dithiocarbazate, we report here the preparation, characterization and photoluminescence properties of metal complexes of Ni(II), Cu(II), Zn(II), Cd(II), Pd(II) and Pb(II) of the bidentate S-hexyl 3-(4-methoxybenzylidene)dithiocarbazate ligand. In order to evaluate

the effect of antimicrobial activity of metal ions upon chelation, both the ligand and their metal complexes were screened for their antibacterial activity by disc diffusion method. The X-ray single crystal structure of the ligand has also been determined.

5.2 Preparation of S-hexyl 3-(4-methoxybenzylidene)dithiocarbazate, 14

To an ethanolic solution of KOH (2.81 g, 0.05 mol) hydrazine hydrate (2.50 g, 0.05 mol, 99%) was added and the mixture was stirred at 0 ^{o}C. To this solution carbon disulfide (3.81 g, 0.05 mol) was added drop wise with constant stirring for one hour. Then 1-bromohexane (8.25 g, 0.05 mol) was added drop wise with vigorous stirring at 0 ^{o}C for an additional hour. Finally, 4-methoxybenzaldehyde (6.81 g, 0.05 mol) in ethanol was added and the mixture refluxed for 30 min. The mixture was filtered while hot and then the filtrate was cooled to 0 ^{o}C giving a precipitate of the Schiff base product (**Scheme 5.2**). It was recrystallized from ethanol at room temperature and dried in a vacuum desiccator over anhydrous $CaCl_2$. Colorless blocks of the title compound were obtained by slow evaporation of an ethanol/chloroform (2:1) solution after 29 days. The physical and spectroscopic data of the Schiff base ligand **14** is as follows:

Colorless, Yield: 74 %; m.p. (95-97 ^{o}C). *Anal. Calc.* for $C_{15}H_{22}N_2OS_2$: C, 58.03; H, 7.14; N, 9.02; S, 20.65 %. Found: C, 58.08; H, 7.15; N, 9.02; S, 20.67 %.

Selected IR data (KBr pellets, cm^{-1}): ν(N-H) 3138m, ν(C-H) 2927m, ν(C=N) 1605s, ν(C=S) 1095s, ν(N-N) 1028s, ν(CSS) 875m.

^{1}H NMR (400 MHz, $CDCl_3$, ppm) δ: 10.66(s, 1H, NH), 7.86(s, 1H, CH=N), 7.68(d, 2H, C- 4,6, J=7.20 MHz), 6.93(d, 2H, C-3,7, J=7.20 MHz), 3.85(s, 3H, -CH_3O), 3.29(t, 2H, -SCH_2), 1.76(p, 2H, C-11), 1.45(p, 2H, C-12), 1.29 -1.40(m, 4H, C-13,14), 0.91(t, 3H, C-15).

^{13}C NMR (125 MHz, $CDCl_3$, ppm) δ: 198.86(C=S), 161.97(CH=N), 145.36(C-5), 129.56(C-4,6), 125.55(C-2), 114.36(C-3,7), 55.40(C-1), 34.59(C-10), 31.41(C-11), 28.73(C-12), 28.56(C-13), 22.53(C-14), 14.03(C-15).

UV-Vis spectrum [CH_2Cl_2, λ_{max} nm (log ε, L mol^{-1} cm^{-1})]: 230(3.86), 262(3.55), 295(3.85), 346(4.45).

HRMS (FAB) Calc. for $C_{15}H_{22}N_2OS_2$ (M+1): 311.1174; Found (M+1): 311.1249.

5.3 Synthesis of bis[S-hexyl 3-(4-methoxybenzylidene)dithiocarbazato-κ^2N^3,S]M(II) complexes 15-20

A solution of $Ni(CH_3COO)_2.4H_2O$ (0.031 g, 0.125 mmol, 7 mL methanol) was added to a solution of the ligand **14**, (0.078 g, 0.25 mmol, 15 mL methanol). The resulting mixture was refluxed for five hours. A dark reddish brown precipitate was formed, filtered off, washed with methanol and dried in vacuo over anhydrous $CaCl_2$ as complex **15**.

The Cu(II), Zn(II), Cd(II), Pd(II) and Pb(II) complexes **16-20** were prepared by the same procedure as described for complex, **15** and using $Cu(CH_3COO)_2.H_2O$, $Zn(CH_3COO)_2.2H_2O$, $Cd(CH_3COO)_2.3H_2O$, $PdCl_2$ and $Pb(CH_3COO)_2.3H_2O$ except Pd(II) complex, **19** that was prepared by refluxing. The product was recrystallized by a mixture of chloroform and acetonitrile (5:1).

The physical and spectroscopic data of the compounds **15-20** are given below:

5.3.1 Bis[S-hexyl 3-(4-methoxybenzylidene)dithiocarbazato-κ^2N^3,S]nickel(II), 15

Dark reddish brown, Yield: 64 %; m.p. (148-150 ^oC). *Anal. Calc.* for $C_{30}H_{42}N_4NiO_2S_4$: C, 53.18; H, 6.25; N, 8.27; S, 18.92 %. Found: C, 53.23; H, 6.26; N, 8.27; S, 18.95 %. Selected IR data (KBr pellets, cm^{-1}): ν(C-H, alkyl) 2926m, ν(C=N) 1601s, ν(N-N) 1027s, ν(CSS) 834m.

^1H NMR (400 MHz, $CDCl_3$, ppm) δ: 7.61(s, 2H, CH=N), 7.98(d, 4H, C-4,6, J=8.40 MHz), 6.87(d, 4H, C-3,7, J=8.40 MHz), 3.85(s, 6H, $-CH_3O$), 3.12(t, 4H, $-SCH_2$), 1.76 (p, 4H, C-11), 1.45(p, 4H, C-12), 1.20-1.35(m, 8H, C -13,14), 0.88(t, 6H, C-15).

UV-Vis spectrum [CH_2Cl_2, λ_{max} nm (log ε, L mol^{-1} cm^{-1})]: 233(4.41), 281(4.57), 329(4.55), 390(4.16), 439((3.87), 534 (2.0).

HRMS (FAB) Calc. for $C_{30}H_{42}N_4NiO_2S_4$ (M+1): 677.1544; Found (M+1): 677.1627. Molar conductivity (1.0×10^{-5} M; CH_2Cl_2, $\Omega^{-1}cm^2mol^{-1}$): 0.00; μ_{eff} = Diamagnetic.

5.3.2 Bis[S-hexyl 3-(4-methoxybenzylidene)dithiocarbazato-κ^2N^3,S]copper(II), 16

Brick red, Yield: 61 %; m.p. (130-132 ^oC). *Anal. Calc.* for $C_{30}H_{42}N_4CuO_2S_4$: C, 52.80; H, 6.20; N, 8.21; S, 18.79 %. Found: C, 52.85; H, 6.22; N, 8.21; S, 18.84 %.

Selected IR data (KBr pellets, cm^{-1}): ν(C-H, alkyl) 2929m, ν(C=N) 1603s, ν(N-N) 1032s, ν(CSS) 827m.

UV-Vis spectrum [CH_2Cl_2, λ_{max} nm (log ε, L mol^{-1} cm^{-1})]: 230(4.25), 279(4.26), 327(4.46), 365(4.61), 443(3.45).

HRMS (FAB) Calc. for $C_{30}H_{42}N_4CuO_2S_4$ (M+1): 682.1487; Found (M+1): 682.1565.

Molar conductivity (1.0×10^{-5} M; CH_2Cl_2, $\Omega^{-1}cm^2mol^{-1}$): 0.00; μ_{eff} = 1.81 B.M.

5.3.3 Bis[S-hexyl 3-(4-methoxybenzylidene)dithiocarbazato-κ^2N^3,S]zinc(II), 17

White, Yield: 55 %; m.p. (120-122 ^oC). *Anal. Calc.* for $C_{30}H_{42}N_4ZnO_2S_4$: C, 52.66; H, 6.19; N, 8.19; S, 18.74 %. Found: C, 52.69; H, 6.20; N, 8.22; S, 18.75 %.

Selected IR data (KBr pellets, cm^{-1}): ν(C-H, alkyl) 2925m, ν(C=N) 1598s, ν(N-N) 1030s, ν(CSS) 835m.

^1H NMR (400 MHz, $CDCl_3$, ppm) δ: 7.64(s, 2H, CH=N), 8.24(d, 4H, C-4,6, J=5.20 MHz), 6.95(d, 4H, C-3,7, J=5.20 MHz), 3.88(s, 6H, $-CH_3O$), 3.26(t, 4H, $-SCH_2$), 1.80 (p, 4H, C-11), 1.48(p, 4H, C-12), 1.25-1.35(m, 8H, C-13,14), 0.88(t, 6H, C-15).

UV-Vis spectrum [CH_2Cl_2, λ_{max} nm (log ε, L mol^{-1} cm^{-1})]: 230(4.25), 281(4.20), 360(4.65).

HRMS (FAB) Calc. for $C_{30}H_{42}N_4ZnO_2S_4$ (M+1): 683.1482; Found (M+1): 683.1556.

Molar conductivity (1.0×10^{-5} M; CH_2Cl_2, $\Omega^{-1}cm^2mol^{-1}$): 0.00; μ_{eff} = Diamagnetic.

5.3.4 Bis[S-hexyl 3-(4-methoxybenzylidene)dithiocarbazato-κ^2N^3,S]cadmium(II), 18

Yellow, Yield: 48 %; m. p. (135-137 ^oC). *Anal. Calc.* for $C_{30}H_{42}N_4CdO_2S_4$: C, 49.27; H, 5.79; N, 7.66; S, 17.53 %. Found: C, 49.30; H, 5.79; N, 7.67; S, 17.53 %.

Selected IR data (KBr pellets, cm^{-1}): ν(C-H, alkyl) 2926m, ν(C=N) 1591s, ν(N-N) 1030s, ν(CSS) 827m.

^1H NMR (400 MHz, $CDCl_3$, ppm) δ: 7.64(s, 2H, CH=N), 8.05(d, 4H, C-4,6, J=9.20 MHz), 6.81(d, 4H, C-3,7, J=9.20 MHz), 3.83(s, 6H, $-CH_3O$), 3.10(t, 4H, $-SCH_2$), 1.67 (p, 4H, C-11), 1.20-1.41(m, 12H, C-12,13,14), 0.88(t, 6H, C-15).

UV-Vis spectrum [CH_2Cl_2, λ_{max} nm (log ε, L mol^{-1} cm^{-1})]: 229(4.34), 353(4.65).

HRMS (FAB) Calc. for $C_{30}H_{42}N_4CdO_2S_4$ (M+1): 733.1224; Found (M+1): 733.1304.
Molar conductivity (1.0×10^{-5} M; CH_2Cl_2, $\Omega^{-1}cm^2mol^{-1}$): 0.00; μ_{eff} = Diamagnetic.

5.3.5 Bis[S-hexyl 3-(4-methoxybenzylidene)dithiocarbazato-κ^2N^3,S]palladium(II), 19

Orange red, Yield: 64 %; m.p. (183-185 ^oC). *Anal. Calc.* for $C_{30}H_{42}N_4PdO_2S_4$: C, 49.68; H, 5.84; N, 7.72; S,17.68 %. Found: C, 49.70; H, 5.84; N, 7.73; S, 17.71 %.
Selected IR data (KBr pellets, cm^{-1}): ν(C-H, alkyl) 2929m, ν(C=N) 1601s, ν(N-N) 1027s, ν(CSS) 834m.
^{1}H NMR (400 MHz, $CDCl_3$, ppm) δ : 7.81(s, 2H, CH=N), 8.03(d, 4H, C-4,6, J=8.80 MHz), 6.89(d, 4H, C-3,7, J=8.80 MHz), 3.87(s, 6H, -CH_3O), 3.13(t, 4H, -SCH_2), 1.76 (p, 4H, C-11), 1.45(p, 4H, C-12), 1.28-1.40(m, 8H, C-13,14), 0.87(t, 6H, C-15).
UV-Vis spectrum [CH_2Cl_2, λ_{max} nm (log ε, L mol^{-1} cm^{-1})]: 240(4.53), 295(4.56), 327(4.61), 393(4.25).
HRMS (FAB) Calc. for $C_{30}H_{42}N_4PdO_2S_4$ (M+1): 725.1225; Found(M+1): 725.1308.
Molar conductivity (1.0×10^{-5} M; CH_2Cl_2, $\Omega^{-1}cm^2mol^{-1}$): 0.00; μ_{eff} = Diamagnetic.

5.3.6 Bis[S-hexyl 3-(4-methoxybenzylidene)dithiocarbazato-κ^2N^3,S]lead(II), 20

Pale yellow, Yield: 55 %; m.p. (124-126 ^oC). *Anal. Calc.* for $C_{30}H_{42}N_4PbO_2S_4$: C, 43.62; H, 5.12; N, 6.78; S, 15.52 %. Found: C, 43.63; H, 5.13; N, 6.77; S,15.54 %.
Selected IR data (KBr pellets, cm^{-1}): ν(C-H, alkyl) 2921m, ν(C=N) 1606s, ν(N-N) 1029s, ν(CSS) 829m.
^{1}H NMR (400 MHz, $CDCl_3$, ppm) δ: 8.05(s, 2H, CH=N), 7.54(d, 4H, C-4,6, J=5.20 MHz), 7.02(d, 4H, C-3,7, J=5.20 MHz), 3.83(s, 6H, -CH_3O), 3.14(t, 4H, -SCH_2), 1.67(p, 4H, C-11), 1.20-1.41(m, 12H, C-12,13,14), 0.88(t, 6H, C-15).
UV-Vis spectrum [CH_2Cl_2, λ_{max} nm (log ε, L mol^{-1} cm^{-1})]: 231(4.45), 345(4.64).
HRMS (FAB) Calc. for $C_{30}H_{42}N_4PbO_2S_4$ (M+1): 827.1957 ; Found (M+1): 827.2040.
Molar conductivity (1.0×10^{-5} M; CH_2Cl_2, $\Omega^{-1}cm^2mol^{-1}$): 0.00; μ_{eff} = Diamagnetic.

5.4 Results and discussion

5.4.1 S-hexyl 3-(4-methoxybenzylidene)dithiocarbazate, 14

The bidentate ligand HL, having N,S donor atoms, was prepared by the 1:1 condensation of S-hexyldithiocarbazate with 4-methoxybenzaldehyde in ethanol.

The IR spectrum of the free ligand **14** (**Section 5.2**) showed a weak band 3138 cm^{-1} for ν(N-H) [3]. Compounds containing the thioamide -N-NH-C(=S) moiety are capable of exhibiting thione-thiol tautomerism and therefore the 4-methoxybenzal dehyde Schiff base of S-hexyldithiocarbazate can exist either as the thione form or the thiol form or as an equilibrium mixture of both forms (**Scheme 5.1**) [13]. But, our previous studies [14] have shown that these ligands remain solely as the thione tautomer both in the solid state as well as in solution. However, the ligand does not exhibit any ν(S-H) band around 2700 cm^{-1}, indicating that in solid state it maintains the thione functional group [15]. Two strong bands exhibited by the ligand at 1605 and 1095 cm^{-1} are assigned to the ν(C=N) and ν(C=S) stretching vibrations, respectively [16-19]. The ν(N=N) band is observed in the free ligand at 1028 cm^{-1} [20]. It also exhibited a medium band at 875 cm^{-1} for the ν(CSS) stretching mode [19].

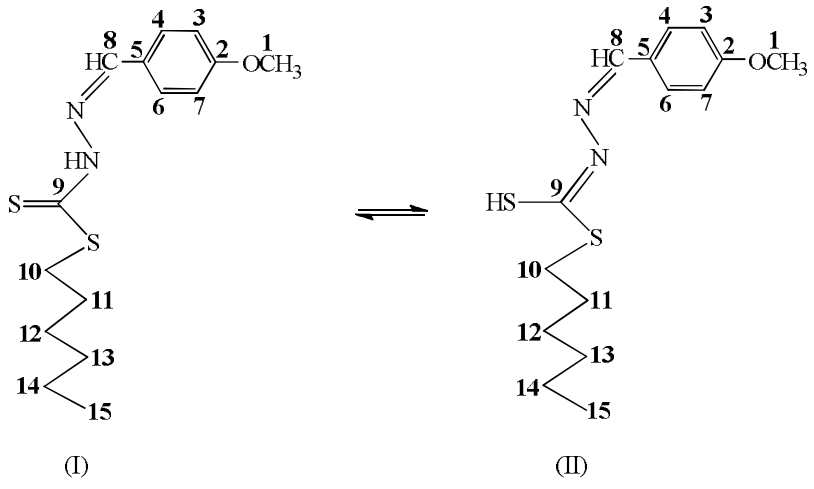

Scheme 5.1: Thione (I) and thiol (II) tautomeric forms of HL, **14**

The ^{1}H NMR of the ligand **14** (**Section 5.2**) showed a broad singlet at 10.66 ppm assigned to the thioamide (N-H) proton[1,21,22] and the absence of any signal at ~ 4.0 ppm for the ligand, suggesting the predominance of the thione tautomer in solution [23]. The azomethine (CH=N) proton observed as a singlet at 7.86 ppm in HL [1,23-26]. The signals at 3.85 and 3.29 ppm for the protons referred to -SCH_2 and C-1 in the ligand [27-29]. The ligand showed other signals at 1.76, 1.45, 1.29 -1.40 and 0.91 ppm for the protons referred to (C-11), (C-12), (C-13,14) and (C-15) of the hexyl group.

The ^{13}C NMR signals of the ligand **14** (**Section 5.2**) are observed at 198.86 and 161.97 ppm for (C=S) and (CH=N) carbons, respectively [24,25,27]. In the ligand the aromatic carbons are observed at 145.36(C-5), 129.56(C-4,6), 125.55(C-2), 114.36(C-3,7) ppm [27]; the methoxy carbon (C-1) at 55.40 ppm [29,30] and the alkyl carbons fall at 34.59(C-10), 31.41(C-11), 28.73(C-12), 28.56(C-13), 22.53(C-14) and 14.03(C-15) ppm.

The mass spectral data by FAB method of the compound **14**, has been given in **Section 5.2**, in its High Resolution Mass Spectrum (HRMS) showed peak at m/z of 311.1249 which consisted with the proposed formula.

The electronic spectrum of the free ligand **14** (**Section 5.2**) exhibited bands at 230 and 262 nm, assigned to the $\pi \rightarrow \pi^*$ transitions for the aromatic ring and azomethine (CH=N) moiety, respectively [25]. Another the two bands at 295 and 346 nm are assigned to $\pi \rightarrow \pi^*$ and $n \rightarrow \pi^*$ transitions of the dithiocarbazate group [24, 25].

5.4.2 Bis[S-hexyl 3-(4-methoxybenzylidene)dithiocarbazato-κ^2N^3,S]M(II), 15-20

Reaction of the ligand with divalent metal ions M(II) [M = Ni, Cu, Zn, Cd, Pd and Pb] in a 2:1 molar ratio in methanol, accompanied by mono-deprotonation, resulted in the formation of bischelated complexes. The *Lasign's* test (halogen test) indicated the absence of chloride ions in the Pd(II) complex **19**, suggesting the uni-negative bidentate complexation of the Schiff bases. All the compounds were soluble in non-coordinating organic solvents such as $CHCl_3$, CH_2Cl_2, DMSO and DMF. The room temperature

molar conductance values of the complexes (10^{-5} M solution in CH_2Cl_2) indicated their non-electrolytic nature [2].

In the infrared spectra of complexes **15-20** (as shown in **Section 5.3**) the disappearance of the ν(N-H) band of the ligand upon complex formation, is an agreement of the coordination of the thiolate sulfur to the metal(II) after deprotonation [31]. The most significant band showed by the ligand at 1605 cm^{-1} assignable to ν(C=N) group which shifted to lower frequency (1603-1591 cm^{-1}), in the corresponding complexes with the exception of Pb(II) complex, hence suggesting the coordination of azomethine nitrogen to the metal atom [16-18].The ν(C=S) band, showed by the ligand **14** at 1095 cm^{-1}, disappeared in the complexes supporting the coordination of the thiolate sulfur atom to the metal [19]. The shifting of the ν(N-N) band in the spectra of the complexes (1032-1027 cm^{-1}), compared to the ligand (1028 cm^{-1}), is another clear indication of the coordination the of azomethine nitrogen to the metal atoms[1,15,21]. The stretching frequency of ν(CSS) in the complexes decreases (835-827 cm^{-1}) as compared to that observed in the ligand (875 cm^{-1}), indicating that complexation have taken place through thiolate sulfur atom [19,32].

The absence of NH signal in the ^1H NMR spectra (as shown in **Section 5.3**) for complexes **15-20** is an agreement with the coordination of thiolate sulfur via deprotonation [3,22,23]. The azomethine (CH=N) proton observed as a singlet at 7.86 ppm in HL, shifted at higher field (7.81-7.61 ppm) in the complexes due to the coordination of azomethine nitrogen [1,23-26]. The signals at 3.85 and 3.29 ppm for the protons referred to -SCH_2 and C-1 in the ligand were shifted to (3.88-3.83 ppm) and (3.26 -3.10 ppm) upon complexation [27-29]. No significant changes observed in the chemical shift for the protons referred to (C-11 to C-15) upon complexation. However, the ^1H NMR spectra for Cu(II)complex **16** was not helpful for the identification of the functional group having the metal ion a paramagnetic electron configuration [28]. The ^1H NMR data are thus consistent with the NS monobasic bidentate binding mode of the ligand.

The mass data by FAB of the compounds **15-20** have been given in **Section 5.3**. The molecular ion peaks of Ni(II), Cu(II), Zn(II), Cd(II), Pd(II) and Pb(II) complexes **15-20** are at m/z 677.1627, 682.1565, 683.1556, 733.1304, 725.1308 and 827.2040, respectively as confirmed by HRMS, suggested the formation of bischelated complexes of the Schiff base ligand **14**.

In the electronic spectra of the complexes **15, 16** and **17** (**Section 5.3**) the thioamide n → π* intra-ligand bands are shifted to high energy (blue shift) upon coordination of the thiol sulfur to the metal [26]. The complexes **15** and **16** showed a medium intensity band at 443 and 431 nm respectively, for the S → M ligand-to-metal charge transfer (LMCT) transition, indicating the coordination of the Schiff base to the metal atom via the thiolate sulfur [33]. The electronic spectrum of the Ni(II) complex exhibited a d-d band at around 534 nm [33]. The diamagnetic nature of the Pd(II) complexes, consistent with the d^8 configuration, suggested a square planar geometry [24,26]. The d-d transition for complex **19** cannot be observed, most probably hidden under the relatively intense LMCT band at 394 nm [34]. The diamagnetic Zn(II) and Cd(II) complexes, consistent with a d^{10} metal ion configuration, do not show *d-d* transition as well, diagnostic of tetrahedral geometry, and that of the diamagnetic Pb(II) complex exhibits an tetrahedral geometry [18]. The Cu(II) complex has magnetic moment of 1.81 B.M. corresponding to a single electron spin [25].

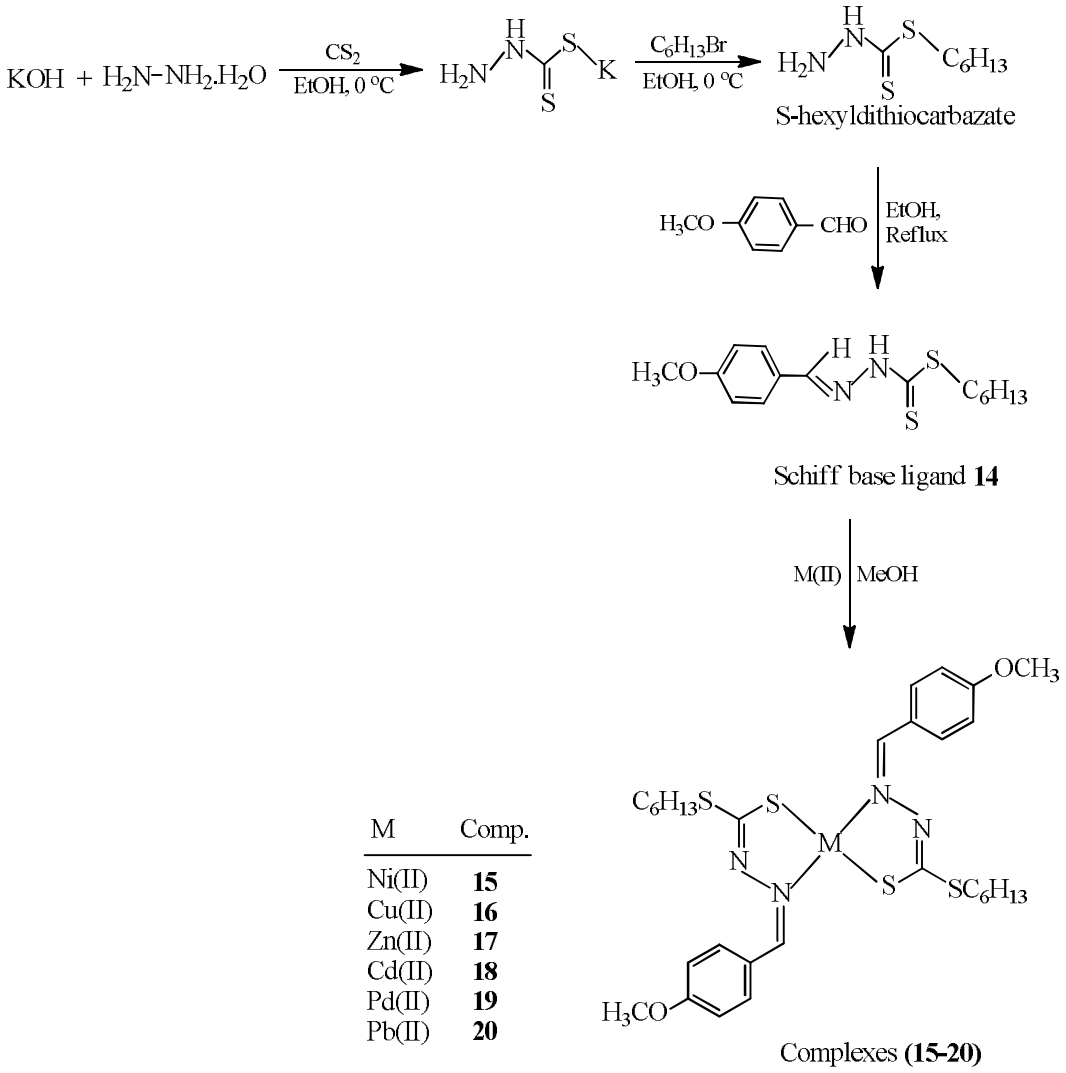

M	Comp.
Ni(II)	**15**
Cu(II)	**16**
Zn(II)	**17**
Cd(II)	**18**
Pd(II)	**19**
Pb(II)	**20**

Scheme 5.2: Synthetic route for the preparation of ligand **14** and the metal complexes **15-20**

5.5 X-ray data collection and crystal structure determination

Crystal structure analysis of the compound **14** reported was carried out at 173 K for **14** on a Rigaku R-AXIS RAPID diffractometer equipped with CCD and Cu-Kα radiation (λ = 1.54187 Å). Cell refinement, indexing and scaling of the data sets were done by using Crystal Structure Rigaku programs [35]. An empirical absorption correction was applied [transmission factors of (0.350, 0.607)] for **14**. All the structures were solved by using SIR92 [36] and subsequent Fourier analyses [37] and refined by the full-matrix least-squares method based on F^2 with all observed reflections [37]. The H atoms were fixed at geometrical positions except that of nitrogen N(2) in **14** which was located on the Fourier map and refined. The ORTEP drawings were done by using the WinGX System, Ver 1.80.05 [38]. Crystal data and details of refinements are given in **Table 5.1**.

5.5.1 Crystal structure description of ligand 14

The molecular and crystal structures of Schiff base ligand S-hexyl 3-(4-methoxybenzy lidene)dithiocarbazate, **14** was determined by single crystal X-ray diffraction method.

The ORTEP drawing of the ligand **14**, which crystallizes in triclinic system space group $P\bar{1}$, is shown in **Fig. 5.1**. In the ligand **14**, the dithiocarbazate group adopts an *E* configuration with respect to the C=N bond of the benzylidene moiety. The *β*-nitrogen and the thioketo sulfur are *trans* located with respect to the C(9)-N(2) bond. The molecule is in its thione tautomeric (also confirmed by IR and NMR) and the co-planarity of atoms (with the exception of the S-hexyl chain) indicates an electron delocalization within it. The C(9)-S(1) and N(2)-C(9) bond length are 1.6713 (19) Å and 1.343 (3) Å, repectively, while N(1)-N(2) bond length is 1.377 (2) Å. All the bond angles are close comparable to those detected in the S-hexyl (*E*)-3-(4-methylbenzylidene)dithiocarbazate [39] which differs for a methyl replacing the methoxy group -O(1)-CH_3. However a different conformation is exhibited by the hexyl chain in the two molecules likely induced by packing requirements. In fact, the torsion angle S(2)-C(10)-C(11)-C(12) is of 173.99(13) and 66.61(1)° in the present complex and in the methyl derivative, respectively.

The crystal packing evidences the ligand molecules piled along axis *a* and connected in pair by N2-H…S1 hydrogen bonds (H…S = 2.51 (3) A, N…S = 3.361 (2) A, O-H…S angle = 154 (2)° as shown in **Fig. 5.2**. On the other hand no appreciable π–π interaction among aromatic rings is present in the crystal packing.

Table 5.1: Crystallographic data and details of refinement for compound **14**

	14
Empirical formula	$C_{15}H_{22}N_2OS_2$
Fw	310.47
Crystal system	Triclinic
Space group	$P\bar{1}$
a, Å	4.55596 (8)
b, Å	12.4224 (3)
c, Å	14.9619 (3)
α, deg	75.7300 (9)
β, deg	84.7599 (10)
γ, deg	84.6141 (9)
V, Å^3	814.99 (3)
Z	2
Dcalcd,g cm^{-3}	1.265
μ(Cu-Kα), mm^{-1}	2.93
F(000)	332
θ max, deg	68.20
No. of reflections collected	9377
No. of indepdent reflections	2932
Rint	0.0816
No. of reflections ($I > 2\sigma(I)$)	2385
Refined parameters	187
goodness-of-fit (F^2)	1.075
R1 ($I>2\sigma(I)$) [a]	0.0509
wR2 (all data) [a]	0.1313
Residuals, e/Å^3	0.550, -0.34

[a] $R1 = \Sigma \; ||Fo| - |Fc|| \; / \Sigma |Fo|$, $wR2 = [\Sigma w (Fo^2 - Fc^2)^2 / \Sigma w (Fo^2)^2]^{1/2}$

Table 5.2: Selected bond lengths (Å) and angles (°) of ligand **14**

	14
S(1)-C(9)	1.6713 (19)
S(2)-C(9)	1.7408 (19)
N(1)-N(2)	1.377 (2)
N(1)-C(8)	1.281 (3)
N(2)-C(9)	1.343 (3)
N(2)-N(1)-C(8)	115.16 (16)
N(1)-N(2)-C(9)	120.57 (16)
S(2)-C(9)-S(1)	126.46 (13)
S(1)-C(9)-N(2)	120.22 (14)
S(2)-C(9)-N(2)	113.32 (13)

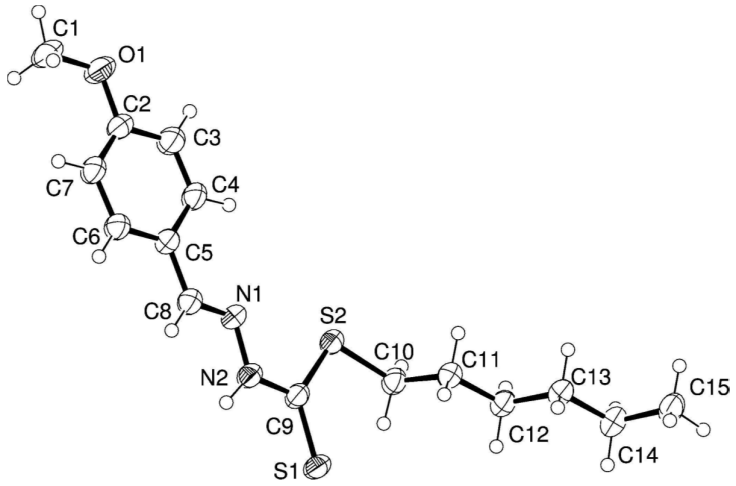

Fig. 5.1: ORTEP drawing (ellipsoid probability at 50%) of compound **14**

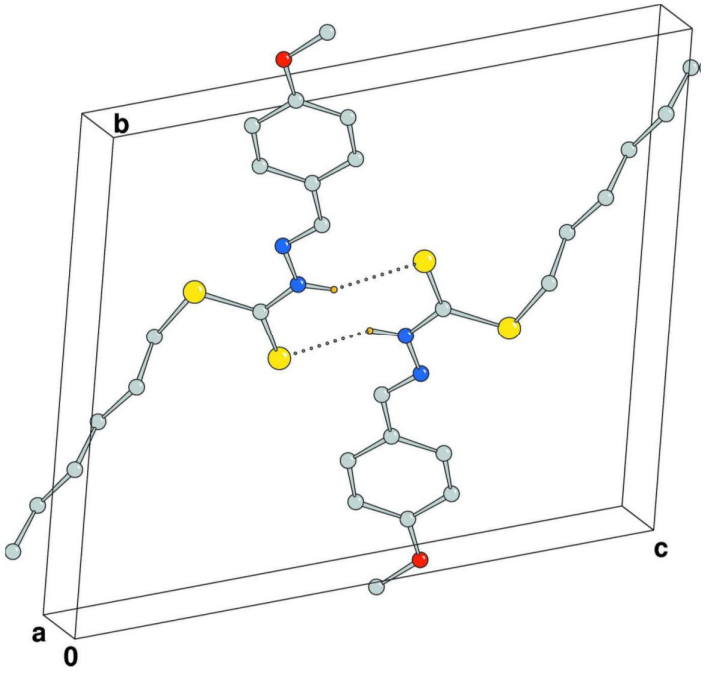

Fig. 5.2: Crystal packing of **14** showing pair of molecules connected by N-H…S interactions (dashed lines). H atoms not involved in hydrogen bonding have been omitted.

5.6 Fluorescence Studies

The photoluminescence properties of the Schiff base ligand **14** and its metal complexes **15-20** were studied of 10^{-5} M solution in CH_2Cl_2 at room temperature. The excitation wavelength dependent emissions of compounds **14-20** have been given in **Table 5.3**. In the emission spectra (as shown in **Fig. 5.3**) of compounds **14-20**, the ligand **14** showed two emission peaks at 391 and 404 nm upon excitation at 346 nm. Excitation of the metal complexes at 281-365 nm gives an emission peak at 313-441 nm. Significant difference in positions of emission maximum of the complexes from those of ligand establish the complexation process [40]. It is interesting that the Ni(II) complex **15** shows a higher fluorescence intensity than that of the free ligand while for the other compounds the fluorescence intensity of the ligand decreases dramatically depending on the complex **16-20** formation with the metal ions.

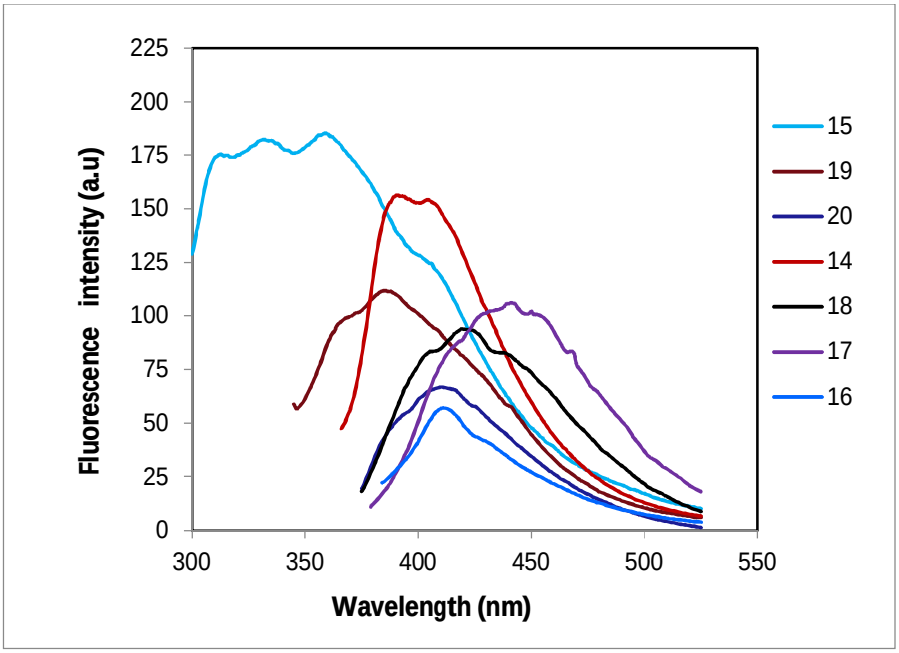

Fig. 5.3: Emission spectra of compounds **14-20** of 10^{-5} M solution in CH_2Cl_2 at room temperature.

Metal ions can enhance or quench the fluorescence emission of some Schiff base ligands containing an aromatic ring. The decrease of emission intensities is due to the formation of coordination complexes of the S and N atom in the ligand with the metal ion. These coordination complexes make the energy transfer from the excited state of the ligand to the metal ions causing decreases of the fluorescence intensity [41]. For this reason the fluorescence intensity of complexes **16-20** is decreased. Quenching of fluorescence of a ligand by transition metal ions during complexation is a rather common phenomenon which is explained by processes such as magnetic perturbation, redox activity, and electronic energy transfer [40-43].

Enhancement of fluorescence through complexation is, however, of much interest as it opens up the opportunity for photochemical applications of these complexes [40,43]. In the absence of metal ions the fluorescence of the ligand is probably quenched by the occurrence of a photoinduced electron transfer (PET) process due to the presence of lone pairs of electrons of the donor atoms in the ligand. Such a PET process is prevented by the complexation of ligand with metal ions; thus the fluorescence

intensity may be greatly enhanced by the coordination of metals. The chelation of the ligand to metals increases the rigidity of the ligand and thus reduces the loss of energy by thermal vibrational decay [44].

Table 5.3: Excitation wavelength dependent emissions of compounds **14-20**

Compound	Excitation wavelength (nm)	Peak wavelength of emission (nm)
14	346	391, 404
15	281	313, 332, 359
16	365	411
17	360	441
18	353	419,408
19	327	385
20	345	401

5.7 Qualitative antibacterial assay

The Schiff base **14** and its metal complexes **15-20** were evaluated for their in vitro antimicrobial activities against three gram-positive bacteria (*Staphylococcus aureus*, *Bacillus subtilis* and *Klebsiella sp.*) and two gram-negative bacteria (*E. coli* and *Pseudomonas aeruginosa*) by disc diffusion methods. The results, as presented in **Table 5.4,** revealed that neither ligand **14** nor any complexes **15-20** were found any activity against the organisms tested. Zone of the test compounds were measured at a dose of 400 µg/disc and ciprofloxacin, a positive control, were evaluated at a dose of 50 µg/disc.

Table 5.4: Qualitative antimicrobial assay of compounds **14-20**

Comp.	Conc. (µg/disc)	Zone of inhibition (mm)			Zone of inhibition (mm)	
14	400	*S. a*	*B. s*	*K. sp.*	*E. c*	*P.a*
15		-	-	-	-	-
16		-	-	-	-	-
17		-	-	-	-	-
18		-	-	-	-	-
19		-	-	-	-	-
20		-	-	-	-	-
Ciprofloxacin	50	24	29	37	22	45

References

1. M.-H.E. Chan, K.A. Crouse, M.I.M. Tahir, R. Rosli, N. Umar-Tsafe, A.R. Cowley, *Polyhedron*, 27 (2008) 1141.
2. K.A. Crouse, K.-B. Chew, M.T.H Tarafder, A. Kasbollah, A.M. Ali, B.M. Yamin, H.-K. Fun, *Polyhedron*, 23 (2004) 161.
3. K.B. Chew, M.T.H. Tarafder, K.A. Crouse, A.M. Ali, B.M. Yamin, H.-K. Fun, *Polyhedron*, 23 (2004) 1385.
4. A.B. Besir, S.K. Guchait, J.A. Gascon, G. Fenteany, *Bioinorganic and Medicinal chemistry*, 18 (2008) 498.
5. M.A. Ali, A.H. Mirza, R. J. Butcher, M.T.H. Tarafder, T.B. Keat, A.M. Ali, *J. Inorg. Biochem.*, 92 (2002) 141.
6. M.A. Ali, A.H. Mirza, R.J. Butcher, K.A. Crouse, *Transition Met. Chem.*, 31 (2006) 79.
7. K. Tampouris, S. Coco, A. Yannopoulos, S. Koinis, *Polyhedron*, 26 (2007) 4269.
8. F.N.-F. How, K.A. Crouse, M.I.M. Tahir, M.T.H. Tarafder, A.R. Cowley, *Polyhedron*, 27 (2008) 3225.
9. M. Yazdanbakhsh, R. Takjoo, *Struct. Chem.*, 19 (2008) 895.
10. R. Takzoo, R. Centore, M. Hakimi, S.A. Beyramabadiand, A. Morsali, *Inorg. Chim. Acta.*, 371 (2011) 36.
11. X.-Y. QIU, S.-Z. Li, A.-R. Shi, Q.-Q. Li, B. Zhai, *Chinese J. Struct. Chem*., 31 (2012) 555.
12. T.B.S.A. Ravoof, K.A. Crouse, M.I.M. Tahir, A.R. Cowley, M.A. Ali, *Polyhedron*, 26 (2007) 1159.
13. M.A. Ali, A.H. Mirza, M. Haniti, S.A. Hamid, P.V. Bernhardt, *Polyhedron*, 24 (2005) 383.
14. M.S. Begum, M.B.H. Howlader, R. Miyatake, E. Zangrando, M.C. Sheikh, *Acta Cryst*. (2015). E**71**, o199.
15. S. Roy, T.N. Mandal, A.K. Barik, S. Gupta, R.J. Butcher, M. Nethaji, S.K. Kar, *Polyhedron*, 27 (2008) 593.

16. M.T.H. Tarafder, T.-J. Khoo, K.A. Crouse, A.M. Ali, B.M. Yamin, H.-K. Fun, *Polyhedron*, 21 (2002) 2691.
17. R.V. Singh, P. Mitharwal, R. Singh, S.P. Mital, *American Chemical Science Journal*, 4 (2014) 117.
18. S.A. Shaker, H.A. Mohammd, A.A. Salih, *Australian Journal of Basic and Applied Sciences*, 4 (2010) 5178-5183.
19. R. Takjoo, R. Centore, L. Rhyman, P. Ramasami, *J. Coord. Chem.*, 65 (2012) 1569.
20. M.A. Ali, H.J.H.A. Bakar, A.H. Mirza, S.J. Smith, L.R. Gahan, P.V. Bernhardt, *Polyhedron*, 28 (2008) 71.
21. P.I.S. Maia, A.G.A. Fernandes, J. Jerley, N. Silva, A.D. Andricopulo, S.S. Lemos, E.S. Lang, U. Abram, V.M. Deflon, *J. Inorg. Biohem.,* 104 (2010) 1276.
22. N.R. Pramanik, S. Ghosh, T.K. Raychaudhuri, S. Ray, R.J. Butcher, S.S. Mandal, *Polyhedron,* 23 (2004) 1595.
23. H. Khaledi, H.M. Ali, M.M. Olmstead, *Inorg. Chim. Acta.,* 366 (2011) 233–240.
24. M.A.A.A. Islam, M.C. Sheikh, M.S. Alam, E. Zangrando, M.A. Alam, M.T.H. Tarafder, R. Myatake, *Transition Met. Chem.,* 39 (2014) 141.
25. M.A.A.A. Islam, M.T.H. Tarafder, M.C. Sheikh, M.A. Alam, E. Zangrando, *Transition Met. Chem.,* 36 (2011) 531.
26. M. Yazdanbaksh, R. Takjoo, W. Frank, A.A. kaju, *J. Coord. Chem.,* (2009) 1.
27. T.B.S.A. Ravoof, K.A. Crouse, M.I.M. Tahir, F.N.-F. How, R. Rosli, D.J. Watkins, *Transition Met. Chem.*, 35 (2010) 871.
28. Y.J. Jang, U.K. Lee, B. Kweon, *Bull. Korean Chem. Soc.* 26 (2011) 925.
29. J.S. Kumaran, S. Priya, N. Jayachandramoni, S. Mahalakshmi, *J. Chem.*, 2013, Article ID260358, 1.
30. K. Singh, S.K. Kushawaha, M.K. Bharty, R. Dulare, R.J. Butcher, *J. Mol. Struc.,* 936 (2009) 257.
31. R. Takjoo, R. Takjoo, M. Yazdanbakhsh, A.A. Kaju, C. Yaguang, *Chin. J. Chem.*, 28 (2010) 221.

32. M. Yazdanbakhsh, M.M. Heravi, R. Takjoo, W. Frank, *Z. Anorg. Allg. Chem.*, 634 (2008) 972.
33. M.A. Ali, A.L. Tan, A.H. Mirza, J.H. Santos, A.H.B.H. Abdullah, *Transition Met. Chem.*, 37 (2012) 651.
34. N.M.H. Salem, L.E. Sayed, M.F. Iskander, *Polyhedron*, 27 (2008) 3115.
35. Rigaku (2010). CrystalStructure. Version 4.0. Rigaku Corporation, Tokyo, Japan.
36. A. Altomare, G. Cascarano, C. Giacovazzo, A. Guagliardi, M. Burla, G. Polidori, M. Camalli, *J. Appl. Cryst.*, 27 (1994) 435.
37. G.M. Sheldrick, *Acta Crystallogr., Sect. A*, 64 (2008) 112.
38. L.J. Farrugia, *J. Appl. Crystallogr.*, 32 (1999) 837.
39. M.B.H. Howlader, M.S. Begum, M.C. Sheikh, R. Miyatake, E. Zangrando, *Acta Cryst.*, (2015). E71, o103.
40. A. Majumder, G.M. Rosair, A. Mallick, N. Chattopadhyay, S. Mitra, *Polyhedron*, 25 (2006) 1753.
41. Z. Önal, H. Zengin, M. Sönmez, *Turk. J. Chem.*, 35 (2011) 905.
42. E.S. Aazam, A.F.EL Husseiny, H.M.A. Amri, *Arabian J. Chem.*, 5 (2012) 45.
43. C. Anitha, C.D. Sheela, P. Tharmaraj, R. Shanmugakala, *Int. J. Inorg. Chem.*, 2013, Article ID 436275, 1.
44. D. Das, B.G. Chand, K.K. Sarker, J. Dinda, C. Sinha, *Polyhedron*, 25 (2006) 2333.

Conclusion and recommendation for future works

This thesis describes the preparation of three NS functionalize Schiff base ligands and their bivalent metal complexes. Three Schiff bases were prepared by the condensation of S-hexyldithiocarbazate with 4-methyl benzaldehyde, thiophene-2-carboxaldeyde and 4-methoxybenzaldehyde, namely, S-hexyl 3-(4-methylbenzylidene)dithiocarbazate **1**, S-hexyl 3-(2-thienylidene)dithiocarbazate **8,** S-hexyl 3-(4-methoxybenzylidene) dithiocarbazate **14**. Single crystals of **1** and **14** were obtained by slow evaporation method. Both the ligands **1** and **14** were crystallized in triclinic system with space group $P\bar{1}$. Spectroscopic and crystallographic data suggest that both **1** and **14** are exist in thione form in the solid and in solution. Upon reaction with the acetate salts of nickel(II), copper(II), zinc(II), cadmium(II) and lead(II), the ligands afforded neutral bis-chelated complexes of nickel(II) (**2**, **9**, **15**), copper(II) (**3**, **10**, **16**), zinc(II) (**4**, **11**, **17**), cadmium(II)(**5**, **12**, **18**) and lead (II) (**7**, 20).They also yielded neutral bis-chelated complexes of palladium(II) (**6**,**13**,**19**) upon the reaction with palladium(II) chloride. Generally, the Schiff bases, in their deprotonated imino thiolate form, act as chelating ligands to the metal centre via the azomethine nitrogen and thiolate sulfur atoms, which was confirmed by the X-ray crystallographic structural analysis for complexes **2**, **6**, **9** and **10**. According to spectroscopic and crystallographic studies, the Ni(II), Cu(II) and Pd(II) complexes exhibit a square planar geometry, the other being tetrahedral.

The fluorescence intensity of all the three Schiff base ligands is quenched upon complexation with metal ions with the exception of complexes **7** and **15** where the fluorescence intensity is enhanced (with respect to the ligand).

The electrochemical properties of Cu(II) complexes **3** and **10** have been studied by cyclic voltammetry. Both the compounds exhibit one electron quasi-reversible redox activity in the applied potential range.

In order to evaluate the effect of antimicrobial activity of metal ions upon chelation, both the ligand **14** and its metal complexes **15-20** were screened for their antibacterial

activity by disc diffusion method. The results revealed that neither ligand **14** nor any complexes **15-20** were found any activity against the organisms tested.

Recommendation for future works

(i) As the antibacterial activity was tested qualitatively for one series, study is needed to determine the antibacterial activity and minimum inhibitory concentration (MIC) as quantitative analysis for other series.

(ii) Literature reported that Schiff bases of S-alkyl/S-aryl dithiocarbazate and their metal complexes can exhibit strong anticancer activity. So, further study is required to determine the cytotoxicity of the ligands and their complexes with cancer cell lines.

(iii) Since Schiff bases of S-alkyl/S-aryl dithiocarbazate and their metal complexes can act as antioxidant agent, further study is recommended to investigate the antioxidant property using EPR spectroscopy.

(iv) Literature reported that some Cu(II) N,S,O/N,N-donor chelators are good anticancer agents due to strong binding ability with DNA base pair (P#19N). So, study is required to investigate the DNA cleavage activity of the synthesized Cu(II) complexes.

(v) Since some Ni(II) and Zn(II) complexes derived from Schiff bases show electrochemical activity, so, study is needed to determine the electrochemical behavior of the synthesized Ni(II) and Zn(II) complexes.

List of publications

1. **M.S. Begum**, M.B.H. Howlader, R. Miyatake, E. Zangrando, M.C. Sheikh, Crystal structure of S-hexyl (E)-3-(4-methoxybenzylidene)dithiocarbazate, *Acta Cryst*., E**71**, o199, (2015).

2. **M.S. Begum**, M.B.H. Howlader, M.C. Sheikh, R. Miyatake, E. Zangrando, Crystal structure of bis[S-hexyl 3-(4-methylbenzylidene)dithiocarbazato-κ^2N^3,S]palladium(II), *Acta Cryst*., E**71**, m63-m64, (2015).

3. M.B.H. Howlader, **M.S. Begum**, M.C. Sheikh, R. Miyatake, E. Zangrando, Crystal structure of bis[S-hexyl 3-(4-methylbenzylidene)dithiocarbazato-κ^2N^3,S]nickel(II), *Acta Cryst*., E**71**, m26-m27, (2015).

4. M.B.H. Howlader, **M.S. Begum**, M.C. Sheikh, R. Miyatake, E. Zangrando, Crystal structure of S-hexyl (E)-3-(4-methylbenzylidene)dithiocarbazate, *Acta Cryst*., E**71**, o103-o104, (2015).

Supplementary crystallographic data of compound 1

***Table A1**: Fractional atomic coordinates and isotropic or equivalent isotropic displacement parameters (Å^2)*

Atom	*x*	*y*	*z*	U_{iso}*/U_{eq}
S1	1.54116 (12)	0.83289 (5)	0.90597 (4)	0.0326 (2)
S2	1.17201 (12)	0.64667 (5)	0.98677 (4)	0.0333 (2)
N1	1.0048 (4)	0.84542 (15)	1.10436 (12)	0.0293 (5)
N2	1.2012 (4)	0.87708 (16)	1.04349 (13)	0.0297 (5)
C1	0.0848 (5)	0.8428 (3)	1.42942 (17)	0.0390 (6)
C2	0.2994 (5)	0.8663 (2)	1.35925 (15)	0.0300 (5)
C3	0.3922 (5)	0.77235 (19)	1.29544 (15)	0.0333 (6)
C4	0.5864 (5)	0.79268 (19)	1.23002 (15)	0.0327 (6)
C5	0.6987 (5)	0.90853 (18)	1.22664 (14)	0.0282 (5)
C6	0.6060 (5)	1.00311 (19)	1.28972 (15)	0.0314 (6)
C7	0.4103 (5)	0.9817 (2)	1.35483 (15)	0.0334 (6)
C8	0.9098 (5)	0.93191 (19)	1.15966 (15)	0.0281 (5)
C9	1.3050 (5)	0.79357 (19)	0.98029 (15)	0.0290 (5)
C10	1.3277 (5)	0.55512 (19)	0.88956 (15)	0.0329 (6)
C11	1.1314 (5)	0.51925 (18)	0.80356 (15)	0.0333 (6)
C12	1.0591 (5)	0.62287 (19)	0.75707 (15)	0.0329 (6)
C13	0.8582 (5)	0.58746 (19)	0.67205 (15)	0.0330 (6)
C14	0.7870 (5)	0.69523 (19)	0.63000 (16)	0.0363 (6)
C15	0.5920 (6)	0.6635 (3)	0.54445 (17)	0.0445 (7)
H1	0.0707	0.7576	1.4338	0.0468*
H2	−0.0975	0.8647	1.4095	0.0468*
H3	0.1417	0.8908	1.4907	0.0468*
H4	0.3201	0.6925	1.2971	0.0400*
H5	0.6440	0.7270	1.1869	0.0393*
H6	0.6778	1.0830	1.2880	0.0377*
H7	0.3505	1.0474	1.3974	0.0401*
H8	0.9772	1.0121	1.1572	0.0337*
H9	1.266 (5)	0.948 (3)	1.0471 (17)	0.044 (8)*
H10	1.4987	0.6000	0.8723	0.0395*

H11	1.3848	0.4817	0.9098	0.0395*
H12	1.2193	0.4603	0.7573	0.0400*
H13	0.9556	0.4791	0.8220	0.0400*
H14	1.2346	0.6621	0.7376	0.0394*
H15	0.9745	0.6826	0.8037	0.0394*
H16	0.9442	0.5300	0.6240	0.0396*
H17	0.6834	0.5467	0.6907	0.0396*
H18	0.6990	0.7519	0.6781	0.0435*
H19	0.9628	0.7367	0.6129	0.0435*
H20	0.5574	0.7366	0.5206	0.0534*
H21	0.4142	0.6253	0.5612	0.0534*
H22	0.6782	0.6081	0.4961	0.0534*

***Table A2**: Atomic displacement parameters (Å^2)*

Atom	U^{11}	U^{22}	U^{33}	U^{12}	U^{13}	U^{23}
S1	0.0382 (4)	0.0272 (4)	0.0329 (4)	0.0014 (3)	0.0096 (3)	0.0062 (3)
S2	0.0453 (5)	0.0245 (3)	0.0317 (4)	0.0021 (3)	0.0077 (3)	0.0087 (3)
N1	0.0353 (12)	0.0273 (10)	0.0259 (10)	0.0011 (9)	0.0034 (9)	0.0070 (8)
N2	0.0342 (12)	0.0236 (10)	0.0318 (11)	0.0010 (9)	0.0072 (9)	0.0062 (8)
C1	0.0374 (15)	0.0452 (14)	0.0383 (14)	0.0048 (12)	0.0056 (11)	0.0169 (11)
C2	0.0308 (14)	0.0345 (12)	0.0266 (12)	0.0037 (10)	−0.0019 (10)	0.0104 (10)
C3	0.0404 (15)	0.0240 (11)	0.0361 (13)	−0.0023 (10)	0.0017 (11)	0.0091 (10)
C4	0.0413 (15)	0.0255 (11)	0.0312 (12)	0.0045 (11)	0.0007 (11)	0.0039 (10)
C5	0.0324 (14)	0.0268 (11)	0.0263 (12)	0.0034 (10)	−0.0014 (10)	0.0071 (9)
C6	0.0350 (14)	0.0238 (11)	0.0364 (13)	0.0016 (10)	0.0032 (11)	0.0079 (10)
C7	0.0399 (15)	0.0290 (12)	0.0314 (12)	0.0060 (11)	0.0044 (11)	0.0033 (10)
C8	0.0296 (13)	0.0255 (11)	0.0304 (12)	0.0025 (10)	0.0003 (10)	0.0083 (9)
C9	0.0333 (14)	0.0280 (11)	0.0274 (11)	0.0054 (10	−0.0011 (10)	0.0084 (9)
C10	0.0406 (15)	0.0249 (11)	0.0346 (13)	0.0086 (11)	0.0042 (11)	0.0061 (10)
C11	0.0416 (15)	0.0245 (11)	0.0350 (13)	0.0034 (11)	0.0046 (11)	0.0074 (10)
C12	0.0396 (15)	0.0254 (11)	0.0345 (13)	0.0044 (10)	0.0050 (11)	0.0069 (10)
C13	0.0362 (14)	0.0272 (12)	0.0364 (13)	0.0021 (10)	0.0056 (11)	0.0077 (10)
C14	0.0416 (16)	0.0301 (12)	0.0388 (13)	0.0035 (11)	0.0048 (12)	0.0100 (10)
C15	0.0494 (17)	0.0415 (14)	0.0449 (15)	0.0004 (13)	−0.0021 (13)	0.0160 (12)

***Table A3**: Geometric parameters (Å º)*

S1− C9	1.670 (3)	C1−H2	0.980
S2− C9	1.759 (3)	C1−H3	0.980
S2−C10	1.814 (3)	C3−H4	0.950
N1−N2	1.375 (3)	C4−H5	0.950
N1−C8	1.277 (3)	C6−H6	0.950
N2−C9	1.335 (3)	C7−H7	0.950
C1−C2	1.505 (4)	C8−H8	0.950
C2−C3	1.395 (3)	C10−H10	0.990
C2−C7	1.389 (4)	C10−H11	0.990
C3−C4	1.380 (4)	C11−H12	0.990
C4−C5	1.392 (3)	C11−H13	0.990
C5−C6	1.394 (3)	C12−H14	0.990
C5−C8	1.460 (4)	C12−H15	0.990
C6−C7	1.384 (4)	C13−H16	0.990
C10−C11	1.524 (3)	C13−H17	0.990
C11−C12	1.518 (4)	C14−H18	0.990
C12−C13	1.526 (3)	C14−H19	0.990
C13−C14	1.523 (4)	C15−H20	0.980
C14−C15	1.512 (4)	C15−H21	0.980
N2−H9	0.84 (3)	C15−H22	0.980
C1−H1	0.980		
C9−S2−C10	103.78 (11)	C2−C7−H7	119.297
N2−N1−C8	115.97 (18)	C6−C7−H7	119.294
N−N2−C9	120.61 (18)	N1−C8−H8	119.724
C1−C2−C3	120.9 (2)	C5−C8−H8	119.729
C1−C2−C7	121.6 (2)	S2−C10−H10	108.909
C3−C2−C7	117.5 (2)	S2−C10−H11	108.910
C2−C3−C4	121.5 (2)	C11−C10−H10	108.900
C3−C4−C5	120.6 (2)	C11−C10−H11	108.913
C4−C5−C6	118.3 (2)	H10−C10−H11	107.737
C4−C5−C8	121.55 (19)	C10−C11−H12	108.647
C6−C5−C8	120.14 (19)	C10−C11−H13	108.645
C5−C6−C7	120.6 (2)	C12−C11−H12	108.656
C2−C7−C6	121.4 (2)	C12−C11−H13	108.654

N1−C8−C5	120.5 (2)	H12−C11−H13	107.587
S1−C9−S2	126.25 (13)	C11−C12−H14	108.631
S1−C9−N2	120.30 (17)	C11−C12−H15	108.636
S2−C9−N2	113.44 (17)	C13−C12−H14	108.637
S2−C10−C11	113.33 (17)	C13−C12−H15	108.627
C10−C11−C12	114.44 (17)	H14−C12−H15	107.578
C11−C12−C13	114.52 (18)	C12−C13−H16	109.166
C12−C13−C14	112.20 (17)	C12−C13−H17	109.171
C13−C14−C15	113.80 (18)	C14−C13−H16	109.159
N1−N2−H9	121.2 (17)	C14−C13−H17	109.167
C9−N2−H9	118.1 (17)	H16−C13−H17	107.879
C2−C1−H1	109.474	C13−C14−H18	108.795
C2−C1−H2	109.467	C13−C14−H19	108.797
C2−C1−H3	109.465	C15−C14−H18	108.803
H1−C1−H2	109.474	C15−C14−H19	108.808
H1−C1−H3	109.480	H18−C14−H19	107.672
H2−C1−H3	109.467	C14−C15−H20	109.472
C2−C3−H4	119.227	C14−C15−H21	109.469
C4−C3−H4	119.232	C14−C15−H22	109.470
C3−C4−H5	119.709	H20−C15−H21	109.471
C5−C4−H5	119.710	H20−C15−H22	109.473
C5−C6−H6	119.686	H21−C15−H22	109.472
C7−C6−H6	119.692		
C9−S2−C10−C11	−99.27 (15)	C3−C4−C5−C6	−1.2 (4)
C10−S2−C9−S1	−4.68 (19)	C3−C4−C5−C8	178.37 (19)
C10−S2−C9−N2	176.19 (15)	C4−C5−C6−C7	0.9 (4)
N2−N1−C8−C5	179.48 (17)	C4−C5−C8−N1	−2.6 (4)
C8−N1−N2−C9	−177.29 (18)	C6−C5−C8−N1	176.96 (19)
N1−N2−C9−S1	179.41 (16)	C8−C5−C6−C7	−178.62 (18)
N1−N2−C9−S2	−1.4 (3)	C5—C6—C7—C2	−0.3 (4)
C1−C2−C3−C4	179.25 (19)	S2−C10−C11−C12	66.6 (2)
C1−C2−C7−C6	−179.50 (19)	C10−C11−C12−C13	−178.90 (17)
C3−C2−C7−C6	−0.1 (4)	C11−C12−C13−C14	178.41 (17)
C7−C2−C3−C4	−0.2 (4)	C12−C13−C14−C15	178.99 (17)
C2−C3−C4−C5	0.8 (4)		

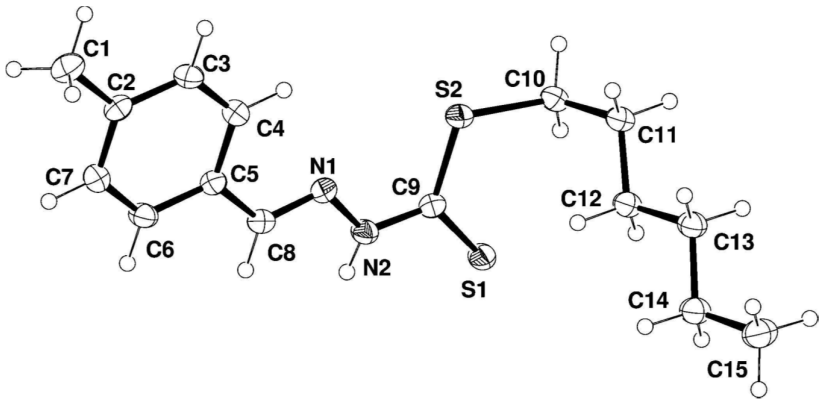

Fig. A1: ORTEP drawing (ellipsoid probability at 50 %) of Schiff base ligand **1**.

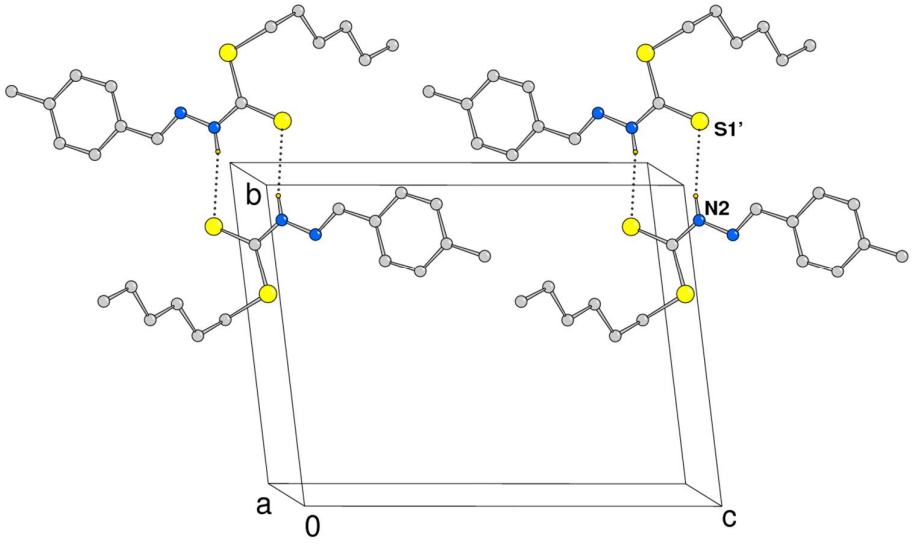

Fig. A2: Crystal packing of the Schiff base ligand **1** showing pair of molecules connected by N-H...S interactions.

Supplementary crystallographic data of compound *2*

***Table A4**: Fractional atomic coordinates and isotropic or equivalent isotropic displacement parameters (Å^2)*

	x	*y*	*z*	U_{iso}*/U_{eq}
Ni	1.0000	1.0000	1.0000	0.0372 (4)
S1	1.1112 (3)	0.83443 (10)	0.92242 (6)	0.0516 (4)
S2	1.4585 (2)	0.80909 (9)	0.76635 (6)	0.0479 (4)
N1	0.7454 (7)	0.9180 (3)	1.07644 (18)	0.0365 (8)
N2	1.3765 (7)	1.0201 (3)	0.85050 (18)	0.0405 (8)
C1	−0.0675 (10)	0.4837 (4)	1.2473 (3)	0.0514 (11)
H1A	−0.0056	0.4630	1.3025	0.077*
H1B	−0.0491	0.4035	1.2184	0.077*
H1C	−0.2717	0.5288	1.2503	0.077*
C2	0.1222 (9)	0.5695 (4)	1.2022 (2)	0.0420 (10)
C3	0.1476 (9)	0.6854 (4)	1.2321 (3)	0.0489 (11)
H3	0.0431	0.7105	1.2825	0.059*
C4	0.3184 (9)	0.7676 (4)	1.1923 (2)	0.0455 (10)
H4	0.3281	0.8471	1.2154	0.055*
C5	0.4769 (8)	0.7344 (4)	1.1181 (2)	0.0390 (9)
C6	0.4513 (10)	0.6168 (4)	1.0883 (3)	0.0522 (12)
H6	0.5555	0.5913	1.0380	0.063*
C7	0.2807 (10)	0.5349 (4)	1.1288 (2)	0.0511 (11)
H7	0.2718	0.4547	1.1063	0.061*
C8	0.6638 (9)	0.8089 (4)	1.0680 (2)	0.0418 (10)
H8	0.7429	0.7691	1.0186	0.050*
C9	1.3189 (8)	0.9071 (4)	0.8487 (2)	0.0370 (9)
C10	1.6632 (9)	0.9110 (4)	0.7013 (3)	0.0469 (11)
H10A	1.7787	0.9530	0.7355	0.056*
H10B	1.8022	0.8559	0.6632	0.056*
C11	1.4718 (9)	1.0153 (4)	0.6522 (2)	0.0463 (10)
H11A	1.3404	1.0736	0.6903	0.056*

H11B	1.3482	0.9738	0.6203	0.056*
C12	1.6461 (9)	1.0959 (4)	0.5943 (2)	0.0467 (10)
H12A	1.7684	1.1383	0.6262	0.056*
H12B	1.7784	1.0378	0.5563	0.056*
C13	1.4508 (9)	1.1991 (4)	0.5453 (2)	0.0488 (11)
H13A	1.3236	1.1563	0.5154	0.059*
H13B	1.3227	1.2580	0.5837	0.059*
C14	1.6143 (10)	1.2790 (4)	0.4849 (3)	0.0545 (12)
H14A	1.7445	1.2204	0.4468	0.065*
H14B	1.7386	1.3235	0.5147	0.065*
C15	1.4131 (11)	1.3796 (5)	0.4361 (3)	0.0670 (14)
H15A	1.3058	1.3358	0.4015	0.100*
H15B	1.5293	1.4337	0.4019	0.100*
H15C	1.2742	1.4342	0.4735	0.100*

***Table A5**: Atomic displacement parameters ($Å^2$)*

Atom	U^{11}	U^{22}	U^{33}	U^{12}	U^{13}	U^{23}
Ni	0.0441 (7)	0.0337 (6)	0.0351 (5)	−0.0150 (4)	0.0033 (4)	0.0027 (4)
S1	0.0706 (9)	0.0392 (6)	0.0472 (6)	−0.0254 (6)	0.0172 (6)	−0.0036 (5)
S2	0.0571 (8)	0.0331 (6)	0.0520 (6)	−0.0121 (5)	0.0142 (5)	−0.0052 (4)
N1	0.044 (2)	0.0325 (16)	0.0337 (16)	−0.0097 (15)	0.0010 (14)	−0.0006 (13)
N2	0.045 (2)	0.0378 (18)	0.0370 (17)	−0.0105 (16)	0.0085 (15)	0.0032 (14)
C1	0.047 (3)	0.047 (2)	0.061 (3)	−0.016 (2)	−0.001 (2)	0.013 (2)
C2	0.034 (2)	0.042 (2)	0.050 (2)	−0.0104 (18)	−0.0010 (18)	0.0111 (18)
C3	0.051 (3)	0.044 (2)	0.051 (2)	−0.013 (2)	0.016 (2)	−0.0023 (19)
C4	0.053 (3)	0.034 (2)	0.049 (2)	−0.015 (2)	0.012 (2)	−0.0064 (17)
C5	0.040 (2)	0.039 (2)	0.038 (2)	−0.0142 (18)	0.0024 (18)	0.0049 (16)
C6	0.071 (3)	0.045 (2)	0.044 (2)	−0.027 (2)	0.013 (2)	−0.0083 (19)
C7	0.068 (3)	0.043 (2)	0.048 (2)	−0.027 (2)	0.004 (2)	−0.0037 (18)
C8	0.050 (3)	0.044 (2)	0.0337 (19)	−0.017 (2)	0.0048 (18)	−0.0028 (16)
C9	0.036 (2)	0.037 (2)	0.036 (2)	−0.0065 (18)	0.0024 (17)	0.0012 (16)

C10	0.049 (3)	0.039 (2)	0.050 (2)	−0.010 (2)	0.016 (2)	−0.0037 (18)
C11	0.050 (3)	0.044 (2)	0.045 (2)	−0.014 (2)	0.007 (2)	−0.0020 (18)
C12	0.048 (3)	0.043 (2)	0.049 (2)	−0.016 (2)	0.009 (2)	−0.0037 (18)
C13	0.051 (3)	0.050 (2)	0.047 (2)	−0.017 (2)	0.007 (2)	−0.0016 (19)
C14	0.061 (3)	0.047 (2)	0.056 (3)	−0.019 (2)	0.011 (2)	−0.001 (2)
C15	0.079 (4)	0.061 (3)	0.063 (3)	−0.026 (3)	0.001 (3)	0.007 (2)

***Table A6**: Geometric parameters (Å, º)*

Ni−N1	1.933 (3)	C6−C7	1.385 (5)
Ni−N1^{i}	1.933 (3)	C6−H6	0.9500
Ni−S1	2.1775 (10)	C7−H7	0.9500
Ni−S1^{i}	2.1775 (10)	C8−H8	0.9500
S1−C9	1.720 (4)	C10−C11	1.519 (5)
S2−C9	1.757 (4)	C10−H10A	0.9900
S2−C10	1.811 (4)	C10−H10B	0.9900
N1−C8	1.294 (5)	C11−C12	1.521 (5)
N1−N2^{i}	1.425 (4)	C11−H11A	0.9900
N2−C9	1.269 (5)	C11−H11B	0.9900
N2−N1^{i}	1.425 (4)	C12−C13	1.521 (6)
C1−C2	1.501 (5)	C12−H12A	0.9900
C1−H1A	0.9800	C12−H12B	0.9900
C1−H1B	0.9800	C13−C14	1.513 (5)
C1−H1C	0.9800	C13−H13A	0.9900
C2−C3	1.371 (6)	C13−H13B	0.9900
C2−C7	1.391 (6)	C14−C15	1.517 (6)
C3−C4	1.383 (5)	C14−H14A	0.9900
C3−H3	0.9500	C14−H14B	0.9900
C4−C5	1.399 (5)	C15−H15A	0.9800
C4−H4	0.9500	C15−H15B	0.9800
C5−C6	1.387 (5)	C15−H15C	0.9800
C5−C8	1.452 (5)		
N1−Ni−N1^{i}	180.00 (14)	N2−C9−S1	125.9 (3)

N1−Ni−S1	93.96 (9)	N2−C9−S2	120.3 (3)
$N1^{i}$−Ni−S1	86.04 (9)	S1−C9−S2	113.9 (2)
N1−Ni−$S1^{i}$	86.04 (9)	C11−C10−S2	113.5 (3)
$N1^{i}$−Ni−$S1^{i}$	93.96 (9)	C11−C10−H10A	108.9
S1−Ni−$S1^{i}$	180.0	S2−C10−H10A	108.9
C9−S1−Ni	95.86 (13)	C11−C10−H10B	108.9
C9−S2−C10	103.09 (19)	S2−C10−H10B	108.9
C8−N1−$N2^{i}$	113.8 (3)	H10A−C10−H10B	107.7
C8−N1−Ni	126.3 (3)	C10−C11−C12	113.2 (3)
$N2^{i}$−N1−Ni	119.9 (2)	C10−C11−H11A	108.9
C9−N2−$N1^{i}$	111.9 (3)	C12−C11−H11A	108.9
C2−C1−H1A	109.5	C10−C11−H11B	108.9
C2−C1−H1B	109.5	C12−C11−H11B	108.9
H1A−C1−H1B	109.5	H11A−C11−H11B	107.8
C2−C1−H1C	109.5	C13−C12−C11	112.4 (3)
H1A−C1−H1C	109.5	C13−C12−H12A	109.1
H1B−C1−H1C	109.5	C11−C12−H12A	109.1
C3−C2−C7	117.1 (4)	C13−C12−H12B	109.1
C3−C2−C1	121.3 (4)	C11−C12−H12B	109.1
C7−C2−C1	121.7 (4)	H12A−C12−H12B	107.9
C2−C3−C4	123.0 (4)	C14−C13−C12	114.4 (4)
C2−C3−H3	118.5	C14−C13−H13A	108.7
C4−C3−H3	118.5	C12−C13−H13A	108.7
C3−C4−C5	120.4 (4)	C14−C13−H13B	108.7
C3−C4−H4	119.8	C12−C13−H13B	108.7
C5−C4−H4	119.8	H13A−C13−H13B	107.6
C6−C5−C4	116.3 (3)	C13−C14−C15	113.0 (4)
C6−C5−C8	116.0 (3)	C13−C14−H14A	109.0
C4−C5−C8	127.8 (4)	C15−C14−H14A	109.0
C7−C6−C5	122.9 (4)	C13−C14−H14B	109.0
C7−C6−H6	118.6	C15−C14−H14B	109.0
C5−C6−H6	118.6	H14A−C14−H14B	107.8
C6−C7−C2	120.3 (4)	C14−C15−H15A	109.5
C6−C7−H7	119.9	C14−C15−H15B	109.5
C2−C7−H7	119.9	H15A−C15−H15B	109.5

N1−C8−C5	133.6 (4)	C14−C15−H15C	109.5
N1−C8−H8	113.2	H15A−C15−H15C	109.5
C5−C8−H8	113.2	H15B−C15−H15C	109.5
C7−C2−C3−C4	0.8 (6)	C4−C5−C8−N1	2.7 (8)
C1−C2−C3−C4	−179.6 (4)	$N1^{i}$−N2−C9−S1	1.8 (5)
C2−C3−C4−C5	−0.2 (7)	$N1^{i}$−N2−C9−S2	−177.5 (2)
C3−C4−C5−C6	0.0 (6)	Ni−S1−C9−N2	2.5 (4)
C3−C4−C5−C8	179.5 (4)	Ni−S1−C9−S2	−178.24 (18)
C4−C5−C6−C7	−0.2 (7)	C10−S2−C9−N2	−0.4 (4)
C8−C5−C6−C7	−179.8 (4)	C10−S2−C9−S1	−179.8 (2)
C5−C6−C7−C2	0.8 (7)	C9−S2−C10−C11	−77.3 (3)
C3−C2−C7−C6	−1.0 (6)	S2−C10−C11−C12	−176.9 (3)
C1−C2−C7−C6	179.3 (4)	C10−C11−C12−C13	179.6 (3)
$N2^{i}$−N1−C8−C5	−1.2 (7)	C11−C12−C13−C14	−178.2 (3)
Ni−N1−C8−C5	−179.8 (3)	C12−C13−C14−C15	179.1 (4)

Symmetry code: (i) −*x*+2, −*y*+2, −*z*+2.

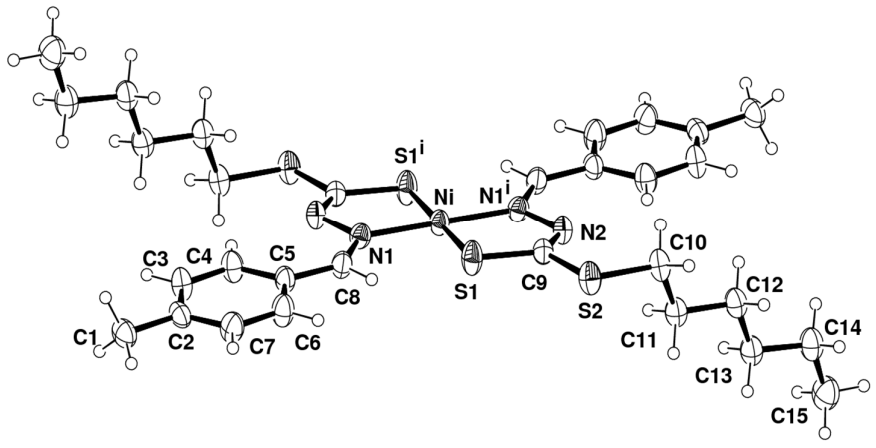

Figure A3: ORTEP drawing (ellipsoid probability at 50%) of the centrosymmetric NiL_2 complex **2**.

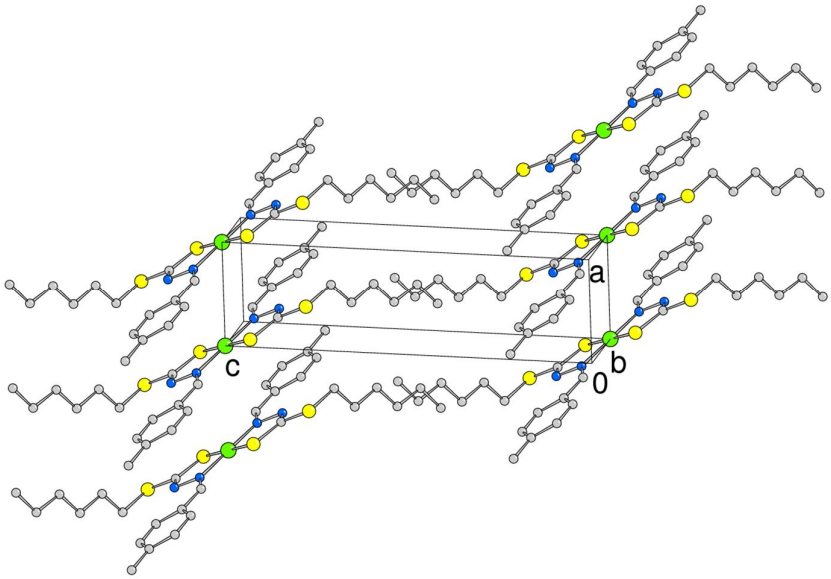

Fig. A4: Crystal packing of the NiL_2 complex **2**

Supplementary crystallographic data of compound *6*

***Table A7**: Fractional atomic coordinates and isotropic or equivalent isotropic displacement parameters (Å^2)*

Atom	*x*	*y*	*z*	U_{iso}*/U_{eq}
Pd1	0.5000	0.5495	0.0000	0.0607 (4)
S1	0.4807 (3)	0.3802 (4)	0.1325 (5)	0.0725 (11)
S2	0.4003 (2)	0.3956 (4)	0.3156 (4)	0.0726 (9)
N1	0.4949 (7)	0.6818 (12)	0.1634 (13)	0.060 (3)
N2	0.4526 (9)	0.6244 (17)	0.2347 (16)	0.071 (4)
C1	0.7185 (10)	1.1510 (17)	0.0408 (17)	0.087 (4)
H1A	0.7670	1.1034	0.0465	0.130*
H1B	0.7353	1.2327	0.1036	0.130*
H1C	0.6839	1.1796	−0.0594	0.130*
C2	0.6712 (6)	1.0545 (19)	0.0900 (11)	0.063 (3)

C3	0.6745 (8)	0.9122 (16)	0.0758 (15)	0.072 (4)
H3	0.7083	0.8746	0.0369	0.086*
C4	0.6290 (7)	0.8236 (13)	0.1178 (14)	0.062 (3)
H4	0.6339	0.7262	0.1124	0.075*
C5	0.5759 (7)	0.8797 (13)	0.1679 (13)	0.061 (3)
C6	0.5741 (8)	1.0255 (14)	0.1841 (14)	0.070 (4)
H6	0.5412	1.0656	0.2234	0.084*
C7	0.6196 (8)	1.1052 (14)	0.1431 (14)	0.071 (3)
H7	0.6161	1.2025	0.1509	0.085*
C8	0.5215 (8)	0.7962 (12)	0.2045 (14)	0.062 (3)
H8	0.5048	0.8378	0.2700	0.074*
C9	0.4449 (11)	0.4926 (16)	0.2274 (18)	0.059 (4)
C10	0.3742 (9)	0.529 (2)	0.4125 (15)	0.080 (5)
H10A	0.4242	0.5722	0.4885	0.096*
H10B	0.3406	0.6025	0.3449	0.096*
C11	0.3247 (9)	0.4534 (18)	0.4821 (16)	0.081 (4)
H11A	0.2809	0.3981	0.4062	0.097*
H11B	0.3617	0.3886	0.5571	0.097*
C12	0.2885 (8)	0.545 (2)	0.5472 (14)	0.081 (3)
H12A	0.2580	0.6183	0.4765	0.097*
H12B	0.3327	0.5904	0.6324	0.097*
C13	0.2311 (9)	0.4735 (19)	0.5952 (19)	0.091 (5)
H13A	0.1951	0.4112	0.5161	0.109*
H13B	0.2642	0.4148	0.6800	0.109*
C14	0.1813 (12)	0.559 (3)	0.632 (2)	0.133 (7)
H14A	0.1500	0.6224	0.5504	0.160*
H14B	0.2165	0.6168	0.7170	0.160*
C15	0.1205 (10)	0.475 (2)	0.670 (2)	0.110 (6)
H15A	0.0888	0.5391	0.6982	0.165*
H15B	0.1512	0.4118	0.7499	0.165*
H15C	0.0835	0.4224	0.5845	0.165*

***Table A8**: Atomic displacement parameters (Å^2)*

Atom	U^{11}	U^{22}	U^{33}	U^{12}	U^{13}	U^{23}
Pd1	0.0664 (7)	0.0506 (7)	0.0761 (7)	0.000	0.0419 (5)	0.000
S1	0.093 (3)	0.051 (2)	0.095 (3)	0.001 (2)	0.062 (2)	0.004 (2)
S2	0.084 (2)	0.059 (2)	0.092 (2)	−0.0072 (17)	0.0542 (19)	0.0009 (17)
N1	0.055 (6)	0.057 (7)	0.076 (7)	−0.011 (5)	0.037 (6)	0.006 (5)
N2	0.067 (8)	0.072 (9)	0.091 (9)	−0.027 (7)	0.050 (7)	−0.017 (7)
C1	0.081 (9)	0.094 (12)	0.096 (11)	−0.013 (8)	0.048 (9)	0.004 (8)
C2	0.063 (6)	0.054 (7)	0.073 (6)	0.014 (9)	0.032 (5)	−0.003 (9)
C3	0.063 (8)	0.084 (11)	0.086 (9)	0.003 (7)	0.048 (7)	−0.002 (7)
C4	0.058 (6)	0.048 (7)	0.082 (8)	0.003 (5)	0.034 (6)	0.003 (6)
C5	0.060 (7)	0.052 (7)	0.076 (8)	0.000 (6)	0.036 (6)	0.001 (5)
C6	0.076 (7)	0.053 (10)	0.093 (8)	0.001 (7)	0.048 (7)	−0.005 (6)
C7	0.074 (8)	0.055 (8)	0.080 (9)	−0.004 (6)	0.032 (7)	0.011 (6)
C8	0.079 (8)	0.030 (6)	0.096 (9)	0.006 (6)	0.057 (7)	0.005 (6)
C9	0.068 (9)	0.052 (9)	0.063 (9)	−0.004 (7)	0.034 (7)	0.000 (6)
C10	0.085 (8)	0.090 (14)	0.081 (8)	−0.017 (10)	0.053 (7)	0.007 (9)
C11	0.084 (9)	0.083 (11)	0.086 (10)	−0.009 (8)	0.048 (8)	0.002 (8)
C12	0.084 (7)	0.088 (9)	0.081 (7)	−0.019 (12)	0.047 (6)	−0.019 (12)
C13	0.082 (10)	0.104 (12)	0.109 (12)	0.010 (9)	0.063 (9)	0.002 (9)
C14	0.162 (16)	0.118 (16)	0.150 (15)	0.043 (19)	0.098 (14)	−0.003 (17)
C15	0.106 (12)	0.112 (14)	0.160 (17)	−0.024 (10)	0.102 (13)	−0.010 (11)

***Table A9**: Geometric parameters (Å, º)*

Pd1−N1	2.154 (12)	C6−C7	1.337 (16)
Pd1−N1^{i}	2.154 (12)	C6−H6	0.9500
Pd1−S1	2.264 (4)	C7−H7	0.9500
Pd1−S1^{i}	2.264 (4)	C8−H8	0.9500
S1−C9	1.777 (17)	C10−C11	1.573 (19)
S2−C9	1.747 (16)	C10−H10A	0.9900
S2−C10	1.829 (18)	C10−H10B	0.9900

N1−C8	1.208 (16)	C11−C12	1.44 (2)
N1−N2	1.404 (17)	C11−H11A	0.9900
N2−C9	1.282 (15)	C11−H11B	0.9900
C1−C2	1.511 (19)	C12−C13	1.52 (2)
C1−H1A	0.9800	C12−H12A	0.9900
C1−H1B	0.9800	C12−H12B	0.9900
C1−H1C	0.9800	C13−C14	1.41 (2)
C2−C7	1.381 (16)	C13−H13A	0.9900
C2−C3	1.39 (2)	C13−H13B	0.9900
C3−C4	1.397 (18)	C14−C15	1.56 (3)
C3−H3	0.9500	C14−H14A	0.9900
C4−C5	1.403 (16)	C14−H14B	0.9900
C4−H4	0.9500	C15−H15A	0.9800
C5−C6	1.423 (17)	C15−H15B	0.9800
C5−C8	1.460 (16)	C15−H15C	0.9800
N1−Pd1−N1^{i}	107.1 (6)	N2−C9−S2	124.7 (15)
N1−Pd1−S1	83.2 (3)	N2−C9−S1	125.6 (15)
N1i−Pd1−S1	168.1 (3)	S2−C9−S1	109.6 (9)
N1−Pd1−S1^{i}	168.1 (3)	C11−C10−S2	105.5 (13)
N1i−Pd1−S1^{i}	83.2 (3)	C11−C10−H10A	110.6
S1−Pd1−S1^{i}	87.3 (2)	S2−C10−H10A	110.6
C9−S1−Pd1	95.1 (5)	C11−C10−H10B	110.6
C9−S2−C10	101.8 (7)	S2−C10−H10B	110.6
C8−N1−N2	114.2 (12)	H10A−C10−H10B	108.8
C8−N1−Pd1	131.8 (10)	C12−C11−C10	114.0 (15)
N2−N1−Pd1	114.0 (9)	C12−C11−H11A	108.7
C9−N2−N1	115.8 (16)	C10−C11−H11A	108.7
C2−C1−H1A	109.5	C12−C11−H11B	108.7
C2−C1−H1B	109.5	C10−C11−H11B	108.7
H1A−C1−H1B	109.5	H11A−C11−H11B	107.6
C2−C1−H1C	109.5	C11−C12−C13	113.9 (18)
H1A−C1−H1C	109.5	C11−C12−H12A	108.8
H1B−C1−H1C	109.5	C13−C12−H12A	108.8
C7−C2−C3	117.7 (14)	C11−C12−H12B	108.8
C7−C2−C1	121.0 (16)	C13−C12−H12B	108.8

C3−C2−C1	121.2 (12)	H12A−C12−H12B	107.7
C2−C3−C4	120.9 (12)	C14−C13−C12	116.7 (19)
C2−C3−H3	119.5	C14−C13−H13A	108.1
C4−C3−H3	119.5	C12−C13−H13A	108.1
C3−C4−C5	119.4 (12)	C14−C13−H13B	108.1
C3−C4−H4	120.3	C12−C13−H13B	108.1
C5−C4−H4	120.3	H13A−C13−H13B	107.3
C4−C5−C6	118.9 (11)	C13−C14−C15	112 (2)
C4−C5−C8	123.5 (11)	C13−C14−H14A	109.1
C6−C5−C8	117.6 (11)	C15−C14−H14A	109.1
C7−C6−C5	118.9 (12)	C13−C14−H14B	109.1
C7−C6−H6	120.5	C15−C14−H14B	109.1
C5−C6−H6	120.5	H14A−C14−H14B	107.8
C6−C7−C2	124.0 (14)	C14−C15−H15A	109.5
C6−C7−H7	118.0	C14−C15−15B	109.5
C2−C7−H7	118.0	H15A−C15−H15B	109.5
N1−C8−C5	129.2 (12)	C14−C15−H15C	109.5
N1−C8−H8	115.4	H15A−C15−H15C	109.5
C5−C8−H8	115.4	H15B−C15−H15C	109.5

Symmetry code: (i) −*x*+1, *y*, −*z*.

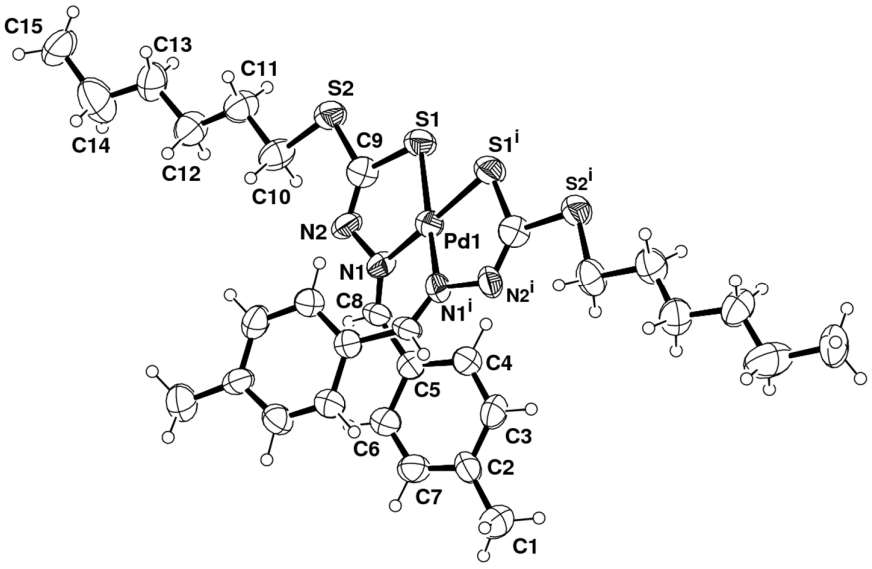

Fig. A5: ORTEP drawing (40% ellipsoid probability) of PdL_2 complex **6**

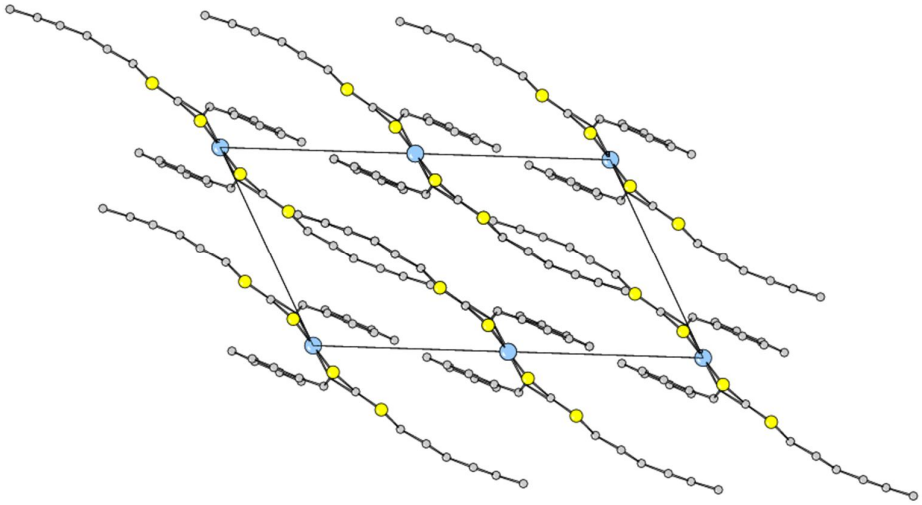

Fig. A6: Crystal packing viewed down axis *b* of PdL_2 complex **6**

Supplementary crystallographic data of complex *9*

Table A10. *Atomic coordinates and B_{iso}/B_{eq} for complex* ***9***

Atom	x	y	z	B_{eq}
Ni1	0.94698(1)	0.12815(2)	0.437919(7)	1.616(5)
S1	1.12925(2)	0.20437(3)	0.24363(2)	1.911(6)
S2	1.04553(2)	0.27580(3)	0.49078(2)	2.394(7)
S3	1.19364(2)	0.42797(3)	0.44263(2)	2.421(7)
S4	0.73766(2)	0.07364(3)	0.62176(2)	2.205(7)
S5	0.83834(2)	-0.00104(3)	0.37870(2)	2.259(7)
S6	0.67614(3)	-0.13677(3)	0.41946(2)	2.667(7)
N1	1.02289(7)	0.13916(9)	0.37076(5)	1.68(2)
N2	1.09267(7)	0.2380(1)	0.37214(5)	1.81(2)
N3	0.87157(8)	0.1143(1)	0.50564(5)	1.78(2)
N4	0.79190(8)	0.0282(1)	0.49842(5)	1.95(2)
C1	1.1270(1)	0.1442(2)	0.16524(6)	2.14(2)
C2	1.07559(9)	0.0307(2)	0.15294(6)	2.14(2)
C3	1.03678(9)	-0.0081(2)	0.20789(6)	1.93(2)
C4	1.05834(8)	0.0769(1)	0.26158(6)	1.68(2)
C5	1.01478(9)	0.0640(1)	0.31865(6)	1.77(2)
C6	1.10728(9)	0.3029(2)	0.42758(6)	1.82(2)
C7	1.2454(1)	0.4199(2)	0.36875(6)	2.24(2)
C8	1.33550(9)	0.5070(2)	0.37672(6)	2.13(2)
C9	1.3775(1)	0.4980(2)	0.31379(7)	2.43(3)
C10	1.4684(1)	0.5805(2)	0.31596(7)	2.43(3)
C11	1.5100(1)	0.5628(2)	0.25324(8)	2.89(3)
C12	1.6016(2)	0.6432(2)	0.25499(9)	3.64(3)
C13	0.7324(1)	0.1391(2)	0.69799(7)	2.43(3)
C14	0.8008(1)	0.2335(2)	0.71773(6)	2.37(2)
C15	0.85855(9)	0.2538(2)	0.67018(6)	2.14(2)
C16	0.83375(9)	0.1744(2)	0.61467(6)	1.82(2)
C17	0.88575(9)	0.1797(2)	0.56120(6)	1.93(2)

C18	0.77327(9)	-0.0278(2)	0.44061(6)	1.97(2)
C19	0.6296(1)	-0.1378(2)	0.49572(7)	2.40(3)
C20	0.5379(1)	-0.2221(2)	0.48696(7)	2.61(3)
C21	0.4958(1)	-0.2172(2)	0.54998(7)	2.42(3)
C22	0.4040(1)	-0.2997(2)	0.54551(7)	2.50(3)
C23	0.3623(1)	-0.2906(2)	0.60850(7)	2.54(3)
C24	0.2724(1)	-0.3757(2)	0.60515(8)	3.07(3)

$B_{eq} = 8/3\ \pi^2(U_{11}(aa^*)^2 + U_{22}(bb^*)^2 + U_{33}(cc^*)^2 + 2U_{12}(aa^*bb^*)\cos\gamma + 2U_{13}(aa^*cc^*)\cos\beta + 2U_{23}(bb^*cc^*)\cos\alpha)$

Table A11**: Atomic coordinates and B_{iso} of hydrogen atoms for complex **9

Atom	x	y	z	B_{iso}
H1	1.1580	0.1852	0.1337	2.57
H2	1.0672	-0.0164	0.1122	2.57
H3	0.9995	-0.0850	0.2082	2.32
H4	0.9742	-0.0100	0.3185	2.13
H5	1.2640	0.3294	0.3614	2.69
H6	1.1957	0.4477	0.3291	2.69
H7	1.3855	0.4794	0.4162	2.56
H8	1.3171	0.5978	0.3838	2.56
H9	1.3939	0.4064	0.3069	2.92
H10	1.3263	0.5249	0.2748	2.92
H11	1.5191	0.5566	0.3559	2.92
H12	1.4517	0.6729	0.3202	2.92
H13	1.5257	0.4702	0.2487	3.47
H14	1.4594	0.5877	0.2134	3.47
H15	1.6542	0.6128	0.2915	4.36
H16	1.5876	0.7345	0.2623	4.36
H17	1.6221	0.6341	0.2123	4.36
H18	0.6868	0.1125	0.7237	2.91
H19	0.8085	0.2799	0.7586	2.84
H20	0.9097	0.3161	0.6757	2.56

H21	0.9383	0.2401	0.5674	2.32
H22	0.6805	-0.1718	0.5331	2.89
H23	0.6137	-0.0482	0.5070	2.89
H24	0.5545	-0.3128	0.4780	3.13
H25	0.4881	-0.1910	0.4481	3.13
H26	0.5466	-0.2470	0.5886	2.91
H27	0.4799	-0.1261	0.5585	2.91
H28	0.4201	-0.3913	0.5382	3.00
H29	0.3535	-0.2713	0.5065	3.00
H30	0.4135	-0.3165	0.6477	3.04
H31	0.3445	-0.1994	0.6151	3.04
H32	0.2208	-0.3493	0.5670	3.68
H33	0.2487	-0.3663	0.6466	3.68
H34	0.2898	-0.4665	0.5996	3.68

Table A12**: Anisotropic displacement parameters for complex **9

Atom	U^{11}	U^{22}	U^{33}	U^{12}	U^{13}	U^{23}
Ni1	0.02236(9)	0.02230(9)	0.01814(8)	-0.00138(5)	0.00744(6)	0.00098(5)
S1	0.0269(2)	0.0256(2)	0.0220(2)	-0.0034(1)	0.0094(1)	-0.0013(1)
S2	0.0336(2)	0.0394(2)	0.0207(2)	-0.0127(2)	0.0121(2)	-0.0057(2)
S3	0.0330(2)	0.0343(2)	0.0273(2)	-0.0120(2)	0.0121(2)	-0.0072(2)
S4	0.0277(2)	0.0323(2)	0.0260(2)	-0.0060(2)	0.0107(2)	-0.0005(1)
S5	0.0313(2)	0.0335(2)	0.0235(2)	-0.0089(2)	0.0114(2)	-0.0048(1)
S6	0.0340(2)	0.0389(2)	0.0306(2)	-0.0145(2)	0.0118(2)	-0.0068(2)
N1	0.0226(5)	0.0214(5)	0.0206(5)	-0.0006(4)	0.0065(4)	0.0022(4)
N2	0.0249(5)	0.0232(5)	0.0224(5)	-0.0029(4)	0.0085(4)	0.0008(4)
N3	0.0223(5)	0.0237(5)	0.0228(5)	-0.0016(4)	0.0074(4)	0.0019(4)
N4	0.0250(5)	0.0259(5)	0.0248(5)	-0.0043(4)	0.0086(4)	0.0005(4)
C1	0.0282(7)	0.0333(7)	0.0221(6)	0.0017(5)	0.0102(5)	0.0003(5)
C2	0.0278(6)	0.0312(7)	0.0231(6)	0.0042(5)	0.0068(5)	-0.0042(5)
C3	0.0243(6)	0.0231(6)	0.0268(6)	0.0014(5)	0.0072(5)	-0.0025(5)
C4	0.0217(6)	0.0209(6)	0.0218(6)	0.0018(4)	0.0062(5)	0.0010(4)
C5	0.0230(6)	0.0218(6)	0.0236(6)	0.0010(4)	0.0074(5)	0.0015(5)

C6	0.0230(6)	0.0252(6)	0.0216(6)	-0.0017(5)	0.0064(5)	0.0019(5)
C7	0.0284(6)	0.0327(7)	0.0260(6)	-0.0065(5)	0.0104(5)	-0.0035(5)
C8	0.0253(6)	0.0282(6)	0.0285(6)	-0.0042(5)	0.0079(5)	-0.0015(5)
C9	0.0289(7)	0.0339(7)	0.0315(7)	-0.0052(5)	0.0108(6)	-0.0027(5)
C10	0.0283(7)	0.0300(7)	0.0358(7)	-0.0023(5)	0.0107(6)	0.0022(5)
C11	0.0338(7)	0.0423(8)	0.0361(7)	-0.0018(6)	0.0128(6)	0.0063(6)
C12	0.0432(9)	0.0446(9)	0.057(1)	-0.0050(7)	0.0245(8)	0.0104(7)
C13	0.0314(7)	0.0375(7)	0.0269(6)	0.0005(5)	0.0141(6)	0.0024(5)
C14	0.0332(7)	0.0343(7)	0.0241(6)	0.0037(5)	0.0098(6)	-0.0011(5)
C15	0.0277(6)	0.0290(6)	0.0254(6)	-0.0015(5)	0.0077(5)	-0.0008(5)
C16	0.0231(6)	0.0250(6)	0.0219(6)	-0.0008(5)	0.0065(5)	0.0020(5)
C17	0.0245(6)	0.0270(6)	0.0233(6)	-0.0018(5)	0.0081(5)	0.0012(5)
C18	0.0244(6)	0.0250(6)	0.0267(6)	-0.0022(5)	0.0079(5)	0.0017(5)
C19	0.0291(7)	0.0346(7)	0.0294(7)	-0.0066(5)	0.0104(6)	-0.0002(5)
C20	0.0305(7)	0.0378(8)	0.0317(7)	-0.0100(6)	0.0088(6)	-0.0010(6)
C21	0.0294(7)	0.0316(7)	0.0319(7)	-0.0048(5)	0.0085(6)	0.0004(5)
C22	0.0291(7)	0.0361(7)	0.0306(7)	-0.0057(6)	0.0084(6)	0.0015(6)
C23	0.0313(7)	0.0348(7)	0.0315(7)	-0.0022(6)	0.0097(6)	0.0010(6)
C24	0.0356(8)	0.0476(9)	0.0362(8)	-0.0087(6)	0.0138(7)	0.0022(6)

The general temperature factor expression: $\exp(-2\pi^2(a^{*2}U_{11}h^2 + b^{*2}U_{22}k^2 + c^{*2}U_{33}l^2 + 2a^*b^*U_{12}hk + 2a^*c^*U_{13}hl + 2b^*c^*U_{23}kl)$

Table A13**: Bond lengths (Å) for complex **9

Atom	Atom	Distance	Atom	Atom	Distance
Ni1	S2	2.1785(4)	Ni1	S5	2.1812(4)
Ni1	N1	1.9112(12)	Ni1	N3	1.9177(12)
S1	C1	1.7133(13)	S1	C4	1.7331(13)
S2	C6	1.7244(14)	S3	C6	1.7484(13)
S3	C7	1.8125(15)	S4	C13	1.7154(15)
S4	C16	1.7289(14)	S5	C18	1.7327(14)
S6	C18	1.7437(13)	S6	C19	1.8148(16)
N1	N2	1.4070(14)	N1	C5	1.3035(16)
N2	C6	1.2948(16)	N3	N4	1.4071(16)
N3	C17	1.2998(16)	N4	C18	1.2915(16)
C1	C2	1.3692(19)	C2	C3	1.4071(19)
C3	C4	1.3869(17)	C4	C5	1.4342(19)
C7	C8	1.5262(19)	C8	C9	1.528(2)
C9	C10	1.522(2)	C10	C11	1.529(3)
C11	C12	1.520(3)	C13	C14	1.3634(19)
C14	C15	1.407(2)	C15	C16	1.3825(18)
C16	C17	1.439(2)	C19	C20	1.528(2)
C20	C21	1.528(3)	C21	C22	1.526(2)
C22	C23	1.527(3)	C23	C24	1.523(2)

Table A14**: Bond lengths involving hydrogens (Å) for complex **9

Atom	Atom	Distance	Atom	Atom	Distance
C1	H1	0.950	C2	H2	0.950
C3	H3	0.950	C5	H4	0.950
C7	H5	0.990	C7	H6	0.990
C8	H7	0.990	C8	H8	0.990
C9	H9	0.990	C9	H10	0.990
C10	H11	0.990	C10	H12	0.990
C11	H13	0.990	C11	H14	0.990
C12	H15	0.980	C12	H16	0.980
C12	H17	0.980	C13	H18	0.950
C14	H19	0.950	C15	H20	0.950
C17	H21	0.950	C19	H22	0.990
C19	H23	0.990	C20	H24	0.990
C20	H25	0.990	C21	H26	0.990
C21	H27	0.990	C22	H28	0.990
C22	H29	0.990	C23	H30	0.990
C23	H31	0.990	C24	H32	0.980
C24	H33	0.980	C24	H34	0.980

Table A15: *Bond angles (°) for complex **9***

Atom	Atom	Atom	Angle	Atom	Atom	Atom	Angle
S2	Ni1	S5	173.288(13)	S2	Ni1	N1	85.74(3)
S2	Ni1	N3	94.61(4)	S5	Ni1	N1	93.71(3)
S5	Ni1	N3	86.03(4)	N1	Ni1	N3	179.08(5)
C1	S1	C4	91.55(7)	Ni1	S2	C6	96.10(5)
C6	S3	C7	101.75(7)	C13	S4	C16	91.45(7)
Ni1	S5	C18	95.95(4)	C18	S6	C19	101.21(7)
Ni1	N1	N2	121.21(8)	Ni1	N1	C5	126.04(9)
N2	N1	C5	112.69(11)	N1	N2	C6	111.74(11)
Ni1	N3	N4	121.09(8)	Ni1	N3	C17	126.08(10)
N4	N3	C17	112.83(11)	N3	N4	C18	112.20(11)
S1	C1	C2	112.66(11)	C1	C2	C3	111.94(12)
C2	C3	C4	113.42(12)	S1	C4	C3	110.42(10)
S1	C4	C5	127.24(9)	C3	C4	C5	121.86(11)
N1	C5	C4	129.25(11)	S2	C6	S3	115.18(7)
S2	C6	N2	124.24(10)	S3	C6	N2	120.58(11)
S3	C7	C8	110.61(9)	C7	C8	C9	109.36(10)
C8	C9	C10	114.26(11)	C9	C10	C11	111.98(12)
C10	C11	C12	112.67(13)	S4	C13	C14	112.71(12)
C13	C14	C15	111.82(12)	C14	C15	C16	113.56(12)
S4	C16	C15	110.46(11)	S4	C16	C17	127.97(10)
C15	C16	C17	121.56(12)	N3	C17	C16	129.64(12)
S5	C18	S6	115.11(7)	S5	C18	N4	124.31(10)
S6	C18	N4	120.57(11)	S6	C19	C20	110.46(10)
C19	C20	C21	110.31(12)	C20	C21	C22	113.66(12)
C21	C22	C23	112.54(12)	C22	C23	C24	112.80(12)

Supplementary crystallographic data of complex 10

Table A16**: Atomic coordinates and B_{iso}/B_{eq} for complex **10

Atom	x	y	z	B_{eq}
Cu1	0.94668(1)	0.12842(2)	0.938407(7)	1.647(4)
S1	1.13059(2)	0.20659(3)	0.74386(2)	1.864(6)
S2	1.04507(3)	0.28941(3)	0.98960(2)	2.405(7)
S3	1.19562(2)	0.43207(3)	0.94163(2)	2.338(7)
S4	0.73497(2)	0.07049(3)	1.12245(2)	2.172(7)
S5	0.83117(3)	-0.00462(3)	0.87785(2)	2.328(7)
S6	0.67189(3)	-0.13962(4)	0.92043(2)	2.639(7)
N1	1.02825(8)	0.1393(1)	0.87046(5)	1.70(2)
N2	1.09787(8)	0.2379(1)	0.87348(5)	1.74(2)
N3	0.86974(8)	0.1075(1)	1.00886(5)	1.84(2)
N4	0.78988(8)	0.0226(1)	0.99969(5)	1.89(2)
C1	1.1264(1)	0.1480(2)	0.66556(6)	2.08(2)
C2	1.07398(9)	0.0357(2)	0.65269(6)	2.08(2)
C3	1.03582(9)	-0.0042(2)	0.70718(6)	1.87(2)
C4	1.05911(9)	0.0795(1)	0.76093(6)	1.63(2)
C5	1.01736(9)	0.0665(2)	0.81794(6)	1.74(2)
C6	1.10909(9)	0.3065(2)	0.92747(6)	1.75(2)
C7	1.2479(1)	0.4218(2)	0.86909(6)	2.16(2)
C8	1.33804(9)	0.5092(2)	0.87689(6)	2.07(2)
C9	1.3795(1)	0.4994(2)	0.81462(7)	2.39(3)
C10	1.4700(1)	0.5822(2)	0.81612(7)	2.40(3)
C11	1.5097(1)	0.5653(2)	0.75365(8)	2.90(3)
C12	1.6016(2)	0.6453(2)	0.75488(9)	3.63(4)
C13	0.7297(1)	0.1368(2)	1.19766(7)	2.44(3)
C14	0.7986(1)	0.2308(2)	1.21762(7)	2.37(3)
C15	0.8573(1)	0.2499(2)	1.17131(6)	2.10(2)
C16	0.83233(9)	0.1699(2)	1.11628(6)	1.80(2)

C17	0.88475(9)	0.1728(2)	1.06399(6)	1.94(2)
C18	0.77009(9)	-0.0311(2)	0.94123(6)	1.94(2)
C19	0.6267(1)	-0.1416(2)	0.99617(7)	2.32(3)
C20	0.5347(1)	-0.2259(2)	0.98758(7)	2.55(3)
C21	0.4929(1)	-0.2200(2)	1.04980(7)	2.37(3)
C22	0.4008(1)	-0.3021(2)	1.04554(7)	2.42(3)
C23	0.3595(1)	-0.2918(2)	1.10774(7)	2.52(3)
C24	0.2690(2)	-0.3756(2)	1.10468(8)	3.10(3)

$B_{eq} = 8/3\ \pi^2(U_{11}(aa^*)^2 + U_{22}(bb^*)^2 + U_{33}(cc^*)^2 + 2U_{12}(aa^*bb^*)\cos\gamma + 2U_{13}(aa^*cc^*)\cos\beta + 2U_{23}(bb^*cc^*)\cos\alpha)$

Table A17: *Atomic coordinates and B_{iso} of hydrogen atoms for complex **10***

Atom	x	y	z	B_{iso}
H1	1.1571	0.1893	0.6345	2.49
H2	1.0644	-0.0103	0.6119	2.49
H3	0.9980	-0.0807	0.7070	2.24
H4	0.9755	-0.0063	0.8173	2.09
H5	1.2671	0.3312	0.8629	2.59
H6	1.1977	0.4479	0.8291	2.59
H7	1.3889	0.4825	0.9164	2.48
H8	1.3193	0.5998	0.8834	2.48
H9	1.3966	0.4080	0.8085	2.87
H10	1.3273	0.5248	0.7756	2.87
H11	1.5222	0.5588	0.8556	2.88
H12	1.4529	0.6743	0.8205	2.88
H13	1.5253	0.4728	0.7488	3.48
H14	1.4578	0.5903	0.7143	3.48
H15	1.5879	0.7364	0.7623	4.36
H16	1.6206	0.6364	0.7122	4.36
H17	1.6554	0.6148	0.7909	4.36
H18	0.6836	0.1108	1.2227	2.93
H19	0.8061	0.2778	1.2580	2.84
H20	0.9090	0.3118	1.1772	2.52
H21	0.9386	0.2315	1.0707	2.33
H22	0.6787	-0.1755	1.0332	2.79
H23	0.6109	-0.0523	1.0076	2.79
H24	0.5515	-0.3165	0.9792	3.06
H25	0.4843	-0.1956	0.9486	3.06
H26	0.5444	-0.2492	1.0885	2.84
H27	0.4770	-0.1289	1.0578	2.84
H28	0.4169	-0.3936	1.0388	2.91
H29	0.3496	-0.2743	1.0064	2.91

H30	0.4114	-0.3175	1.1469	3.02
H31	0.3422	-0.2004	1.1139	3.02
H32	0.2860	-0.4665	1.0998	3.72
H33	0.2167	-0.3495	1.0665	3.72
H34	0.2458	-0.3648	1.1458	3.72

Table A18**: Anisotropic displacement parameters for complex **10

Atom	U^{11}	U^{22}	U^{33}	U^{12}	U^{13}	U^{23}
Cu1	0.02254(9)	0.02301(9)	0.01925(8)	-0.00168(5)	0.00938(6)	0.00137(5)
S1	0.0257(2)	0.0256(2)	0.0220(2)	-0.0037(1)	0.0105(2)	-0.0016(1)
S2	0.0350(2)	0.0388(2)	0.0218(2)	-0.0131(2)	0.0152(2)	-0.0065(2)
S3	0.0314(2)	0.0338(2)	0.0268(2)	-0.0118(2)	0.0132(2)	-0.0070(2)
S4	0.0264(2)	0.0323(2)	0.0268(2)	-0.0062(2)	0.0122(2)	-0.0002(2)
S5	0.0320(2)	0.0352(2)	0.0247(2)	-0.0097(2)	0.0137(2)	-0.0056(2)
S6	0.0336(2)	0.0382(2)	0.0312(2)	-0.0148(2)	0.0132(2)	-0.0069(2)
N1	0.0227(5)	0.0216(5)	0.0220(5)	-0.0012(4)	0.0088(4)	0.0017(4)
N2	0.0231(5)	0.0238(5)	0.0214(5)	-0.0030(4)	0.0094(4)	0.0004(4)
N3	0.0236(5)	0.0254(5)	0.0226(5)	-0.0032(4)	0.0089(4)	0.0013(4)
N4	0.0238(5)	0.0256(5)	0.0244(5)	-0.0047(4)	0.0098(5)	0.0010(4)
C1	0.0271(7)	0.0328(7)	0.0215(6)	0.0018(5)	0.0105(5)	0.0003(5)
C2	0.0271(7)	0.0303(7)	0.0227(6)	0.0042(5)	0.0081(5)	-0.0039(5)
C3	0.0235(6)	0.0221(6)	0.0264(6)	0.0020(5)	0.0078(5)	-0.0021(5)
C4	0.0210(6)	0.0208(6)	0.0214(6)	0.0013(5)	0.0075(5)	0.0011(5)
C5	0.0225(6)	0.0215(6)	0.0240(6)	-0.0002(5)	0.0090(5)	0.0009(5)
C6	0.0217(6)	0.0254(6)	0.0209(6)	-0.0015(5)	0.0077(5)	0.0014(5)
C7	0.0267(6)	0.0323(7)	0.0259(6)	-0.0069(5)	0.0119(5)	-0.0032(5)
C8	0.0237(6)	0.0277(7)	0.0286(7)	-0.0044(5)	0.0092(5)	-0.0013(5)
C9	0.0278(7)	0.0342(7)	0.0315(7)	-0.0050(6)	0.0124(6)	-0.0024(6)
C10	0.0269(7)	0.0300(7)	0.0369(7)	-0.0018(5)	0.0126(6)	0.0032(6)
C11	0.0327(8)	0.0443(9)	0.0364(8)	-0.0019(6)	0.0143(6)	0.0062(7)
C12	0.0448(9)	0.0453(9)	0.056(1)	-0.0056(7)	0.0279(8)	0.0098(8)
C13	0.0306(7)	0.0384(8)	0.0281(7)	0.0012(6)	0.0157(6)	0.0031(6)

C14	0.0340(7)	0.0334(7)	0.0250(6)	0.0036(6)	0.0115(6)	-0.0006(5)
C15	0.0271(6)	0.0287(7)	0.0253(6)	-0.0022(5)	0.0088(5)	-0.0002(5)
C16	0.0218(6)	0.0260(6)	0.0220(6)	-0.0012(5)	0.0080(5)	0.0027(5)
C17	0.0239(6)	0.0283(7)	0.0232(6)	-0.0037(5)	0.0086(5)	0.0014(5)
C18	0.0239(6)	0.0245(6)	0.0272(6)	-0.0026(5)	0.0099(5)	0.0014(5)
C19	0.0274(7)	0.0340(7)	0.0294(7)	-0.0069(6)	0.0115(6)	0.0008(6)
C20	0.0289(7)	0.0364(8)	0.0331(7)	-0.0102(6)	0.0100(6)	-0.0004(6)
C21	0.0280(7)	0.0310(7)	0.0326(7)	-0.0048(5)	0.0100(6)	0.0005(6)
C22	0.0270(7)	0.0353(7)	0.0311(7)	-0.0052(6)	0.0094(6)	0.0019(6)
C23	0.0295(7)	0.0353(8)	0.0325(7)	-0.0032(6)	0.0105(6)	0.0009(6)
C24	0.0350(8)	0.050(1)	0.0368(8)	-0.0091(7)	0.0157(7)	0.0014(7)

The general temperature factor expression: $\exp(-2\pi^2(a^{*2}U_{11}h^2 + b^{*2}U_{22}k^2 + c^{*2}U_{33}l^2 + 2a^*b^*U_{12}hk + 2a^*c^*U_{13}hl + 2b^*c^*U_{23}kl)$

Table A19: *Bond lengths (Å) for complex* ***10***

Atom	Atom	Distance	Atom	Atom	Distance
Cu1	S2	2.2591(4)	Cu1	S5	2.2637(4)
Cu1	N1	1.9988(12)	Cu1	N3	2.0047(12)
S1	C1	1.7141(14)	S1	C4	1.7323(13)
S2	C6	1.7295(15)	S3	C6	1.7495(13)
S3	C7	1.8106(15)	S4	C13	1.7136(16)
S4	C16	1.7290(14)	S5	C18	1.7367(15)
S6	C18	1.7453(13)	S6	C19	1.8132(17)
N1	N2	1.3981(16)	N1	C5	1.3000(16)
N2	C6	1.3003(16)	N3	N4	1.3953(16)
N3	C17	1.2985(17)	N4	C18	1.2991(16)
C1	C2	1.3654(19)	C2	C3	1.410(2)
C3	C4	1.3859(17)	C4	C5	1.433(2)
C7	C8	1.5253(19)	C8	C9	1.528(2)
C9	C10	1.518(2)	C10	C11	1.524(3)
C11	C12	1.518(3)	C13	C14	1.362(2)
C14	C15	1.406(3)	C15	C16	1.3839(18)
C16	C17	1.434(2)	C19	C20	1.526(2)
C20	C21	1.527(3)	C21	C22	1.523(2)
C22	C23	1.525(3)	C23	C24	1.519(3)

Table A20**: Bond lengths involving hydrogen atoms (Å) for complex **10

Atom	Atom	Distance	Atom	Atom	Distance
C1	H1	0.950	C2	H2	0.950
C3	H3	0.950	C5	H4	0.950
C7	H5	0.990	C7	H6	0.990
C8	H7	0.990	C8	H8	0.990
C9	H9	0.990	C9	H10	0.990
C10	H11	0.990	C10	H12	0.990
C11	H13	0.990	C11	H14	0.990
C12	H15	0.980	C12	H16	0.980
C12	H17	0.980	C13	H18	0.950
C14	H19	0.950	C15	H20	0.950
C17	H21	0.950	C19	H22	0.990
C19	H23	0.990	C20	H24	0.990
C20	H25	0.990	C21	H26	0.990
C21	H27	0.990	C22	H28	0.990
C22	H29	0.990	C23	H30	0.990
C23	H31	0.990	C24	H32	0.980
C24	H33	0.980	C24	H34	0.980

Table A21**: Bond angles (°) for complex **10

Atom	Atom	Atom	Angle	Atom	Atom	Atom	Angle
S2	Cu1	S5	169.960(14)	S2	Cu1	N1	84.59(3)
S2	Cu1	N3	96.18(3)	S5	Cu1	N1	95.31(3)
S5	Cu1	N3	84.55(3)	N1	Cu1	N3	176.37(5)
C1	S1	C4	91.49(7)	Cu1	S2	C6	95.09(5)
C6	S3	C7	102.09(7)	C13	S4	C16	91.44(7)
Cu1	S5	C18	95.05(4)	C18	S6	C19	101.62(7)
Cu1	N1	N2	120.59(8)	Cu1	N1	C5	125.13(10)
N2	N1	C5	114.04(12)	N1	N2	C6	112.51(11)
Cu1	N3	N4	120.70(8)	Cu1	N3	C17	125.00(10)
N4	N3	C17	114.22(12)	N3	N4	C18	112.85(12)
S1	C1	C2	112.70(11)	C1	C2	C3	112.03(12)
C2	C3	C4	113.20(12)	S1	C4	C3	110.57(10)
S1	C4	C5	126.72(9)	C3	C4	C5	122.28(12)
N1	C5	C4	129.67(12)	S2	C6	S3	113.81(7)
S2	C6	N2	126.72(10)	S3	C6	N2	119.46(11)
S3	C7	C8	110.74(9)	C7	C8	C9	109.39(11)
C8	C9	C10	114.64(12)	C9	C10	C11	112.16(12)
C10	C11	C12	112.92(13)	S4	C13	C14	112.75(13)
C13	C14	C15	111.92(13)	C14	C15	C16	113.45(13)
S4	C16	C15	110.44(11)	S4	C16	C17	127.58(10)
C15	C16	C17	121.97(12)	N3	C17	C16	129.83(12)
S5	C18	S6	113.99(7)	S5	C18	N4	126.57(10)
S6	C18	N4	119.43(11)	S6	C19	C20	110.68(10)
C19	C20	C21	110.49(12)	C20	C21	C22	113.96(12)
C21	C22	C23	112.73(12)	C22	C23	C24	113.19(12)

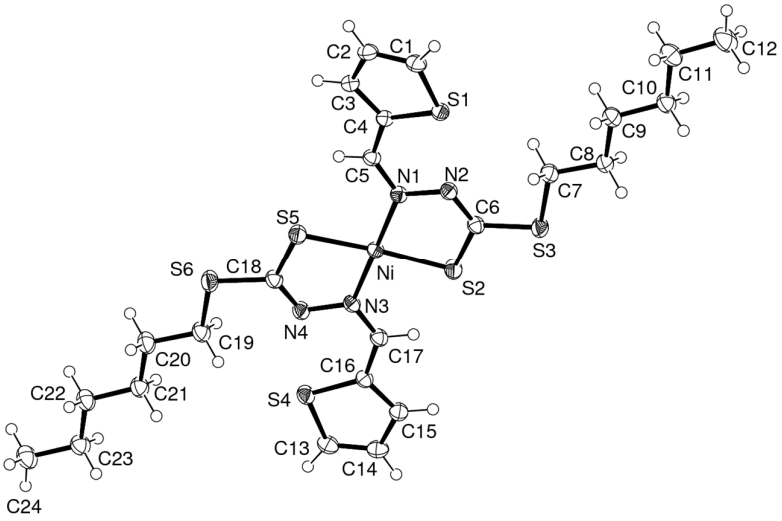

Fig. A7: ORTEP drawing (ellipsoid probability at 50%) of Ni(II) complex, **9**

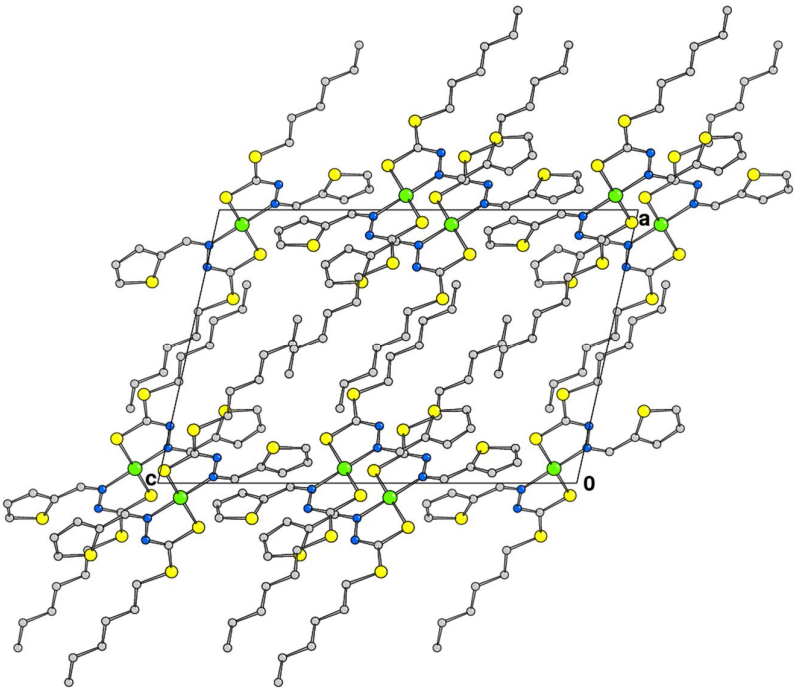

Fig. A8: Crystal packing viewed down axis *b* of the Ni(II) complex **9** (the same arrangement is observed in the copper derivative).

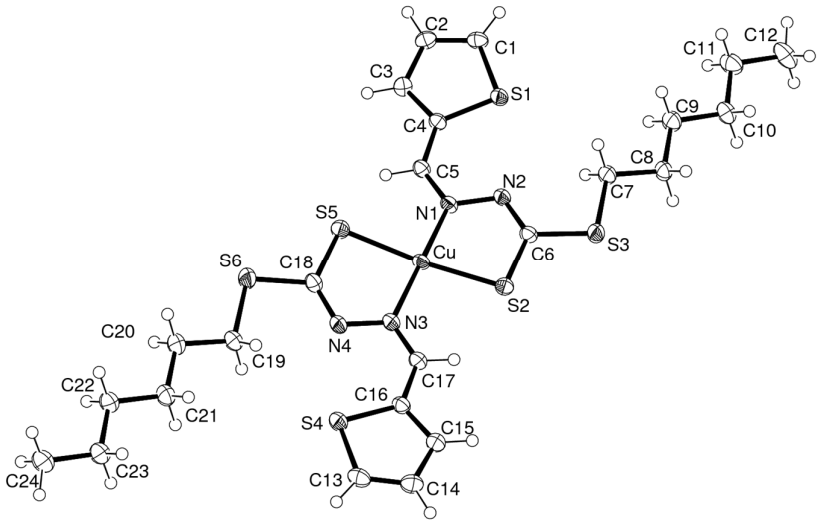

Fig. A9: ORTEP drawing (ellipsoid probability at 50%) of Cu complex **10**